

Electroporation of biomimetic vesicles

Perrier, Dayinta

DOI

[10.4233/uuid:dd37171a-f008-4874-9616-fb50367b8089](https://doi.org/10.4233/uuid:dd37171a-f008-4874-9616-fb50367b8089)

Publication date

2018

Document Version

Final published version

Citation (APA)

Perrier, D. (2018). *Electroporation of biomimetic vesicles*. [Dissertation (TU Delft), Delft University of Technology]. <https://doi.org/10.4233/uuid:dd37171a-f008-4874-9616-fb50367b8089>

Important note

To cite this publication, please use the final published version (if applicable).
Please check the document version above.

Copyright

Other than for strictly personal use, it is not permitted to download, forward or distribute the text or part of it, without the consent of the author(s) and/or copyright holder(s), unless the work is under an open content license such as Creative Commons.

Takedown policy

Please contact us and provide details if you believe this document breaches copyrights.
We will remove access to the work immediately and investigate your claim.

Electroporation of biomimetic vesicles

Electroporation of biomimetic vesicles

Proefschrift

ter verkrijging van de graad van doctor
aan de Technische Universiteit Delft,
op gezag van de Rector Magnificus prof. dr. ir. T.H.J.J. van der Hagen,
voorzitter van het College voor Promoties,
in het openbaar te verdedigen op
maandag 26 november 2018
om 15.00 uur

door

Dayinta Liem PERRIER

Master of Science in Chemistry,
Universiteit Utrecht, Utrecht, Nederland
geboren te Amsterdam, Nederland.

Dit proefschrift is goedgekeurd door de

promotor: prof. dr. ir. M. T. Kreutzer

copromotor: dr. P. E. Boukany

Samenstelling promotiecommissie:

Rector Magnificus,
Prof. dr. ir. M. T. Kreutzer,
Dr. P. E. Boukany

voorzitter
Technische Universiteit Delft, promotor
Technische Universiteit Delft, copromotor

Onafhankelijke leden:

Prof. dr. H. Lin
Prof. dr. E.J.R. Sudhölter
Prof. dr. S.J. Picken
Dr. S. Le Gac

State U. New Jersey, Rutgers
Technische Universiteit Delft
Technische Universiteit Delft
Universiteit Twente



Keywords: electroporation, electropermeabilization, electric field, lipid vesicles, giant unilamellar vesicles, GUVs, gel-phase lipids, fluid-phase lipids, binary-phase, actin network

Printed by: Gildeprint, Enschede

Front & Back: The little scientist by Dayinta Perrier

Copyright © 2018 by Dayinta L. Perrier

Casimir PhD series: 2018-41

ISBN: 978.90.8593.371.7

An electronic version of this dissertation is available at <https://repository.tudelft.nl/>.

*“It is the time you have wasted for your rose that
makes your rose so important”*

The little Prince by Antoine de Saint-Exupéry



Content

Summary	xi
Samenvatting	xv
1 Introduction	1
1.1 Electroporation of cells	3
1.1.1 The electroporation mechanism(s)	3
1.1.2 Challenges in the electroporation of cells	7
1.2 Towards understanding the electroporation mechanism	7
1.2.1 Using simplified models to mimic the cell	7
1.2.2 Scope of this thesis	8
1.3 Outline of this thesis	8
1.4 References	9
2 Lipid vesicles in pulsed electric fields: fundamental principles of the membrane response and its biomedical applications	17
2.1 Introduction	18
2.2 Vesicles as simple models of cells in electric fields	19
2.2.1 The basic principles of membranes in electric fields	19
2.2.2 Responses of GUVs in pulsed electric fields	22
2.2.3 Electrofusion	34



2.2.4 Approaching towards more realistic cell models	38
2.3 Future perspectives	39
2.4 References	41
 3 The role of gel-phase domains in electroporation of vesicles	 59
3.1 Introduction	60
3.2 Results	61
3.2.1 Fluid-phase and gel-phase GUVs	62
3.2.2 Binary GUVs containing fluid-phase and gel-phase lipids	65
3.3 Discussion	68
3.4 Conclusion	71
3.5 Methods	72
3.5.1 GUV preparation	72
3.5.2 Microscopy	73
3.5.3 Electroporation setup	73
3.5.4 Data analysis	74
3.6 References	74
S3 Appendix	78
S3.1 Movie captions	78
S3.2 Lipid loss in DPhPC fluid-phase GUVs and buckling DPPC gel-phase GUVs	79
S3.3 Calculation of the efflux for the GUVs exposed to the electric pulses	80
S3.4 Joule heating during electroporation of vesicles	81
S3.5 Evaporation of the exterior liquid during experiments	81
S3.6 References	82
 4 Unraveling the response of a biomimetic actin cortex to electric pulses in vesicles	 85
4.1 Introduction	86
4.2 Materials and Methods	88
4.2.1 Preparation of the GUVs	88
4.2.2 Polymerization and binding of the actin to the membrane	89
4.2.3 Electroporation setup combined with high speed imaging	89

4.2.4 Electroporation setup for pore dynamics	90
4.2.5 Electroporation chamber combined with confocal imaging	91
4.2.6 Data analysis of GUV response	91
4.3 Results and discussion	92
4.3.1 The dynamics of the GUVs	92
4.3.2 Resealing of the permeabilized membrane	95
4.3.3 Stability of the actin network	97
4.4 Conclusion	100
4.5 References	101
S4 Appendix	108
S4.1 Movie captions	108
S4.2 Visualization of the actin shell	108
S4.3 Polymerisation on the outside of the GUV	109
S4.4 Photobleaching correction	110
S4.5 Background signal of confocal experiments	111
S4.6 Thickness of the actin network	113
S4.7 Electric field inside an electroporated GUV	114
S4.8 Actin intensity versus transmembrane voltage	116
S4.9 References	117
5 Conclusions and outlook	119
5.1 Conclusions	120
5.1.1 Empty vesicles in electric fields	120
5.1.2 The response of a heterogeneous membrane to the electric pulse	121
5.1.3 Electroporation of an actin-supported membrane	122
5.2 Outlook	122
5.2.1 Further increase the complexity of the GUV	123
5.2.2 Single pore imaging	124
5.2.3 Reveal shielding effects of multiple GUVs	125
5.2.4 Systematic study on engineered cellular tissue	126
5.3 References	127



Acknowledgements	133
Curriculum Vitae	141
List of publications	143

Summary

Electroporation is a popular technique to permeabilize the membrane for different purposes such as medical treatments, food processing and biomass processing. In this thesis, we use the bottom-up approach to unravel the role of specific cellular components in the electroporation of cellular membranes. We have studied the role of the gel-phase domains in the membrane and the contribution of the actin-cortex during electroporation. In order to do so, we have prepared binary-phase vesicles, containing fluid- and gel-phase lipids, and actin-cortex encapsulated vesicles. Consequently, the electroporation mechanisms of these two samples provide systematic insight in the electroporation mechanism of a single cell.

In the first chapter, single cell electroporation is introduced, where the current status is discussed together with the gap(s) in the knowledge of the underlying mechanism(s). In the absence of an electric field, all cells possess a resting transmembrane voltage, which is equally distributed over the cell membrane. As soon as the electric field is applied, the cell membrane is charged with an angular dependence leading to an electrically induced transmembrane voltage. The induced transmembrane voltage is maximum at the poles, where facing the electrodes, and zero at the equator of the cell. As soon as the induced transmembrane voltage exceeds a threshold value, the five-step electroporation process starts, consisting of (1) the trigger of the electroporation, (2) expansion of the defects, (3) stabilization of the defects,



(4) resealing of the defects, and (5) the recovery of the membrane in the resealed state, called the memory of the cell. While these electroporation steps are generally accepted, the structure of these defects is unknown. In addition, their long life-time cannot be explained purely by the motion of the lipids. Moreover, the transport of large molecules, as DNA, remains unexplained and also the trafficking of the DNA after the entrance to the cell is not clear. Therefore, in order to improve electroporation as a tool for medical, food and biomass processing purposes, fundamental knowledge of the mechanism(s) is crucial.

Electroporation of lipid vesicles has provided insight in the response of the membrane to an electric field, presented in *the second chapter*, where the state-of-the-art of vesicle electroporation is discussed. The electric field induces Maxwell stresses on the membrane of the vesicles, increasing the membrane tension and causing elliptical deformations. As the transmembrane voltage exceeds the critical voltage for pore formation, macro-pores are formed accompanied with an outflow of the internal fluid, releasing the membrane tension. In addition to the observation of macro-pores, fluid-phase vesicles in electric fields have shown lipid ejection in the form of small vesicles, tubules or a combination of both. Altering the composition of the membrane by adding cholesterol or changing the lipid composition controls the critical transmembrane voltage, where the phase-state is the dominant factor determining the critical transmembrane voltage. Moreover, the gel-phase vesicles appear to obey a different electroporation mechanism. In summary, the critical transmembrane voltage of vesicles is governed by the phase state of the lipids, exhibited in the form of macropores, vesicle expel and tubulation. Hitherto, the underlying physics of these phenomena is unknown. In chapter three, we address these phenomena for a mechanistic insight.

In *the third chapter*, we present our study to the difference in the electroporation mechanism of fluid- and gel-phase vesicles and the effect of mixing the two phases. We have studied single-phase and binary-phase vesicles in electric fields. Whereas fluid-phase vesicles can expel their lipid due to the electrical tension acting during the electric field, the surface viscosity of the gel-phase lipids is too high to be expelled. Consequently, the gel-phase vesicles exhibit buckling by expelling the inner fluid, without losing its lipids. The binary-phase vesicles show a mix of both mechanisms, displaying both fluid-phase lipid expel and buckling of the gel-phase lipids. In addition, based on an estimate outflow of vesicles deducted from the post-pulse shrinkage of the different vesicles, it appears that the pore sizes of the binary vesicles are similar to the pore sizes of the fluid-phase vesicles. These results provide insights in the role of the gel-phase domains in the cell membrane during electroporation, increasing the electrical stability of the bilayer while not (significantly) affecting the sizes of the formed electro-pores. Concluding, this chapter unravels electroporation mechanism(s) of fluid-phase, gel-phase and binary vesicles, and consequently shines light on the role of lipid rafts in the electroporation of cells.

To reveal the dominating cellular components governing the pore size and the closure of

the pores during single cell electroporation, we have studied actin-cortex encapsulated vesicles, discussed in the *fourth chapter*. Experiments on living cells have indicated that the actin-cortex may play an important role in the closure of the electro-pores. High-speed imaging of biomimetic vesicles encapsulating an actin shell have shown that the actin-shell suppresses electro-deformations and inhibits the expansion of small pores to macro-pores. In addition, these biomimetic vesicles have shown tiny pores with a long lifetime after one single pulse, whereas empty vesicles require multiple pulses to be permeabilized long term. Above the critical transmembrane voltage, the pulses can disintegrate the actin-shell by the electrical forces. Consequently, our study has shown that this biomimetic shell plays a pivotal role in both the expansion of the pores and the resealing of the pores and that high electroporative pulses can provide insight into the role of the actin-cortex in the electroporation mechanism and during the resealing process.

In the *fifth chapter*, the thesis is concluded with a summary of the main results of this work and various suggestions how to apply the results from our studies presented in this thesis. Empty vesicles have been used as simplified models to reveal how large molecules as DNA can travel through the membrane by electroporation. As we have shown in our studies, the actin shell limits the growth of the pores into macro-pores for vesicles. Therefore, these biomimetic vesicles are well-suited to continue the search for the transport mechanism of large molecules through the membrane. In addition, synthetic biology can provide the help to fabricate more cell-like vesicles containing anchoring proteins for the cortex binding, linking proteins governing the strength of the cortex and microtubules including motor proteins. These more complex and realistic vesicle models can further unravel the electroporation mechanism of the membrane and additionally be used to study the DNA transport through the membrane and the trafficking towards the nucleus of the cell. Moreover, some preliminary results of high speed atomic force microscopy experiments have shown the potential of this setup to reveal structural changes in the lipid bilayer, during the increased conductivity of the membrane. These experiments would enable the visualization of single pores, unravelling their physical structure. Furthermore, biomimetic vesicle systems can be used as a step towards mimicking the cellular tissue by studying the electroporation of dense vesicle solutions. Shielding effects and its influence on the transmembrane voltage of the vesicle solution can be investigated in depth. Results of these studies can be used for two purposes: (1) enabling the control of these two parameters during the electroporation of dense solutions, and (2) confirming theoretical models of these systems. Finally, the usage of tissue engineering can provide a controlled fashion to study the complex, heterogeneous tissue. Similarly as the vesicle solutions, these are suitable samples for validation of theoretical models of tissue electroporation. Additionally, electroporation of engineered tissue can unravel the electroporation mechanism for medical usage on the human tissue.



Samenvatting

Elektroporatie is een populaire techniek voor het doordringen van het celmembraan ten behoeve van verschillende doeleinden; zoals medische behandelingen, voedselverwerking en verwerking van biomassa. In dit proefschrift gebruiken we de bottom-up benadering om de rol van specifieke cellulaire componenten in de elektroporatie van celmembranen te ontrafelen. We hebben de rol van de gelfase domeinen in het membraan bestudeerd en de bijdrage van de actine cortex tijdens elektroporatie. Om dit te doen hebben we binairefase vesikels bereid, i.e. lipiden in vloeistof en gelfase, en vesikels met een actine cortex. De elektroporatiemechanismen van deze twee soorten vesikels bieden systematisch inzicht in het elektroporatiemechanisme van een cel.

In het eerste hoofdstuk wordt de elektroporatie van een cel geïntroduceerd, waarbij de huidige status van de kennis van de onderliggende mechanismen wordt besproken tezamen met de hiaten in de huidige kennis. In rust bezitten alle cellen een spanning, het rustpotentiaal, dat gelijkmatig over het celmembraan verdeeld is. Zodra het elektrische veld is aangebracht, wordt het celmembraan geladen met een elektrisch geïnduceerde transmembraanvoltage. Het geïnduceerde transmembraanvoltage is maximaal bij de polen van de cel waar de cel op de elektroden is gericht en nul bij de evenaar. Zodra het geïnduceerde transmembraanvoltage een drempelwaarde overschrijdt start het vijfstaps elektroporatieproces



bestaande uit: (1) het in werking zetten van de elektroporatie waarbij defecten in het membraan worden gevormd; (2) de groei van deze defecten; (3) de stabilisatie van de defecten; (4) het sluiten van de defecten; (5) het herstel van het reeds gesloten membraan, ook wel “het geheugen” van de cel genoemd. Deze elektroporatiestappen zijn algemeen aanvaard, terwijl de structuur van deze defecten onbekend is. Daarnaast kan hun lange levensduur niet louter worden verklaard door de dynamiek van de lipiden. Bovendien is het transport van grote moleculen, zoals DNA, door het membraan onverklaard en het transport van het DNA binnenin de cel is niet bekend. Daarom is fundamentele kennis van de mechanismen cruciaal om elektroporatie te verbeteren bij het gebruik voor medische, voedsel- en biomassabewerkingsdoeleinden.

Elektroporatie van lipide vesikels heeft inzicht verschaft in de reactie van het membraan op een elektrische veld, gepresenteerd in *het tweede hoofdstuk*, waar de state-of-the-art van vesikelelektroporatie wordt besproken. Het elektrische veld induceert Maxwell spanning op het membraan van de vesikels, waardoor de membraanspanning toeneemt en elliptische vervormingen ontstaan. Naarmate het transmembraanvoltage de kritische waarde voor porievorming overschrijdt worden macroporiën gevormd vergezeld met een uitstroom van het interne fluïdum waardoor de membraanspanning verlaagt. Naast de macroporiën hebben vloeistof fase vesikels in elektrische velden lipide ejectie vertoond in de vorm van kleine vesikels, tubuli of een combinatie van beide. Het aanpassen van de membraansamenstelling door cholesterol toe te voegen of de lipidesamenstelling te veranderen bepaalt de kritische transmembraanspanning, waarbij de fasetoestand de dominante factor is. Bovendien lijken de gelfase vesikels aan een ander elektroporatiemechanisme te gehoorzamen. Samenvattend wordt het kritische transmembraanvoltage van vesikels beheerst door de fase van de lipiden uitgedrukt in de vorm van macroporiën, vesikeluitstoting en tubuli formatie. Tot nu toe is de onderliggende fysica van deze verschijnselen onbekend. In hoofdstuk drie behandelen we de verschijnselen om een mechanistisch inzicht te verschaffen.

In *het derde hoofdstuk* presenteren we onze studie over het verschil in het elektroporatiemechanisme van fluïde en gelfase vesikels en het effect van het mengen van de twee fasen. We hebben vesikels in elektrische velden bestudeerd van enkele fase en binair fase. Vloeistoffase vesikels kunnen hun lipiden afstoten door de spanning van het elektrische veld terwijl de oppervlakteviscositeit van de gelfase lipiden te hoog is om te worden verdreven. Daarom vertonen de gelfase vesikels rimpels die veroorzaakt zijn door de uitstoot van de interne vloeistof zonder zijn lipiden te verliezen. De binaire fase vesikels vertonen een mengsel van beide mechanismen: het uitstoten van de lipiden in de vloeistoffase en het rimpelen van de gelfase domeinen. Daarnaast lijken de poriegroottes van de binaire vesikels vergelijkbaar te zijn met de poriegroottes van de pure vloeistoffase vesikels, gebaseerd op de geschatte uitstroom van de verschillende vesikels afgeleid van hun postpulsrimp. Deze resultaten bieden inzicht in de rol van de gelfase domeinen in het celmembraan tijdens elektroporatie, die de elektrische stabiliteit van de lipide bilaag verhogen terwijl de grootte van de gevormde elektroporiën niet (significant) wordt

beïnvloed. Concluderend ontrafelt dit hoofdstuk elektroporatiemechanisme(n) van fluïde fase, gelfase en binaire vesikels. Daarmee schijnt het onderzoek zijn licht op de rol van gelachtige lipide domeinen in de elektroporatie van cellen.

Om de cellulaire componenten te onthullen die de poriegrootte en het sluiten van de poriën tijdens een elektroporatie van een cel domineren, hebben we vesikels met een actine cortex bestudeerd en besproken *in het vierde hoofdstuk*. Experimenten op levende cellen hebben erop gewezen dat de actine cortex een belangrijke rol kan spelen in het sluiten van de elektroporiën. Hogesnelheidsmicroscopie van biomimetische vesikels met een ingekapselde actine schil heeft aangetoond dat de actine elektrische vervormingen onderdrukt en de ontwikkeling van kleine poriën tot macroporiën remt. Daarnaast vertonen deze biomimetische vesikels kleine poriën met een lange levensduur na één enkele puls, terwijl lege vesikels meerdere pulsen vereisen om langdurig permeabel te worden. Boven het kritische transmembraanvoltage kunnen de elektrische krachten van de pulsen de actine schil desintegreren. Daarmee heeft onze studie aangetoond dat deze biomimetische schil een cruciale rol speelt in zowel de groei van de poriën als het sluiten van de poriën en dat hoge elektroporatieve pulsen inzicht kunnen geven in de rol van de actin cortex in het elektroporatiemechanisme en tijdens het sluitingsproces.

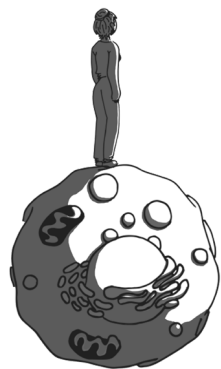
In het vijfde hoofdstuk wordt het proefschrift afgesloten met een samenvatting van de belangrijkste resultaten van dit werk en verschillende suggesties om de resultaten van onze studies toe te passen. Lege vesikels zijn gebruikt als vereenvoudigde modellen om te onthullen hoe grote moleculen, zoals DNA, door het membraan kunnen passeren door middel van elektroporatie. Zoals we in onze studies hebben aangetoond, beperkt de actine schil de groei van de poriën in macroporiën in vesikels. Daarom zijn deze biomimetische vesikels geschikt om het onderzoek naar het transportmechanisme van grote moleculen door het membraan voort te zetten. Bovendien kan synthetische biologie helpen bij het maken van meer celachtige vesikels die bijvoorbeeld verankerende eiwitten bevatten voor de cortexbinding of crosslink eiwitten hebben die de sterkte van de cortex bepalen of microtubuli bevatten inclusief motoreiwitten. Deze meer complexe en realistische vesikel modellen kunnen het elektroporatiemechanisme van het membraan verder ontrafelen en daarnaast gebruikt worden voor het bestuderen van het DNA transport door het membraan en de verplaatsing naar de kern van de cel. Daarnaast hebben enkele voorlopige resultaten van experimenten met hogesnelheidsatoomkrachtmicroscopie de potentie aangetoond om structurele veranderingen in de lipide bilag te onthullen. Deze experimenten zouden de visualisatie van afzonderlijke poriën mogelijk maken om hun fysieke structuur te ontrafelen. Daarbij kunnen de biomimetische vesiclesystemen worden gebruikt als een stap in de richting van het nabootsen van de elektroporatie van cellulaire weefsel door vesikeloplossingen met een hoge dichtheid in elektrische velden te bestuderen. Afschermingseffecten en hun invloed op het kritisch transmembraanvoltage van de vesikeloplossing kunnen diepgaand onderzocht worden. De resultaten van deze onderzoeken kunnen voor twee doeleinden worden gebruikt: (1) het besturen van deze twee parameters tijdens de elektroporatie van oplossingen met een hoge vesikeldichtheid;



(2) de bevestiging van theoretische modellen van deze systemen. Tenslotte kan het gebruik van weefselengineering een gecontroleerde manier bieden om het complexe, heterogene weefsel te bestuderen. Evenals de vesikeloplossingen zijn dit geschikte monsters voor de validatie van theoretische modellen van weefselektroporatie. Bovendien kan elektroporatie van geconstrueerd weefsel het elektroporatiemechanisme van menselijk weefsel ontrafelen voor medisch gebruik.



1. INTRODUCTION



1

Introduction



The plasma membrane of a cell acts as a selective barrier between the interior and the exterior of the cell. It regulates the molecular transport through the membrane inwards and outwards, either through the lipid bilayer or via embedded proteins, providing the activity and function of the cell. By applying electric pulses, the membrane can be temporarily perturbed or permeabilized to allow molecular transport through the membrane, called electroporation or electroporeabilization. Throughout this thesis, we refer to this phenomenon as electroporation [1]. Depending on the duration and the strength of the electric pulse, the electroporation of the membrane is either reversible or not. The technique has been found to be applicable to all cell types. Based on the various structural rearrangements in the membrane triggered by the electric pulses (Figure 1), this technique is widely applicable for different fields as medical treatments [2] (e.g. transdermal drug delivery [3-6], cancer treatment [7-11] and gene therapy [12-15]), in the food processing (e.g. to alter the viscoelastic properties of potatoes [16, 17], pasteurizing juices [18-20] and sugar extraction of sugar beet [21-24]) and in biomass processing [25-27].

The various applications of electroporation are possible because the extent of electroporation can be tailored by the electric pulse parameters. In order to determine the pulse parameters required for specific applications, knowledge of all aspects of the electroporation mechanism(s) is needed which forms the base of most research in this field. Electrochemotherapy, for example, is based on the use of non- or poorly permeable chemotherapeutic drugs, which can be delivered to tumour cells [2]. For this treatment, careful control of the permeabilized area within the targeted tissue is required combined with a local delivery of the drugs. This therapy is already in an advanced stage, where several treatments are used in cancer centres in Europe [28]. In the case of transdermal

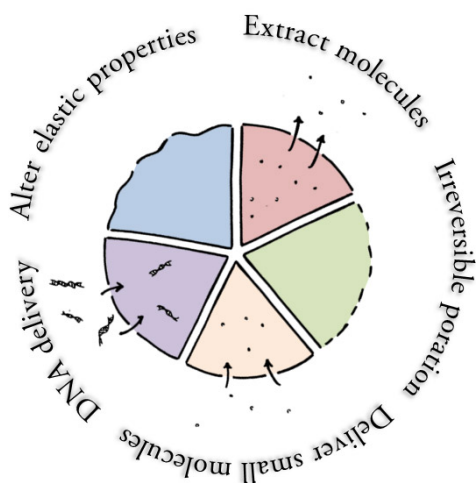


Figure 1.1. A schematic of the various results of the electroporation of a living cell: altering the physical properties of the cell, extracting molecules from a living cell, irreversible electroporating the membrane, transporting small molecules into the cell and delivering DNA. These strategies can be applied for all different kinds of applications, as discussed in the text.

drug delivery a drug transport through several cell layers of the skin is required to the target tissue, requiring different pulse parameters [3, 4]. Finally, gene therapy demands both a high control of gene transport through the membrane and knowledge of the translocation of the gene to the nucleus in order to get to expression [29]. These examples of different purposes of electroporation illustrate the required understanding of the mechanism(s) to optimize the different applications.

1.1 ELECTROPORATION OF SINGLE CELLS

1.1.1 The electroporation mechanism(s)

The electroporation technique was already discovered around the end of 1950 [30-32], followed by extensive studies to reveal the underlying mechanism(s) to the permeabilization of the cell [33]. To date, the fundamental mechanism(s) acting during electroporation or electropermeabilization are still not fully understood [34]. Furthermore, the physical mechanisms behind membrane permeabilization are highly debated, due to lack of understanding and experimental evidence at the subcellular level. Despite the limited knowledge at the subcellular level, *in vitro* studies on different types of cells have led to the general acceptance that electroporation is a multi-step process (Table 1.1 and Figure 1.2) [33, 35]. It is disputed to refer to this multiple-step process as either electroporation or electropermeabilization. The name electroporation suggests the physical formation of aqueous (i.e. hydrophilic) pores during the pulse, confirmed by theoretical studies [36-38], experiments on vesicles [39, 40] and planar lipid bilayers [41-45], and molecular dynamic (MD) simulations [46-49]. The biggest gap between theory and experiments is the inability to explain the long post-pulse permeability of the cell membrane, at least much longer than the predicted lifetime of the pores [50]. This may either be caused by the failure of the theory predicting the pore closure in the cell membrane or by other transport mechanisms in the perturbed cell membrane, possibly involving biological processes. Consequently, the term electropermeabilization has been proposed as an alternative name. In this thesis we are mainly focussing on lipid vesicle systems. Therefore, we will

Table 1.1. The different stages during electroporation, adapted from Rems & Miklavčič, J. Appl. Phys. 119, 201101 (2016) [33].

Electroporation steps		
Trigger	As the electric pulse is applied, the transmembrane voltage builds up until the critical transmembrane voltage is reached.	ns – μ s
Expansion	Expansion of the defects as long as the transmembrane voltage remains above the critical transmembrane voltage.	ns – ms
Stabilizing	When the transmembrane voltage drops below the critical value, the defects are initially stabilized.	ms – s
Resealing	In case of a reversible pulse, the membrane reseals gradually after the pulse.	s – min



A Cellular level

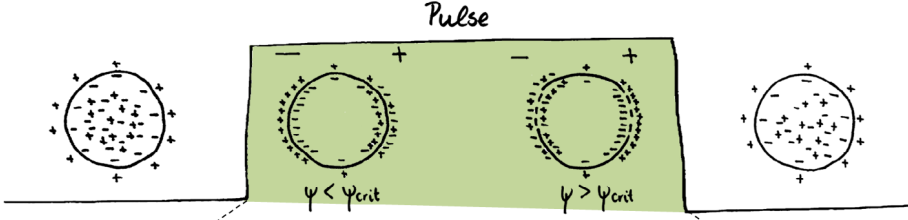
B Membrane level, $\Psi > \Psi_{crit}$ 

Figure 1.2. (A) A schematic of a cell before, during and after the electric pulse application. Before and after the pulse, the cell has a resting transmembrane voltage. During the pulse, before the transmembrane voltage exceeds the critical transmembrane voltage, the cell is charged. As the transmembrane voltage exceeds the critical value, the membrane is permeabilized according to the five steps of electroporation in (B) and Table 1.1. (B) The five-electroporation steps are displayed in table 1.1.

use the term electroporation in this thesis, due to focus on the electroporation of vesicles.

The effect of an electric field on a single cell can be described based on the electrical properties of the cell. In absence of the field, ion channels in the membrane impose a resting voltage on the cell, equally distributed over the cell membrane. As an electric field is applied, assuming that the membrane is a pure insulator, the cell acts as a capacitor and an induced transmembrane voltage builds up like [51]:

$$\Psi_m = 1.5ER \cos \theta (1 - e^{-t/\tau}) \quad (1.1)$$

where E , R and t represent the electric field strength, the radius of the cell and the time since the start of the pulse, respectively (Figure 1.3). θ is the angle with respect to the direction of the electric field, showing the angular dependence of the electrically induced transmembrane voltage. τ is the charging time of the membrane, which is the time it takes for the ions to reorganize at the membrane as the pulse is applied. Under physiological conditions the charging times are in the range of hundreds of nanoseconds. Therefore, the exponential factor can be neglected:

$$\Psi_m = 1.5ER \cos \theta \quad (1.2)$$

This equation, referred to as the Schwan equation, is only valid for a non-permeabilized (referred as a dielectric) membrane. To determine the total transmembrane voltage (Ψ_{total}),

the electrically induced transmembrane voltage must be added to the resting voltage as follows [52, 53]:

$$\Psi_{total} = \Psi_{rest} + \Psi_m = \Psi_{rest} + 1.5ER \cos \theta \quad (1.3)$$

where Ψ_{rest} is the resting voltage of the cell. Based on the angular dependence of the induced transmembrane voltage, the total transmembrane voltage is maximum at the poles facing the electrodes, and minimum at the equator. Moreover, since the resting voltage is equally distributed over the membrane, theoretically the cell contains a hyperpolarised pole and a depolarised pole during the pulse (see Figure 1.3) [35]. At the poles of the cell, wherever the transmembrane voltage Ψ_{total} exceeds a critical transmembrane voltage ($\Psi_{crit} \sim 100 - 1000$ mV) [33], the cell membrane is permeabilized. The degree of permeabilization within the permeabilized area, on the other hand, is dependent on the number and the duration of the pulse(s) [34, 35, 54]. Consequently, the permeabilized area of the cell is determined by the strength of the electric field and the degree of permeabilization by the dynamics (e.g. number and duration) of the electric pulse(s).

To explore the electroporation mechanism(s) experimentally, many single cell studies have been conducted. Several of these experiments corroborate the theory discussed above. Voltage-sensitive dye has been used to visualise the hyperpolarisation and depolarisation of the cells at the poles facing the electrodes [55]. Moreover, the asymmetric permeabilization of the membrane at the poles due to the angular dependence of the electrically induced transmembrane voltage is supported by the delivery of small tracers by electric pulses (see Figure 1.3). The transport through the membrane of tracers that were added after the pulse application, indicates that the pulses can induce long-lived pores in the cell (\sim minutes) and/or an alternative transport through the membrane. These microscopic experiments are limited by the temporal and spatial resolution of the microscopic techniques. On the contrary, conductivity measurements can detect the transport of ions through the permeabilized membrane, for example by the use of patch-clamp experiments. These studies have revealed the dynamics of the membrane to ion-permeabilization and, implied, the kinetics of the pores [56]. Both methods are strongly dependent on the tracer particles used, e.g. the size of the molecules determines the detection of the onset of permeabilization. In conclusion, these various experiments combined with theory provide a first insight into the location and the dynamics of the electroporation of a single cell.

The agreement between the theory and the experiments gives a solid foundation for the electroporation mechanism, however some crucial aspects are still unknown. In contrast to the accepted five steps of the electroporation of the membrane discussed above, the actual structure of the formed defects has not been revealed. In addition, the lifetime of the pores cannot be explained by the pure motion of the lipids. The resealing time of pure lipid bilayers has shown to be less than seconds [57-59], whereas some defects in cells take up to minutes to reseal after electroporation [50]. Moreover, the delivery



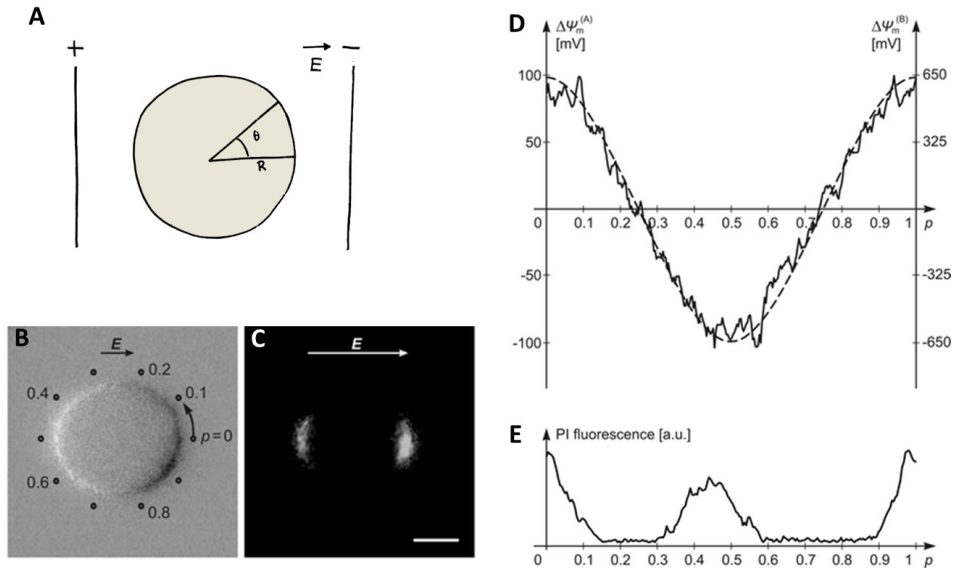


Figure 1.3. The induced transmembrane voltage of a cell during a pulse. (A) A schematic of a cell in an electric field. (B) A spherical Chinese hamster ovary (CHO) cell exposed to a non-porating electric pulse of 50 ms and 100 V/cm. The changes in fluorescence of a voltage-sensitive dye indicate the induced transmembrane voltage. The dark regions correspond to membrane depolarization and the bright regions correspond to membrane hyperpolarization. (C) The uptake of Propidium iodide (PI) molecules into the CHO cell by a porating electric pulse of 1.5 ms and 650 V/cm. The PI fluorescence indicates the transport of PI across the electroporated membrane. (D) The transmembrane voltage ($\Delta\psi_m$) along the path shown in (B) as measured (solid) and as predicted by numerical computation (dashed). (E) Fluorescence of PI, indicating the cellular uptake, along the path shown in (B). Adapted from Kotnik et al., *J. Membr. Biol.* 236, 3 (2010) [51].

of larger molecules (molecular weight > 4 kDa) appears to obey a different mechanism than that proposed above [60]. Small molecules, such as Propidium iodide (PI) dye and ions, enter the cell based on diffusional transport [61]. Due to the long lifetime of the permeabilization of the membrane, the small molecules can also enter the cell when added to the suspension after the pulse application. In contrast to this passive transport of small molecules, the delivery of larger molecules, as DNA, has shown to be more complicated. These macromolecules cannot be taken up by the cell when added to the solution after pulse application, contrarily to small molecules. Therefore, three different electric field-mediated transport of genes have been proposed. Firstly, electrophoretic forces acting on the DNA during the pulse may play a role in the transport through the membrane. Secondly, pulse-mediated membrane-DNA complexes have been observed leading to slow vesicular uptake of the DNA long after the pulse. Thirdly, pulse-mediated interaction between the DNA and active macro-domains in the membrane has been proposed to initiate the uptake through channels in the membrane [60]. The precise delivery mechanism of genes through the membrane by electric pulses remains unknown. These illustrative examples of the unknown features of the electroporation mechanism show that, despite the wide

applicability of this technique, acquiring more fundamental knowledge is essential for a full control of the phenomenon.

1.1.2 Challenges in the electroporation of cells

To progress the development of electroporation applications, gaining more insights into the molecular, cellular and tissue level are essential. At the molecular level, the electroporation mechanism strongly depends on the size of the molecules delivered to the living cells. Understanding and control of the different delivery mechanisms especially play an important role in gene therapy and DNA delivery, where large macromolecules must be delivered to the cell. Different electric pulse parameters can be used for various purposes, while strong and short pulses can permeabilize the membrane, long and weak pulses can mediate active transport through the membrane and inside the cell. At the tissue level, also the heterogeneity of the tissue and the shielding of the electric field due to the closely packed cells must be taken into account during/after electroporation. Therefore, a combination of the various electric pulse parameters might be used for different purposes. Fundamental questions still remain unanswered as: what is the pore formation mechanism? What is the actual structure of these pores? What is the role of the heterogeneity of the membrane? What governs the resealing of the membrane? How are other cellular components involved? Why does the gene delivery differ from the transport of small molecules? Providing insights on these topics for single cell studies, this knowledge can subsequently be translated to the tissue level, eventually leading to better medical applications.

1.2 TOWARDS UNDERSTANDING THE ELECTROPORATION MECHANISM

1.2.1 Using simplified models to mimic the cell

To systematically elucidate the cascade of mechanisms acting during the electroporation mechanism, bottom up approaches have been used inspired by the synthetic biology. Simplified models of the cell have been developed to mimic the cell and isolate specific cellular components [62-65]. The most popular experimental models used to study electroporation are lipid bilayers, either supported or free-standing, and vesicles, ranging from small vesicles ($\sim 10 - 100$ nm) to giant unilamellar vesicles (> 1 μ m) [66]. Both of these lipid systems provide the benefit of easy preparation and control over the composition. Free-standing lipid bilayers enable facile integration of electrodes on both sides of the membrane. Therefore, this system has been used for conductivity measurements similar to patch-clamp experiments on cells [67, 68]. Consequently, the relation between the membrane composition and the onset of irreversible electroporation can be determined. However, due to the low stability of these bilayers, no reversible electroporation can be



obtained. Supported lipid bilayers, on the other hand, possess a much higher stability. Using these lipid samples, visualisation of single pores has been attempted [69, 70], showing the preference of pores to form in the fluid-phase domains of the membrane. These studies reveal the interaction of the lipid bilayer with the electric field.

Lipid vesicles are ideal 3D-models to mimic the membrane of the cell. Topologically, they resemble the real cells and therefore include curvature effects. Additionally, giant vesicles can be imaged microscopically for single vesicle studies. Finally, the composition of the membrane, the vesicle size and the content of the vesicle can be tuned. Therefore, they are great candidates to study both the influence of the lipid composition and phase state, and the contribution of the interior of the cell. Mimicking the cytoplasm with agarose encapsulated by the membrane has shown a great influence of the interior on the deformations and the pore dynamics during electroporation [71]. In addition, the expansion of the synthetic biology increases the opportunities to further unravel the electroporation mechanism step-by-step.

1.2.2 Scope of this thesis

In this thesis we work towards understanding the electroporation mechanism at the single cell level, specifically the contribution of different cellular components. By studying giant vesicles to mimic the cell, we focus on the electroporation mechanism at and directly under the membrane, isolating different cellular components. We focus on the contribution of, firstly, the rigid gel domains in the membrane and, secondly, the actin cortex adjacent to the membrane. This way, we provide systematic insights on the electroporation mechanism of a single cell and the contribution of cellular components.

The electric field-mediated delivery mechanisms of large macromolecules as DNA plasmids and the electroporation mechanisms at the tissue level are not in the scope of this thesis. However, the vesicle models developed in this work, containing gel-phase patches and an actin-cortex, can be used to study delivery of DNA plasmids by use of electroporation. Additionally, the revelations at the cellular level of this thesis can be used for understanding the electroporation at the tissue level. Consequently, the single cell insights of this thesis can be used for expanding the knowledge on both the delivery mechanisms of DNA and electroporation at the tissue level.

1.3 OUTLINE OF THIS THESIS

The outline of the thesis is as follows. In Chapter 2, we introduce the state-of-the-art of vesicle responses in electric fields. The fundamentals of electrodeformation and electroporation mechanism are explained and a perspective on expanding the empty vesicle as a simplified model of the cell is given. In Chapter 3, we have studied binary-phase

vesicles containing gel-phase domains. Pure fluid- and gel-phase vesicles have been studied to elucidate the lipid loss mechanism of vesicles during electroporation. Consequently, this mechanism is applied to the results of electroporation of the binary-phase vesicles. In Chapter 4, we address the role of the actin-cortex in the electroporation of vesicles. Vesicles with encapsulated actin-cortex provide a model to study its contribution during the pulse. Finally, in Chapter 5, we close the thesis with a future perspective, proposing studies to further unravel the electroporation mechanism expanding the knowledge of electroporation towards molecular and tissue level.

1.4 REFERENCES

1. Pakhomov, A.G., Miklavcic, D., and Markov, M.S., *Advanced Electroporation Techniques in Biology and Medicine*. 2010: CRC Press.
2. Yarmush, M.L., Golberg, A., Serša, G., Kotnik, T., and Miklavčič, D., *Electroporation-Based Technologies for Medicine: Principles, Applications, and Challenges*. *Annual Review of Biomedical Engineering*, Vol 16, 2014. 16: p. 295-320.
3. Denet, A.-R., Vanbever, R., and Prétat, V., *Skin electroporation for transdermal and topical delivery*. *Advanced drug delivery reviews*, 2004. 56(5): p. 659-674.
4. Prausnitz, M.R., and Langer, R., *Transdermal drug delivery*. *Nature biotechnology*, 2008. 26(11): p. 1261.
5. Pavšelj, N., Prétat, V., and Miklavčič, D., *A numerical model of skin electropermeabilization based on in vivo experiments*. *Annals of biomedical engineering*, 2007. 35(12): p. 2138-2144.
6. Pliquett, U., and Weaver, J.C., *Feasibility of an electrode-reservoir device for transdermal drug delivery by noninvasive skin electroporation*. *IEEE transactions on biomedical engineering*, 2007. 54(3): p. 536-538.
7. Sersa, G., Cufer, T., Paulin, S.M., Cemazar, M., and Snoj, M., *Electrochemotherapy of chest wall breast cancer recurrence*. *Cancer Treatment Reviews*, 2012. 38(5): p. 379-386.
8. Testori, A., Rossi, C.R., and Tosti, G., *Utility of electrochemotherapy in melanoma treatment*. *Current opinion in oncology*, 2012. 24(2): p. 155-161.
9. Marty, M., Sersa, G., Garbay, J.R., Gehl, J., Collins, C.G., Snoj, M., Billard, V., Geertsens, P.F., Larkin, J.O., Miklavčič, D., Pavlovic, I., Paulin-Kosir, S.M., Cemazar, M., Morsli, N., Soden, D.M., Rudolf, Z., Robert, C., O'Sullivan, G.C., and Mir, L.M., *Electrochemotherapy – An easy, highly effective and safe treatment of cutaneous and subcutaneous metastases: Results of ESOPE (European Standard Operating Procedures of Electrochemotherapy) study*. *European Journal of Cancer Supplements*, 2006. 4(11): p. 3-13.



10. Spratt, D.E., Gordon Spratt, E.A., Wu, S., DeRosa, A., Lee, N.Y., Lacouture M.E., and Barker, C.A., Efficacy of Skin-Directed Therapy for Cutaneous Metastases From Advanced Cancer: A Meta-Analysis. *Journal of Clinical Oncology*, 2014. 32(28): p. 3144-3155.
11. Miklavčič, D., Mali, B., Kos, B., Heller, R., and Serša, G., Electrochemotherapy: from the drawing board into medical practice. *BioMedical Engineering OnLine*, 2014. 13: p. 29-29.
12. Vandermeulen, G., Staes, E., Vanderhaeghen, M.L., Bureau, M.F., Scherman, D., and Préat, V., Optimisation of intradermal DNA electrotransfer for immunisation. *Journal of Controlled Release*, 2007. 124(1): p. 81-87.
13. Mir, L.M., Nucleic Acids Electrotransfer-Based Gene Therapy (Electrogenethrapy): Past, Current, and Future. *Molecular Biotechnology*, 2009. 43(2): p. 167.
14. Broderick, K.E., and Humeau, L.M., Electroporation-enhanced delivery of nucleic acid vaccines. *Expert Review of Vaccines*, 2015. 14(2): p. 195-204.
15. C Heller, L., and Heller, R., Electroporation gene therapy preclinical and clinical trials for melanoma. *Current gene therapy*, 2010. 10(4): p. 312-317.
16. Fincan, M., and Dejmek, P., Effect of osmotic pretreatment and pulsed electric field on the viscoelastic properties of potato tissue. *Journal of Food Engineering*, 2003. 59(2): p. 169-175.
17. McHugh, T., and Toepfl, S., Pulsed electric field processing for fruits and vegetables. *Food Technol*, 2016. 70(1): p. 73-5.
18. Martín-Belloso, O., and Sobrino-López, A., Combination of Pulsed Electric Fields with Other Preservation Techniques. *Food and Bioprocess Technology*, 2011. 4(6): p. 954-968.
19. Toepfl, S., Heinz, V., and Knorr, D., High intensity pulsed electric fields applied for food preservation. *Chemical Engineering and Processing: Process Intensification*, 2007. 46(6): p. 537-546.
20. Mahnič-Kalamiza, S., Vorobiev, E., and Miklavčič, D., Electroporation in Food Processing and Biorefinery. *The Journal of Membrane Biology*, 2014. 247(12): p. 1279-1304.
21. Loginova, K.V., Vorobiev, E., Bals, O., and Lebovka, N.I., Pilot study of countercurrent cold and mild heat extraction of sugar from sugar beets, assisted by pulsed electric fields. *Journal of Food Engineering*, 2011. 102(4): p. 340-347.
22. Bouzrara, H., and Vorobiev, E., Beet juice extraction by pressing and pulsed electric fields. *International Sugar Journal*, 2000. 102(1216): p. 194-200.
23. Bluhm, H., and Sack, M., Electrotechnologies for extraction from food plants and

biomaterials. Food engineering series. Springer, Berlin, 2008: p. 237-269.

24. Mhemdi, H., Bals, O., Grimi, N., and Vorobiev, E., Alternative pressing/ultrafiltration process for sugar beet valorization: impact of pulsed electric field and cossettes preheating on the qualitative characteristics of juices. *Food and bioprocess technology*, 2014. 7(3): p. 795-805.

25. Golberg, A., Sack, M., Teissie, J., Pataro, G., Pliquett, U., Saulis, G., Stefan, T., Miklavčič, D., Vorobiev, E., and Frey, W., Energy-efficient biomass processing with pulsed electric fields for bioeconomy and sustainable development. *Biotechnology for Biofuels*, 2016. 9(1): p. 94.

26. Sack, M., Eing, C., Buth, L., Berghofer, T., Frey, and W., Bluhm, H., Electroporation as an optimizing step in drying of green biomass. in 2007 16th IEEE International Pulsed Power Conference. 2007.

27. Bluhm, H., and Sack, M., Industrial-Scale Treatment of Biological Tissues with Pulsed Electric Fields, in *Electrotechnologies for Extraction from Food Plants and Biomaterials*. 2008, Springer New York: New York, NY. p. 237-269.

28. Testori, A., Faries, M.B., Thompson, J.F., Pennacchioli, E., Deroose, J.P., van Geel, A.N., Verhoef, C., Verrecchia, F., and Soteldo, J., Local and intralesional therapy of in-transit melanoma metastases. *J Surg Oncol*, 2011. 104(4): p. 391-6.

29. Rosazza, C., Meglic, S.H., Zumbusch, A., Rols, M.P., Miklavčič, D., Gene Electrotransfer: A Mechanistic Perspective. *Current Gene Therapy*, 2016. 16(2): p. 98-129.

30. Stampfli, R., Reversible electrical breakdown of the excitable membrane of a Ranvier node. *An Acad Brasil Ciens*, 1958. 30: p. 57-63.

31. Coster, H., A quantitative analysis of the voltage-current relationships of fixed charge membranes and the associated property of "punch-through". *Biophysical journal*, 1965. 5(5): p. 669-686.

32. Neumann, E., and Rosenheck, K., Permeability changes induced by electric impulses in vesicular membranes. *The Journal of membrane biology*, 1972. 10(1): p. 279-290.

33. Rems, L., and Miklavčič, D., Tutorial: Electroporation of cells in complex materials and tissue. *Journal of Applied Physics*, 2016. 119(20): p. 201101.

34. Teissie, J., Golzio, M., and Rols, M.-P., Mechanisms of cell membrane electroporation: A minireview of our present (lack of ?) knowledge. *Biochimica et Biophysica Acta (BBA) - General Subjects*, 2005. 1724(3): p. 270-280.

35. Krassowska, W., and Filev, P.D., Modeling Electroporation in a Single Cell. *Biophysical Journal*, 2007. 92(2): p. 404-417.



36. Weaver, J.C., and Chizmadzhev, Y.A., Theory of electroporation: a review. *Bioelectrochemistry and bioenergetics*, 1996. 41(2): p. 135-160.
37. Powell, K.T., and Weaver, J.C., Transient aqueous pores in bilayer membranes: A statistical theory. *Bioelectrochemistry and Bioenergetics*, 1986. 15(2): p. 211-227.
38. Escoffre, J.M., Dean, D.S., Hubert, M., Rols, M.-P., and Favard, C., Membrane perturbation by an external electric field: a mechanism to permit molecular uptake. *European Biophysics Journal*, 2007. 36(8): p. 973.
39. Kakorin, S., Stoylov, S., and Neumann, E., Electro-optics of membrane electroporation in diphenylhexatriene-doped lipid bilayer vesicles. *Biophysical chemistry*, 1996. 58(1-2): p. 109-116.
40. Portet, T., and Dimova, R., A new method for measuring edge tensions and stability of lipid bilayers: effect of membrane composition. *Biophysical journal*, 2010. 99(10): p. 3264-3273.
41. Abidor, I., Arakelyan, V.B., Chernomordik, L.V., Chizmadzhev, Y.A., Pastushenko, V.F., and Tarasevich, M.P., Electric breakdown of bilayer lipid membranes: I. The main experimental facts and their qualitative discussion. *Journal of electroanalytical chemistry and interfacial electrochemistry*, 1979. 104: p. 37-52.
42. Chernomordik, L., and Abidor, I., 322-The voltage-induced local defects in unmodified BLM. *Bioelectrochemistry and Bioenergetics*, 1980. 7(4): p. 617-624.
43. Glaser, R.W., Leikin, S.L., Chernomordik, L.V., Pastushenko, V.F., and Sokirko, A.I., Reversible electrical breakdown of lipid bilayers: formation and evolution of pores. *Biochimica et Biophysica Acta (BBA)-Biomembranes*, 1988. 940(2): p. 275-287.
44. Melikov, K.C., Frolov, V.A., Shcherbakov, A., Samsonov, A.V., Chizmadzhev, Y.A., and Chernomordik, L.V., Voltage-induced nonconductive pre-pores and metastable single pores in unmodified planar lipid bilayer. *Biophysical journal*, 2001. 80(4): p. 1829-1836.
45. Szabo, M., and Wallace, M.I., Imaging potassium-flux through individual electropores in droplet interface bilayers. *Biochimica et Biophysica Acta (BBA) - Biomembranes*, 2016. 1858(3): p. 613-617.
46. Gurtovenko, A.A., Anwar, J., and Vattulainen, I., Defect-mediated trafficking across cell membranes: Insights from in silico modeling. *Chemical Reviews*, 2010. 110(10): p. 6077-6103.
47. Tieleman, D.P., The molecular basis of electroporation. *BMC biochemistry*, 2004. 5(1): p. 10.
48. Tarek, M., Membrane electroporation: a molecular dynamics simulation. *Biophysical journal*, 2005. 88(6): p. 4045-4053.

49. Vernier, P.T., Levine, Z.A., and Gundersen, M.A., Water bridges in electroporabilized phospholipid bilayers. *Proceedings of the IEEE*, 2013. 101(2): p. 494-504.
50. Rols, M.-P., and Teissié, J., Electroporabilization of mammalian cells. Quantitative analysis of the phenomenon. *Biophysical Journal*, 1990. 58(5): p. 1089-1098.
51. Kotnik, T., Pucihar, G., and Miklavčič, D., Induced Transmembrane Voltage and Its Correlation with Electroporation-Mediated Molecular Transport. *Journal of Membrane Biology*, 2010. 236(1): p. 3-13.
52. Mehrle, W., Hampp, R., and Zimmermann, U., Electric pulse induced membrane permeabilisation. Spatial orientation and kinetics of solute efflux in freely suspended and dielectrophoretically aligned plant mesophyll protoplasts. *Biochimica et Biophysica Acta (BBA) - Biomembranes*, 1989. 978(2): p. 267-275.
53. Kotnik, T., and Miklavčič, D., Analytical description of transmembrane voltage induced by electric fields on spheroidal cells. *Biophysical Journal*, 2000. 79(2): p. 670-679.
54. DeBruin, K.A., and Krassowska, W., Modeling Electroporation in a Single Cell. I. Effects of Field Strength and Rest Potential. *Biophysical Journal*, 1999. 77(3): p. 1213-1224.
55. Hibino, M., Itoh, H., and Kinoshita Jr, K., Time courses of cell electroporation as revealed by submicrosecond imaging of transmembrane potential. *Biophysical Journal*, 1993. 64(6): p. 1789-1800.
56. Ryttsén, F., Farre, C., Brennan, C., Weber, S.G., Nolkranz, K., Jardemark, K., Chiu, D.T., and Orwar, O., Characterization of Single-Cell Electroporation by Using Patch-Clamp and Fluorescence Microscopy. *Biophysical Journal*, 2000. 79(4): p. 1993-2001.
57. Tekle, E., Astumian, R.D., Friauf, W.A., and Chock, P.B., Asymmetric pore distribution and loss of membrane lipid in electroporated DOPC vesicles. *Biophysical Journal*, 2001. 81(2): p. 960-968.
58. Benz, R., and Zimmermann, U., Relaxation Studies on Cell-Membranes and Lipid Bilayers in the High Electric-Field Range. *Bioelectrochemistry and Bioenergetics*, 1980. 7(4): p. 723-739.
59. Teissie, J., and Tsong, T.Y., Electric field induced transient pores in phospholipid bilayer vesicles. *Biochemistry*, 1981. 20(6): p. 1548-1554.
60. Escoffre, J.-M., Portet, T., Wasungu, L., Teissié, J., Dean, D., and Rols, M.-P., What is (Still not) Known of the Mechanism by Which Electroporation Mediates Gene Transfer and Expression in Cells and Tissues. *Molecular Biotechnology*, 2009. 41(3): p. 286-295.
61. Henslee, B.E., Morss, A., Hu, X., Lafyatis, G.P., and Lee, L.J., Electroporation Dependence on Cell Size: Optical Tweezers Study. *Analytical Chemistry*, 2011. 83(11): p. 3998-4003.



62. Szathmary, E., Life: In search of the simplest cell. *Nature*, 2005. 433(7025): p. 469-470.
63. Liu, A.P., and Fletcher, D.A., Biology under construction: in vitro reconstitution of cellular function. *Nat Rev Mol Cell Biol*, 2009. 10(9): p. 644-650.
64. Sens, P., Johannes, L., and Bassereau, P., Biophysical approaches to protein-induced membrane deformations in trafficking. *Current Opinion in Cell Biology*, 2008. 20(4): p. 476-482.
65. Schwille, P., Bottom-Up Synthetic Biology: Engineering in a Tinkerer's World. *Science*, 2011. 333(6047): p. 1252-1254.
66. Jesorka, A., and Orwar, O., Liposomes: technologies and analytical applications. *Annu. Rev. Anal. Chem.*, 2008. 1: p. 801-832.
67. Kramar, P., Miklavčič, D., Kotulska, M., and Lebar, A.M., Chapter two - Voltage- and Current-Clamp Methods for Determination of Planar Lipid Bilayer Properties, in *Advances in Planar Lipid Bilayers and Liposomes*, i. Aleš, Editor. 2010, Academic Press. p. 29-69.
68. Kotnik, T., Kramar, P., Pucihar, G., Miklavčič, D., and Tarek, M., Cell membrane electroporation- Part 1: The phenomenon. *Electrical Insulation Magazine*, IEEE, 2012. 28(5): p. 14-23.
69. Jeuken, L.J.C., AFM Study on the Electric-Field Effects on Supported Bilayer Lipid Membranes. *Biophysical journal*, 2008. 94(12): p. 4711-4717.
70. Sengel, J.T., and Wallace, M.I., Imaging the dynamics of individual electropores. *Proceedings of the National Academy of Sciences*, 2016. 113(19): p. 5281-5286.
71. Lira, R.B., Dimova, R., and Riske, K.A., Giant Unilamellar Vesicles Formed by Hybrid Films of Agarose and Lipids Display Altered Mechanical Properties. *Biophysical Journal*, 2014. 107(7): p. 1609-1619.





2

Lipid vesicles in pulsed electric fields: fundamental principles of the membrane response and its biomedical applications

The present review focuses on the effects of pulsed electric fields on lipid vesicles ranging from giant unilamellar vesicles (GUVs) to small unilamellar vesicles (SUVs), from fundamental perspectives. Lipid vesicles are the most popular model membrane systems for studying biophysical and biological processes in living cells. Furthermore, as vesicles are made from biocompatible and biodegradable materials, they provide a strategy to create safe and functionalized drug delivery systems in health-care applications. Exposure of lipid vesicles to pulsed electric fields is a common physical method to transiently increase the permeability of the lipid membrane. This method, termed electroporation, has shown many advantages for delivering exogenous molecules including drugs and genetic material into vesicles and living cells. In addition, electroporation can be applied to induce fusion between vesicles and/or cells. First, we discuss in detail how research on cell-size GUVs as model cell systems has provided novel insight into the basic mechanisms of cell electroporation and associated phenomena. Afterwards, we conclude by summarizing the open questions in the field of electroporation and possible future directions for vesicles in the biomedical field.



2.1 INTRODUCTION

Biological cells are soft microscopic entities corresponding to a class of active colloidal systems. These living systems exhibit rich mechanical responses in the presence of external forces as a result of far-from-equilibrium interactions between the cells and their surrounding environment. Many of the paramount functions of living cells are governed by the cell membrane, which encloses the cell and separates its “inside” from the “outside”. Traditionally, biologists put tremendous efforts to explain how the cell membrane contributes to the cellular shape, trafficking, motility, and communication by employing top-down approaches [1-3]. In contrast to this classical strategy, biophysicists have succeeded in developing minimal model membrane systems that decipher how cellular membranes behave and interact with intra/extracellular components ranging from nanoparticles, DNA, to proteins such as cytoskeleton [4-7]. In fact, much of our current understanding about cell biology has emerged from such simple model studies [3, 8].

Understanding of the cellular phenomena using fundamental (colloidal) laws based on soft matter physics is still far away. To overcome this issue, lipid vesicles are used as an idealized system to study fundamental biophysical and biochemical cell processes [9]. Lipid vesicles can be prepared in a variety of sizes ranging from tens of nanometres to tens of micrometres, which corresponds to the smallest membrane-enclosed intracellular organelles and to dimensions of almost any type of prokaryotic and eukaryotic cells [10-12]. Based on their size and lamellarity, the vesicles are categorized into four different groups: small unilamellar vesicles (SUVs) with diameters of $\sim 10 - 100$ nm, large unilamellar vesicles (LUVs) with diameters of $\sim 100 - 1000$ nm, giant unilamellar vesicles (GUVs) with diameters $> 1 \mu\text{m}$, and multilamellar vesicles (MLVs) containing multiple bilayers [13]. Various types and mixtures of lipids can be used to prepare the vesicles [14, 15]. Moreover, several techniques are being developed for embedding proteins into the membrane, as well as for encapsulating a wide variety of materials inside the vesicle's aqueous core [16-22]. The versatile character of vesicles in terms of their size, surface functionality, and vesicle interior makes them attractive as simple cell models and ultrasmall biomimetic reactors [23-28]. Furthermore, as lipid vesicles are made from biocompatible and biodegradable materials, they provide a strategy to create safe and functionalized drug delivery systems in health-care applications [29, 30].

Cells and lipid vesicles are also characterized by heterogeneous electrical properties, for which they can be manipulated in electric field. By subjecting cells or vesicles to DC pulses, an electric potential difference (i.e. voltage) builds across the membrane, causing various phenomena. At weak pulses these membrane structures can deform under the influence of the induced electric stresses. At strong pulses, transient pores form in the lipid bilayer, which dramatically increases the membrane permeability. This phenomenon, called electroporation or electropermeabilisation, is nowadays becoming a platform technology for enhancing the transmembrane transport of drugs, genetic material, and

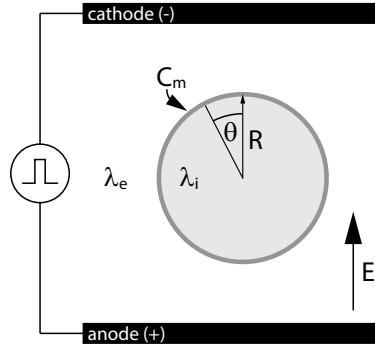


Figure 2.1. Schematic of a vesicle exposed to an electric pulse.

other molecules in the areas of medicine, food processing, and in some environmental applications [31-33]. Additionally, electroporation of two cells or vesicles, which are in close proximity, can lead to fusion of the two bodies, allowing one to create hybrid cell-cell, vesicle-vesicle, or cell-vesicle fusion products [34, 35].

In this review, we discuss the responses of lipid vesicles in pulsed electric fields. We describe how vesicles respond to electric pulses based on theoretical and experimental work on GUVs, concluding with a section about the possibilities to improve the GUV as a model of cell electroporation. this review complements the previous reviews [36-39] and covers the recent insights.

2.2 VESICLES AS SIMPLE MODELS OF CELLS IN PULSED ELECTRIC FIELDS

2.2.1 The basic principles of membranes in electric fields

Induced transmembrane voltage

The amphiphilic structure of the lipid bilayer makes lipid membranes practically impermeable to ions. In addition, the hydrophobic core of the lipid bilayer is weakly polarizable in an external electric field. Thus, the lipid membrane can be viewed as a thin dielectric layer characterized by practically negligible electrical conductivity and low dielectric permittivity as compared to the surrounding aqueous solutions [40]. The theoretical models, considering the lipid membrane as a thin dielectric layer, have provided an explanation for different phenomena observed in low AC fields including electrorotation, electrodeformation, and dielectrophoretic movement of vesicles/cells [41-44]. Additionally, the models have provided insights into electroporation and electrofusion, both observed when exposing cells or vesicles to strong DC electric pulses [42].

To understand how electric pulses act on a lipid vesicle, first consider an isolated,



spherical vesicle exposed to a homogeneous DC electric field (see Figure 2.1). The electric field electrophoretically drives the charged particles (ions) in the internal and external solutions, for which the membrane becomes charged similarly as a capacitor. The build-up of charges along the membrane leads to an induced transmembrane voltage (U_m). After a step increase in the electric field intensity E , U_m increases with time according to the Schwan's equation [45]:

$$U_m = 1.5 ER \cos \theta (1 - e^{-t/\tau_{chg}}) \quad (2.1)$$

Note that U_m is proportional to the vesicle radius R and varies with the angle position θ on the membrane, as shown in Figure 2.1, such that it reaches the highest absolute value at the areas facing the electrodes. The characteristic charging time τ_{chg} of the membrane depends on the vesicle radius, membrane capacitance ($C_m \approx 0.7 \mu\text{F}/\text{cm}$ [43, 46]), and the conductivities of the internal (λ_i) and external (λ_e) solutions:

$$\tau_{chg} = RC_m \frac{2\lambda_e + \lambda_i}{2\lambda_e \lambda_i} \quad (2.2)$$

If the duration of the exposure to the electric field (i.e. the duration of the electric pulse) is longer than the charging time, $t_{pulse} \gg \tau_{chg}$, U_m reaches a steady state, $U_m = 1.5 ER \cos \theta$. Otherwise, the membrane remains in the charging phase throughout the duration of the electric pulse. In typical experiments with GUVs, where the aqueous solutions consist of dissolved sucrose and glucose ($\lambda_i \approx \lambda_e \approx 5 \mu\text{S}/\text{cm}$ [47]), the charging time for a vesicle with radius of $20 \mu\text{m}$ is about $420 \mu\text{s}$. When such GUVs are exposed to electric pulses with duration on the order of $100 \mu\text{s}$, the membrane remains in the charging phase. Upon addition of ions into aqueous solutions, the charging time considerably decreases.

Note that equations (2.1–2.2) are valid only for a spherical, nondeformed vesicle, and until the membrane can be considered as electrically nonconductive, i.e., before the membrane becomes electroporated [48, 49]. Furthermore, the equations are valid as long as the dielectric permittivities of the external (ϵ_e) and internal (ϵ_i) aqueous solution can be neglected, i.e., for pulse duration considerably longer than the Maxwell-Wagner polarization time $\tau_{MW} = (2\epsilon_e + \epsilon_i) / (2\lambda_e + \lambda_i)$ [50]. To determine U_m on deformed or electroporated vesicles, often numerical calculations need to be employed.

Theoretical background on electroporation

Natural pores can be nucleated spontaneously in the lipid membrane due to thermal fluctuations of the lipid molecules. But as the free energy for pore nucleation is much higher than the thermal energy kT (where k is the Boltzmann's constant and T is the absolute temperature), spontaneous occurrence of pores is a very rare event. This free energy can be reduced either by applying lateral (stretching) tension on the membrane or by exposing the membrane to an electric field [51, 52]. Since the bilayer behaves as

a dielectric shell, the electric field induces electric stresses on the membrane, which act similarly to a lateral tension, as proposed in different models based on continuum theories [53-55]. If the decrease in the free energy for pore nucleation is governed by electric stresses, the rate of pore nucleation can be written as [56]

$$v = A \exp \left(-\frac{\delta_c}{kT} + \frac{BU_m^2}{kT} \right) \quad (2.3)$$

where δ_c is the nucleation free energy in the absence of U_m , A is a pre-exponential factor and B is a proportionality constant. The free energy δ_c has been estimated to be $\sim 45 kT$ based on measurements on planar lipid bilayers, however it is expected to depend on the composition of the lipid bilayer [57]. After pore nucleation, the Maxwell stress expands the pores further [58]. Once the electric field is removed, the edge tension (the energy of the pore edge per unit length of the pore circumference) tends to close the pores [59, 60].

During the last decade, molecular dynamics (MD) simulations have provided an additional insight into the molecular mechanisms of pore formation [61]. When the bilayer is exposed to an electric field, the pore nucleation is initiated by formation of a water column spanning the bilayer, which (in typical zwitterionic phospholipid bilayer) is followed by migration of lipid head groups into the wall of the pore [62]. (An example of the pore nucleation sequence taken from MD simulations is shown in Figure 2.6.) The average lag time before the onset of pore nucleation is a stochastic variable, but on average the nucleation rate increases exponentially with an increase in U_m [63, 64]. Although in a broader sense, the insights from MD agree with earlier theoretical predictions [65], MD suggest that the pore nucleation is predominantly mediated by the electric-field-driven reorientation of the water dipoles at the water-bilayer interface, and not by tensile electric stresses [64, 66].

Both continuum models and MD simulations indicate that U_m influences the rate of pore nucleation. Hence, it is impossible to theoretically define an absolute critical U_m above which electroporation of the lipid membrane takes place. However, as the nucleation rate increases exponentially with U_m , electroporation experimentally appears as a threshold-like phenomenon [67]. Thus, it is possible to define a relative threshold as the critical value $U_{m,crit}$ above which electroporation can be detected in a given amount of time and under the given experimental conditions. Additionally, since electroporation is generally detected through a dramatic increase in the membrane permeability and associated molecular transport across the membrane, it is important to note that the pulse parameters influence the growth of the pores, and thus directly control the transmembrane molecular flux. As such, the determined $U_{m,crit}$ depends on the size of the molecular probe and the sensitivity of the detection system [68]. A well-known technique for detecting $U_{m,crit}$ of GUVs is through determining the contrast loss from sucrose-filled GUVs in a glucose environment. Using sucrose in the interior and glucose in the exterior of the GUV leads to a contrast difference when using phase-contrast optical microscopy. However, the presence of the pores allows the sugar molecules to exchange across the membrane, which



diminishes the contrast difference after electroporation. Using of this technique $U_{m,crit}$ of fluid phase GUVs is found to be around 1 V [60]. Another method to detect $U_{m,crit}$, recently established by Mauroy *et al.*, is based on detecting the transmembrane transport of manganese ions [68]. With this novel technique they have been able to measure a significantly lower $U_{m,crit}$ of about 6 mV for the same type of GUVs. This extremely low $U_{m,crit}$ is assigned to the small size of the manganese ions, which thus require only small defects in order to cross the bilayer. Moreover, $U_{m,crit}$ of ~ 650 mV is found for similar type of GUVs by tracking Ca^{2+} influx [69]. It is further worth mentioning that $U_{m,crit}$ is generally determined based on calculating the maximum absolute U_m reached at $\theta = 0$ and π from equation (2.1). This equation is valid only for a spherical vesicle and does not take into account the shape deformations, which are induced by electric stresses.

Besides these parameters, that can unintentionally change the measured $U_{m,crit}$, it has also shown that $U_{m,crit}$ can be tuned intentionally. Since both mechanical tension and electric stresses promote pore formation, $U_{m,crit}$ can be reduced by mechanically increasing the lateral tension of the membrane, e.g. by aspirating part of the GUV into a micropipette [54]. For this reason, GUVs which have some initial tension, i.e., GUVs which do not exhibit any visible thermal undulations, electroporate at lower $U_{m,crit}$ [47]. In addition, different membrane compositions influence $U_{m,crit}$. MD simulations showed that $U_{m,crit}$ is to some extent correlated with the thickness of the bilayer [70], though in general, it greatly depends on the detailed architecture of both the lipid head groups and the lipid tails, as well as the lipid phase and the temperature [71-73]. The parameter, on which $U_{m,crit}$ appears to depend predominantly, is the local pressure profile in both the head group and the tail group region, which could affect the mobility of water molecules inside the bilayer [72, 74]. Furthermore, the strong influence of the lipid architecture was also found in MD calculations of the pore nucleation free energy in the absence of the electric field (δ_ϵ in equation (2.3)) [75, 76]. This shows that the ability of a bilayer to resist poration is an intrinsic property of its constituting lipids. The effect of the lipid composition on the electroporation of GUVs is discussed in greater detail below.

2.2.2 Responses of GUVs in pulsed electric fields

Due to the micrometre size of GUVs, their responses to electric pulses can be monitored and investigated at the microscopic level. In particular, the development of high-speed imaging has dramatically increased the knowledge on the dynamic behaviour of GUVs during and after the exposure to electric pulses. The basic responses have been determined on GUVs made from zwitterionic phospholipids in the fluid phase such as Egg PC [47, 77, 78] and DOPC [69, 79, 80]. These experiments revealed details on the electrodeformation of the GUVs, which is in high electric fields accompanied by the formation of macropores and lipid loss (associated with electroporation). Experiments on GUVs made from different lipids and lipid mixtures provided further insights into the effect of the lipid composition on electroporation and the stability of GUVs in an electric field. These observations are

outlined below. For completeness we review recent reports together with older data. More comprehensive reviews on this topic (conducted until 2012) can be found in [36-38].

Electrodeformation

The exposure of a GUV to an electric field induces an electrical tension on the membrane, given by the Maxwell stress tensor, which can cause deformation and stretching of the GUV. Depending on the intensity and the duration of the electric pulse, as well as the conductivity of the inner and outer solutions, the shape and the degree of GUV deformation can be significantly varied [36]. Deformation of the GUV is accompanied by an increase in the projected membrane area, which can be categorized into two regimes. For small deformations (low tension), the projected area increases as the weak electric stresses flatten the thermal undulations of the membrane. This regime is often referred to as the entropic regime and is governed by the bending rigidity of the membrane. For stronger deformations (high tension), where all membrane undulations are flattened, the electric stresses lead to elastic stretching of membrane, increasing the area-per-lipid in the bilayer [81, 82]. This regime is governed by the elastic stretching modulus of the membrane. The first studies on GUV electrodeformation were conducted in AC electric fields, which induced ellipsoidal deformations, as predicted by theory [83-88] (see Dimova *et al.* [36, 37] for reviews). Depending on the frequency of the applied AC field and the ratio between the conductivity of the internal and the external aqueous solutions ($\chi = \lambda_i / \lambda_e$), the GUV can deform into either a prolate or an oblate ellipsoid, with the long axis aligned either parallel or perpendicular to the direction of the electric field, respectively. By measuring electrodeformations of GUVs in AC field, it is possible to extract the information on the mechanical properties of the membrane, such as the bending rigidity [89], and the electrical properties, such as capacitance [46].

Unlike in continuous AC fields, the electrodeformation induced by DC pulses are transient and the GUVs relax back into their spherical shape rapidly after the end of the pulse; therefore, these deformations are experimentally difficult to capture with conventional cameras having a temporal resolution in the millisecond range. The first experimental observations of GUV electrodeformation induced by a 1.2 ms-long pulse were reported by Kinosita *et al.* [90]. They imaged fluorescently labelled GUVs using a pulsed-laser fluorescence imaging system with a temporal resolution of 100 μ s. They observed that, similarly as in AC field, the shape of the deformed GUV depends on the ratio χ ; if the internal conductivity is higher than the external conductivity ($\chi > 1$), the GUV deforms into a prolate shape, whereas for $\chi < 1$ the GUV deforms into an oblate shape. These observations were qualitatively corroborated by theoretical work of Hyuga *et al.* [91, 92]. Later, Riske and Dimova [47, 77] studied the electrodeformation of GUVs exposed to 50 – 300 μ s pulses (where $t_{\text{pulse}} < \tau_{\text{chg}}$) with a time resolution down to 33 μ s, using phase-contrast microscopy and a high-speed digital camera. They observed a similar dependence of the GUV shape on χ , but also highlighted the influence of ions in the external solution. In the absence of ions, the GUVs were deformed into prolate ellipsoids for $\chi > 1$ [47]. Upon



addition of ions, the GUVs were transiently deformed into peculiar cylindrical shapes, again depending on the ratio χ (Figure 2.2) [77]. For $\chi > 1$ tube-like shapes were observed analogous to prolate ellipsoids, for $\chi \approx 1$ square-like deformations were reported, and for $\chi < 1$ disk-like deformations were observed comparable to oblate shapes. Such “squaring” of the GUV shape was also noted in the presence of gold nanoparticles [36]. Moreover, Riske and Dimova [47, 77] measured the degree of deformation by determining the aspect ratio a/b of the deformed GUVs (Figure 2.2c). They demonstrated that the degree of deformation increases with the increasing electric field strength and/or the pulse duration, while it also depends on the initial tension of the GUV. Sadik *et al.* [78] further studied the prolate deformations by systematically varying χ (between 1.92 and 53.0). At constant χ the aspect ratio scaled quadratically with the electric field strength, confirming the dominant role of the electric stresses in driving the deformations. With increasing χ at a constant electric field strength, the aspect ratio asymptotically approached a maximum value. Note that in the experiments described above, the electrodeformations were often accompanied by macroporation of the GUV membrane.

Analytical modelling results based on balancing the stresses acting on the GUV membrane (electric, hydrodynamic, bending, and tension) demonstrated that the shape of deformation during an electric pulse relates to the different charging kinetics on the external and internal side of the membrane (see Figure 2.3) [93]. If $\chi > 1$, the charges accumulate faster on the internal side and the resulting electric stresses tend to elongate the GUV along the direction of the electric field inducing a prolate deformation (Figure 2.3a). On the contrary, if $\chi < 1$, a transient oblate deformation can occur during the charging phase of the membrane, since the charges accumulate faster on the external side, and the electric stresses tend to compress the GUV in the direction of the electric field (Figure 2.3b). Once the membrane is fully charged, the accumulated charges on the internal and

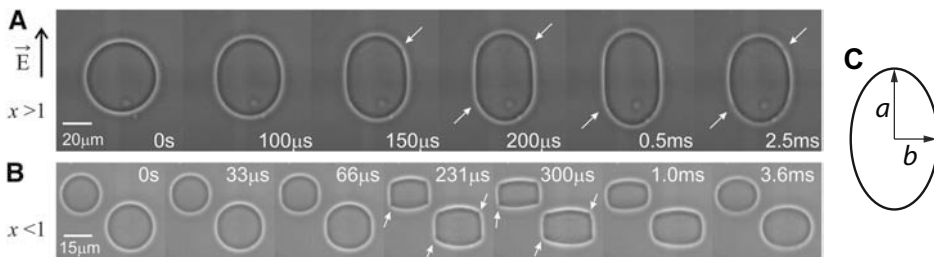


Figure 2.2. Time sequence of phase contrast images showing deformation and macroporation of GUVs exposed to a DC electric pulse under two different conductivity conditions. (A) shows the tube-like deformation of a GUV, exposed to 200 μs, 2 kV/cm pulse, at conductivity condition $\chi = 1.38$, $\lambda_i = 16.5 \mu\text{S/cm}$, $\lambda_e = 12 \mu\text{S/cm}$. (B) Shows two disk-like deformation of two GUVs exposed to 300 μs, 3 kV/cm pulse under conductivity condition $\chi = 0.05$, $\lambda_i = 6 \mu\text{S/cm}$, $\lambda_e = 120 \mu\text{S/cm}$. Time 0 s corresponds to the onset of the pulse. In both cases the pulse duration is comparable to the charging time of the membrane. White arrows indicate locations of macropores. Reprinted with permission from [77]. Copyright 2006 Elsevier. (C) A schematic representation of the semi-axes for determining the aspect ratio a/b of deformed GUVs.

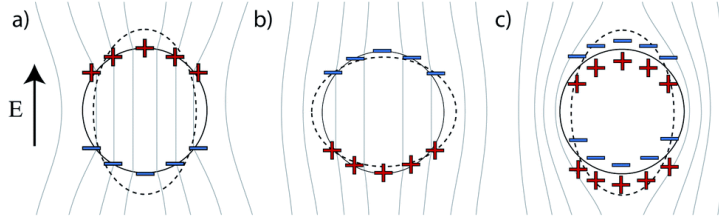


Figure 2.3. Sketch of the electric field and induced charge distribution around a GUV immersed in an electrolyte solution, following the imposition of a uniform DC field: (a,b) during the membrane charging phase under condition (a) $\chi > 1$ and (b) $\chi < 1$, and (c) after the membrane becomes fully charged. The dashed lines indicate the vesicle deformation. Reprinted with permission from [79]. Copyright 2014 The Royal Society of Chemistry.

external sides are balanced, the electric field is expelled from the interior, and the GUV is deformed into a prolate ellipsoid (Figure 2.3c). Hence, under the condition $\chi > 1$, the shape deformation can only be prolate, as corroborated by experiments [47, 78]. Under the condition $\chi < 1$, an oblate-to-prolate shape transition is predicted [93]. However, the oblate-to-prolate transition is difficult to observe experimentally, as explained by Salipante and Vlahovska [79]. On one hand, the GUV can attain an oblate shape only during the charging phase of the membrane, $t < \tau_{chg}$. On the other hand, significant deformation can only occur for times longer than the characteristic time in which the electric stresses can deform the GUV during the pulse [93]

$$\tau_{el} = \frac{\mu_e(1+\mu_i/\mu_e)}{\varepsilon_0 \varepsilon_e E^2} \quad (2.4)$$

where μ_e and μ_i are the viscosities of the external and internal solution, respectively. In low electric field, where $\tau_{el} > \tau_{chg}$, the deformation occurs after the membrane is fully charged and only a prolate shape can be observed. In a high electric field, where $\tau_{el} < \tau_{chg}$, the deformation occurs while the membrane is still charging. However, in typical experimental conditions, such an electric field strength leads to electroporation and the associated increase in the membrane conductivity. If the membrane becomes conductive, theory predicts that the GUV can remain oblate when $\chi < 1$ [91, 92, 94]. To demonstrate experimentally the oblate-to-prolate transition, Salipante and Vlahovska [79] used a double-pulse protocol consisting of a strong 20 μ s pulse followed by a longer 50 ms pulse with a lower intensity. The first pulse was strong enough to induce an oblate deformation but short enough to avoid electroporation, whereas the second pulse allowed full charging of the membrane leading to a prolate deformation. More complex numerical models based on electrohydrodynamic principles further corroborated the predicted oblate-to-prolate transition, and in addition revealed more complicated shapes of GUVs, including the squared shapes [94-97], resembling those observed by Riske and Dimova [77]. In summary, electrodeformation of a GUV during the pulse is dynamic and depends on the pulse duration, strength, presence of ions in the external solution, conductivity ratio χ , and

membrane electroporation. As it is challenging to model the highly nonlinear dependence of pore nucleation and pore growth on U_m and associated tensile stresses, as well as the ionic and fluid exchanges across the pores, current models of GUV electrodeformation are either limited to treatment of a nonconductive membrane and are strictly valid only before the onset of electroporation [93-97], or consider a simplified case of a completely conductive membrane and are based on semi-empirical treatment of the hydrodynamic forces [78, 91, 92].

After the exposure of a GUV to an electric pulse, which leads to electrodeformation, the GUV relaxes back to the spherical shape (in the absence of electric field). Provided that the GUV has not been electroporated, the characteristic relaxation time depends on the stretching regime attained by the membrane during the pulse. Relaxation of an elastically stretched GUV proceeds with a characteristic time on the order of 100 μ s [47], whereas relaxation of membrane undulations strongly depends on the initial (pre-pulse) tension of the GUV. Yu *et al.* [98] theoretically analysed relaxation of GUVs deformed in the second (entropic) regime and showed that such analysis can be applied to measure the bending rigidity and the initial membrane tension of GUVs.

Electroporation: macropores and lipid loss

When applying weak electric pulses, a GUV can be electrodeformed in the absence of detectable electroporation, as discussed above. By increasing the intensity and/or duration of the electric pulse, electrodeformation becomes accompanied by electroporation of the GUV membrane. Experiments on GUVs have shown two interesting phenomena associated with electroporation, which are not observed in living cells: the creation of micrometre-sized pores (macropores) and the expel of lipids from the GUV membrane [47, 69, 77, 80, 90]. Kinoshita *et al.* [90] reported that formation of macropores was preceded by a measurable increase in the membrane conductivity, indicating the presence of optically-undetectable nanoscale pores. Thus they postulated that macropores could arise from growth or coalescence of smaller pores, or as a consequence of electrodeformation. In the following studies, the formation of macropores was linked to the increase in the membrane tension caused by the electric field [47, 60]. As inferred from the measurements on GUVs aspirated into a micropipette, when the membrane tension exceeds a critical value called the lysis tension, the bilayer ruptures due to unlimited growth of unstable pore(s) [99]. Unlike in the aspiration experiments where the tension imposed on the membrane is controlled by the micropipette, the tension induced by an electric field relaxes as the pores grow and the fluid leaks out from the GUV [60, 100]. Therefore, large macropores can form without disintegrating the membrane. The value of the lysis tension depends on the lipid composition and varies roughly between 3 and 10 mN/m for phospholipid fluid GUVs [54, 101], although it also depends on the time and rate at which the tension is imposed [99, 102, 103]. To compare the electric tension σ_{el} induced on the membrane at given U_m with the lysis tension σ_{lys} , Needham and Hochmuth proposed a simple derivation [54]

$$\sigma_{el} = \frac{1}{2} \frac{\epsilon_m}{h_e} \left(\frac{h}{h_e} \right) U_m^2 \quad (2.5)$$

where ϵ_m and h_e represent the dielectric permittivity and the thickness of the hydrophobic lipid core, respectively, whereas h represents the total thickness of the membrane. By inserting typical values for fluid phospholipids $\epsilon_m = 2 \cdot 10^{-11}$ F/m, $h_e = 2.8$ nm, and $h = 3.9$ nm, the lysis tension of 5 mN/m is reached at $U_m \approx 1$ V [54]. This was corroborated by the experimental observation of macropores at $U_m \approx 1$ V when exposing GUVs to an electric pulse with a duration in the order of 100 μ s [47, 54].

Under the conditions which lead to prolate deformation of a GUV, macropores are generally formed near the poles of the GUV, where the highest U_m and largest electrical tension are predicted based on theory [47, 78, 95]. Compared with non-macroporated GUVs, macroporated GUVs attain a higher aspect ratio during the pulse and relax more slowly back to spherical shape after the pulse [47]. The post-pulse relaxation of the GUV shape is governed by the closure of macropores, which takes about 10 ms to few 100 ms, depending on the size of the macropores and the residual membrane tension [47, 60]. The velocity of pore closure is determined by the interplay between the edge tension of the pore and the leak-out of the internal fluid from the GUV [47, 59, 60]. The analysis of the closure kinetics of macropores thus provides a method for measuring the edge tension in GUVs with different lipid compositions [60]. Additionally, since the leak out of the internal fluid depends on the viscosity of this fluid, the pore closure can be slowed down by increasing the viscosity, e.g. by adding glycerol to water [100].

When cylindrical deformations occurred, Riske and Dimova observed macropores at the corners of the deformed membrane (as indicated in Figure 2.2 with white arrows) [77]. McConnell *et al.* [94, 95, 104] attempted to theoretically understand this observation by numerically calculating the time-dependent evolution of the induced membrane tension (Figure 2.4). The results showed that when the GUV deforms into a cylindrical shape, the highest positive (stretching) tension is induced at the corners of the deformed GUV (Figure 2.4c), which is expected to promote formation and growth of pores in these regions. If the membrane does not porate at this point of time, the highest tension shifts to the poles of the GUV (Figure 2.4d-e). Indeed, Portet and Dimova [60] used similar experimental conditions as in Figure 2.2b, but they exposed the GUVs to longer 5 ms pulses with lower intensity and captured macropores at the poles of the GUVs towards the end of the pulse. Note that the tension shown in Figure 2.4 is not equal to the one in equation (2.5), but was determined numerically by a more rigorous calculation of the electric and hydrodynamic stresses acting on the membrane. More specifically, the tension in Figure 2.4 corresponds to the Lagrange multiplier that enforces incompressibility of the membrane area [94].

Several reports further showed an asymmetric pattern of the pore distribution [60, 69, 80, 90]. Kinosita *et al.* [90] reported that macropores in asolectin (soybean phospholipid)



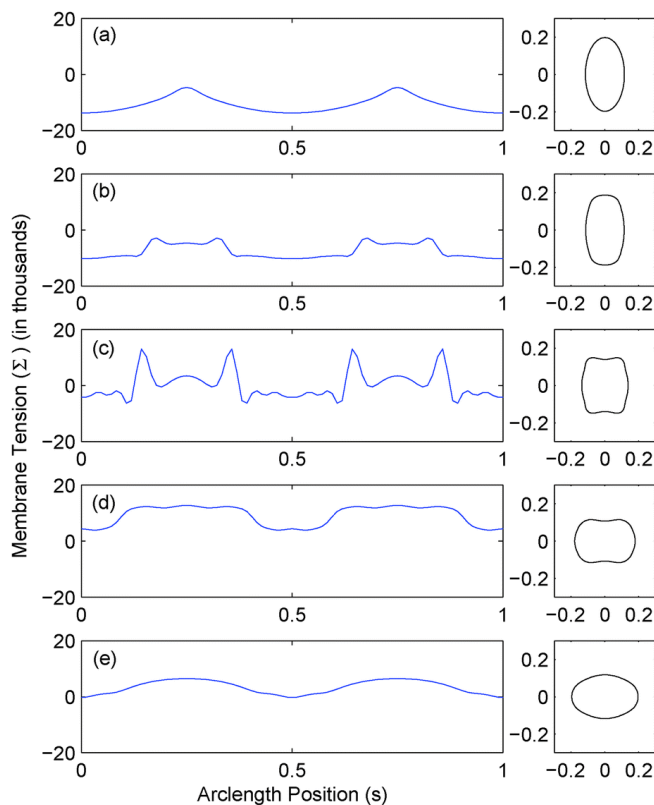


Figure 2.4. Numerical calculations of the membrane tension for a GUV exposed to a DC pulse under conductivity condition $\chi = 0.1$. Membrane tension is plotted as a function of arclength measured from the vesicle equator (0 and 0.5 correspond to the equator, 0.25 and 0.75 to the poles of the GUV). The images on the right-hand side show the associated vesicle profile at dimensionless time (a) $t/t_m = 0$, (b) 0.1, (c) 0.17, (d) 0.22 and (e) 0.6, where $t_m = RC_m/\lambda_c$ is a measure for the membrane charging time. The electric field is directed from top to bottom. The numerical results were reported in dimensionless form. For experimental parameters similar to those in Figure 2.2A, the electric field strength in dimensional form is ~ 4 kV/cm and the pulse duration is ~ 150 μ s. Note that the GUV is initially shaped as prolate spheroid since the numerical model assumes conservation of the membrane area and vesicle volume, and thus cannot predict electrodeformations for idealized spheres without any access area. Reprinted with permission from [94]. Copyright 2015 The Royal Society of Chemistry.

GUVs formed preferentially on the side facing the positive electrode (anode). In contrast, Tekle *et al.* [69] observed that macropores preferentially formed on the side facing the negative electrode (cathode) in DOPC GUVs. Macropores were rarely found on the anodic hemisphere, but the results suggested that the anodic side is permeabilized by a greater number of smaller (optically undetectable) pores [69]. Preferential macroporation of the cathodic side was also observed by Portet *et al.* in DOPC and Egg PC vesicles [60, 80]. Furthermore, both Tekle *et al.* [69] and Portet *et al.* [60, 80] detected macropores in

combination with a reduced size of the GUVs after the pulse. The size reduction can be attributed to the expel of lipids in the form of small vesicles and/or tubules, as reported by Portet *et al.* [80] based on imaging of fluorescently-labelled GUVs (Figure 2.5). In some cases, multiple pulses were applied to detect visible lipid ejection, and by increasing the number of pulses, the size of the GUVs progressively decreased [80]. Mauroy *et al.* [105] showed similar lipid ejection by use of CARS microscopy, confirming that lipid loss is not an artefact of membrane labelling. Moreover, they demonstrated that lipid loss is controlled by the pulse duration and can be detected at a significantly lower electric field when GUVs are exposed to 5 ms pulses compared to 100 μ s pulses. Portet *et al.* [80] assumed that the amount of ejected lipids is proportional to the permeabilized membrane area, showing good agreement with the experimental results, whereas Sadik *et al.* [78] reported a correlation between the post-pulse reduction in the membrane area and the aspect ratio attained by GUVs during electrodeformation. However, the mechanisms responsible for the asymmetric distribution of pores and lipid ejection are not yet completely understood. It also remains unclear whether electroporation and lipid loss are either coincident or interrelated phenomena. For instance, tubule formation can also be observed in GUVs exposed to non-electroporating AC fields [106]. Theoretical works on the instability of a lipid membrane in an electric field suggested that a bilayer can undergo undulations with an increasing amplitude [107–111], which may eventually lead to tubulation and loss of lipids. When the membrane is separating fluids with an equal conductivity and permittivity, such a membrane instability could result from ionic currents in the electric double layer

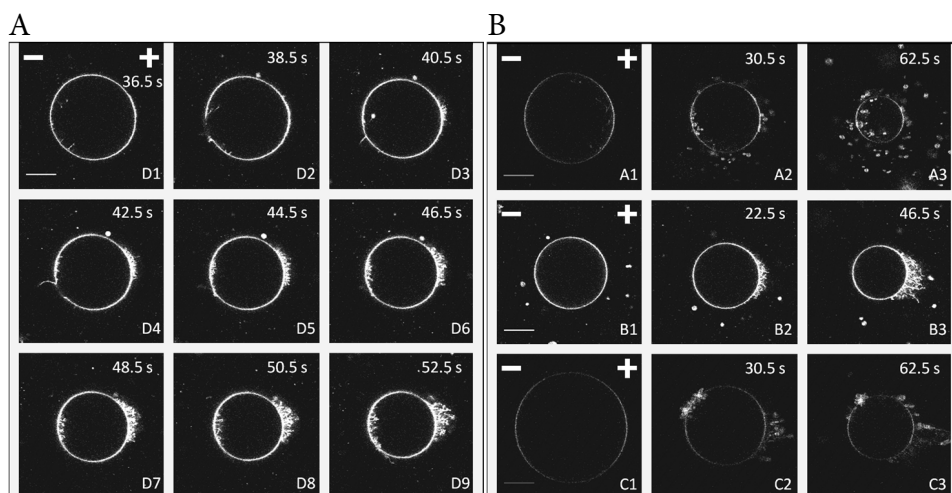


Figure 2.5. (a) Image sequence of a fluorescently labelled GUV showing formation of macropores on the cathodic side of the membrane. The GUV was exposed to multiple 5 ms, 300 V/cm pulses. Image D1 is acquired after 15 pulses, D2 after 16 pulses, D3 after 17 pulses, etc. (b) Images of three GUVs, denoted as A, B, and C, showing the different mechanisms of lipid ejection: vesicle and tubule formation. The parameters of applied pulses were similar as in (a). Images with index 1, 2, and 3, were captured after application of 0, 12, and 24 pulses, respectively. Reprinted with permission from [80]. Copyright 2009 Elsevier.

next to the membrane surface [108, 109]. When the membrane is separating fluids with asymmetric electrical properties, particularly different conductivities, such an instability could also be a consequence of the transient mismatch between the ionic accumulation at the two sides of the membrane [110, 111]. These instabilities were predicted both for a nonconducting and a conducting (electroporated) membrane.

Influence of membrane composition on electroporation

One of the main advantages of using vesicles is that the membrane composition can be controlled and thus the mechanical properties can be tuned. So far, the lipids of all systems discussed in this review have been in the fluid phase (or liquid-disordered phase), where the lipids possess high mobility and chain disorder. Lowering the temperature below the transition temperature of a lipid, brings the lipid in the so-called gel phase (or solid-ordered phase), where the lipids are tightly packed and exhibit low mobility. The transition temperature varies with different types of lipids, whereby some lipids exist in the fluid and others in the gel phase at room temperature [112]. Therefore, a simple method to change the mechanical properties of the membrane is to select a lipid with a different phase or create a two-phase system with both liquid and gel domains. The addition of cholesterol to fluid phase lipids brings the lipids in an intermediate phase, the liquid-ordered phase. Cholesterol organizes the hydrophobic core of the membrane causing ordering of the lipids while maintaining the lateral mobility [113]. Mixing cholesterol in a binary mixture of lipids induces a two-phase liquid system of liquid-ordered, containing saturated lipids and cholesterol, and liquid-disordered domains, containing unsaturated lipids and possibly a low level of cholesterol. Below, we discuss the influence of altering the lipid composition of the membrane on the critical U_m at which electroporation is detected (i.e. $U_{m,crit}$). This influence has been studied both at the molecular level by the use of MD simulations, and at the microscopic level by the use of GUVs.

Both MD simulations and experiments on GUVs demonstrated that $U_{m,crit}$ in fluid phase lipids depends on the structure of the lipid tails as well as the head groups. MD simulations indicated that for lipids with a PC head group, $U_{m,crit}$ increases with the chain length of the lipid tails [70]. In contrast with simulations, Mauroy *et al.*, studied GUVs from different PC lipids experimentally, showing no influence of the hydrophobic chain length on $U_{m,crit}$ [68]. Apart from the influence of the chain length, MD simulations also demonstrated a considerable effect of methyl branches in the lipid tails, as well as the type of linkage between the head group and the carbonyl region [73]. Polak *et al.* observed that $U_{m,crit}$ increases, respectively, in linear-chained DPPC lipids, methyl-branched DPhPC with ester linkages, and DPhPC with ether linkages, all in the fluid phase. Based on their analysis, they proposed that the presence of methyl branches could reduce the mobility of water molecules in the hydrophobic core and hence increase $U_{m,crit}$. Additionally, Polak *et al.* also studied $U_{m,crit}$ of archaeal lipids, which have the same tail structure as DPhPC-ether lipids, whereas the archaeal head groups are formed by large sugar moieties [72]. Compared with DPhPC-ether, archaeal lipids exhibit higher $U_{m,crit}$, associated with stronger interactions

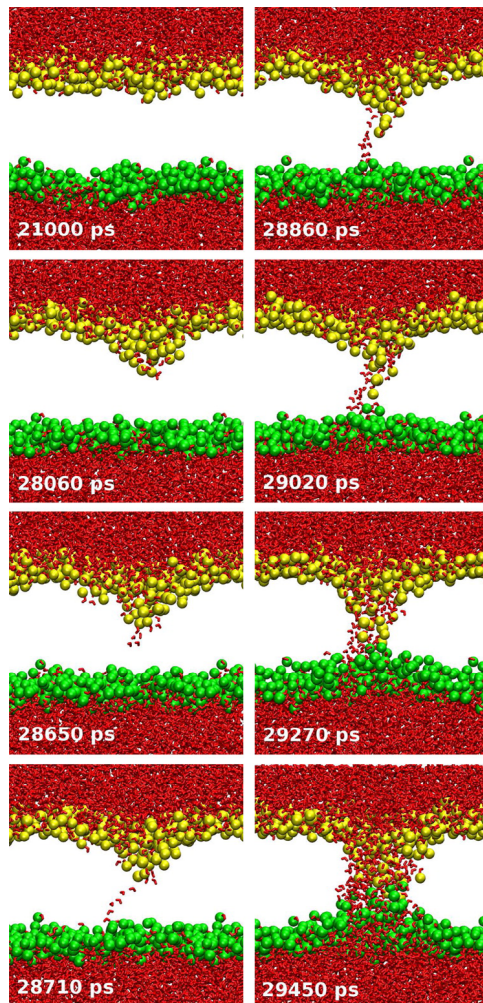


Figure 2.6. Snapshots from MD showing the creation of a pore in an asymmetric bilayer composed of POPE (green) and POPC (yellow) induced by an electric field. Reprinted with permission from [74]. Copyright 2014 American Chemical Society.

between the archaeal head groups. $U_{m,crit}$ was decreased when archaeal lipids were mixed with DPPC. Similarly, Gurtovenko and Lyulina showed higher $U_{m,crit}$ in a POPE lipid bilayer with respect to POPC [74]. Higher $U_{m,crit}$ has been attributed to the primary amines in the POPE head groups capable of intra and intermolecular hydrogen bonding, in contrast to the choline moieties in the POPC head groups. POPE lipids are thus packed more densely than the POPC lipids, which hinders the penetration of water molecules in the bilayer and slows down the reorientation of the lipid head groups into the pore, as shown in Figure 2.6. Mixing these two lipids in an asymmetric bilayer (POPE in one and POPC in the other leaflet) results in $U_{m,crit}$ in between the $U_{m,crit}$ of pure POPC and POPE.

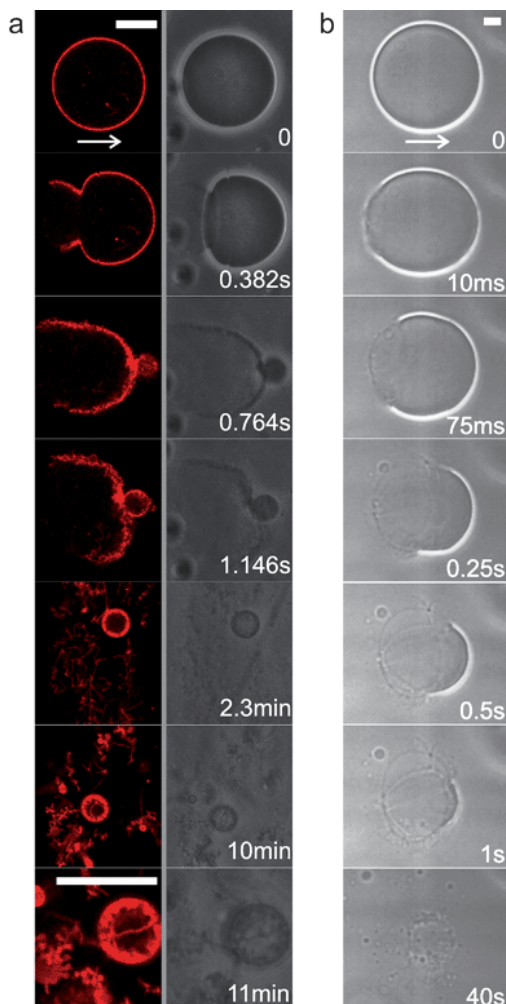


Figure 2.7. (a) Confocal fluorescence microscopy (left) and phase-contrast (right) images of the bursting effect of charged GUVs (1:1 PG:PC) in salt solution. Pulse parameters: 1.4 kV/cm, $t_{\text{pulse}} = 200 \mu\text{s}$. (b) Fast camera image sequence of a bursting GUV, made from lipid extract of human red blood cell membranes. Pulse parameters: 2 kV/cm, $t_{\text{pulse}} = 300 \mu\text{s}$. The scale bar corresponds to 15 μm . Reprinted with permission from [114]. Copyright 2009 The Royal Society of Chemistry.

Besides the physical properties of the lipids, also the effect of the membrane charge was studied. When the negatively charged GUVs consisting of PC and PG lipids (1:1 ratio) were exposed to an electric pulse, a bursting effect was observed, as reported by Riske *et al.*, and shown in Figure 2.7 [114]. Despite the lack of understanding of this bursting effect, they were able to prevent the bursting effect by the addition of EDTA. However, the mechanism of the stabilizing effect of EDTA remains unknown.

Several studies have further shown that $U_{m,\text{crit}}$ in gel phase GUVs is higher than in fluid

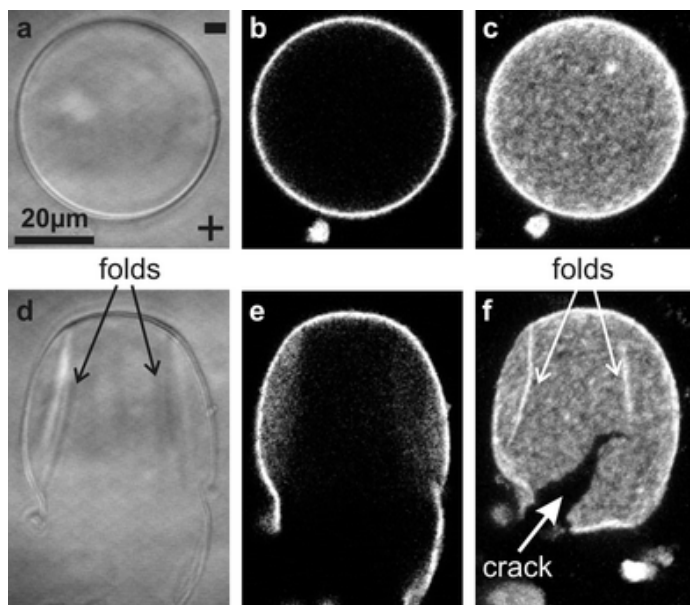


Figure 2.8. Images of a gel phase DPPC GUV with $R = 25 \mu\text{m}$, before and after the pulse ($E = 6 \text{ kV/cm}$, $t_{\text{pulse}} = 300 \mu\text{s}$) in (a,d) DIC, (b,e) confocal, and (c,f) a 3D projection of the upper half of the GUV. Reprinted with permission from [115]. Copyright 2010 The Royal Society of Chemistry.

phase GUVs. Knorr *et al.* used a classical method to determine $U_{m,crit}$ based on the contrast loss of the GUV [115]. $U_{m,crit}$ of gel phase DPPC GUVs was found to be at $9.8 \pm 1.1 \text{ V}$, compared to the 1 V for the liquid phase POPC GUVs, which they attributed to a higher bending rigidity and thickness of the gel phase membrane. The observed pores appeared to be arrested (irreversible) and were often visualized as cracks (see Figure 2.8). Additionally, they reported the deformation dynamics of the gel phase GUVs during the pulse below $U_{m,crit}$. The GUVs show only small deformations below the electroporation threshold, and show a so-called intra-pulse relaxation of their deformation already during the pulse. Moreover, the deformations of these gel phase GUVs were expressed as wrinkling of the membrane instead of the ellipsoidal deformations occurring in fluid phase lipids [115]. A more detailed study by Mauroy *et al.* on $U_{m,crit}$ of different GUVs has elucidated that the phase state, and not the membrane thickness, plays the decisive role in the increased $U_{m,crit}$ of gel phase GUVs with respect to fluid phase GUVs [68]. The increased $U_{m,crit}$ of gel phase GUVs with respect to fluid phase GUVs is also supported by Liu *et al.*, who determined $U_{m,crit}$ by detecting the release of 5(6)-Carboxyfluorescein (5(6)-CF) [116]. Additionally, when mixing fluid and gel phase lipids, Liu *et al.* reported a decrease in the membrane permeability with an increasing percentage of gel phase lipids [116]. Recently, Majhi *et al.* also reported an increase in $U_{m,crit}$ when going from liquid to gel phase lipids, based on results from MD simulations [71]. Additionally, they observed slower pore resealing dynamics for DPPC in the gel phase than in the fluid phase, which shows a correlation with the experimental studies of Knorr *et al.* [115].

As cholesterol is added to the system, the lipids organise in the liquid-ordered phase [117]. The cholesterol organizes itself in the hydrophobic core of the bilayer, where it can condense the lipids and it can alter the mechanical properties of the membrane, such as the thickness, the bending stiffness and the fluidity [118]. However, the addition of cholesterol does not always lead to the same results. Depending on the concentration of the cholesterol and the architecture of the lipid, cholesterol can either decrease or raise the electroporation threshold [60]. Also, mechanical studies on bilayers have shown the non-universal and lipid-specific effect of cholesterol [89, 119, 120]. Recent studies of Mauroy *et al.* have shown that an increasing concentration of cholesterol on POPC leads to a higher $U_{m,crit}$ whereas this increased cholesterol shows no significant influence on $U_{m,crit}$ of Egg PC [68]. Similar results for Egg PC have been shown before by Portet and Dimova [60]. In addition, they reported that increasing cholesterol could decrease $U_{m,crit}$ for DOPC vesicles. Surprisingly, the experimental results on the effect of cholesterol on $U_{m,crit}$ of different lipid bilayers have not been fully supported by MD simulations. Simulations on the effect of cholesterol on $U_{m,crit}$ of POPC show similar results as found experimentally on GUVs [121]. Nevertheless, MD simulations of Fernandez *et al.* on DOPC showed an increase of $U_{m,crit}$ when adding cholesterol [122], which is in disagreement with the experimental results on GUVs [60]. Overall, the influence of cholesterol on $U_{m,crit}$ of a lipid bilayer is non-universal and strongly dependent on the architecture of the lipids. By mixing two different lipids together with cholesterol, coexisting liquid-ordered and liquid-disordered phases can occur in the membrane. Van Uiter *et al.* studied this effect of cholesterol on $U_{m,crit}$ in planar bilayers made from binary lipid mixtures [117]. They observed that the effect of cholesterol on $U_{m,crit}$ is dependent on the cholesterol percentage. At low percentages, $U_{m,crit}$ decreased slightly with respect to $U_{m,crit}$ of the pure binary mixture without cholesterol. However, above a certain threshold percentage, $U_{m,crit}$ increased together with the increase in cholesterol. From the experimental results it is difficult to interpret the molecular mechanisms of this biphasic influence of cholesterol percentage on $U_{m,crit}$. With MD simulations on heterogeneous membranes, Reigada showed that the probability of pore formation is highest in the middle of the liquid disordered phase [123].

2.2.3 Electrofusion

Fusion of biological membranes is a ubiquitous phenomenon in nature, which for example occurs in exocytosis, fertilization, muscle fibre and bone development, tissue regeneration, viral infection, and carcinogenesis [124-126]. Since spontaneous fusion is prevented by large electrostatic and hydration repulsive forces between the membranes, nature utilizes specialized membrane proteins, which facilitate and control the fusion process [127-129]. Artificially, fusion can be induced by virus-based methods [130], by chemical methods such as the addition of polyethylene glycol (PEG) [131], by ultraviolet laser [132], or by electroporation-mediated fusion [42]. Artificial fusion between two cells of different types enables one to create a hybrid cell which expresses the properties of both parental cells. Electric-field induced fusion (i.e. electrofusion) has gained notable attention particularly

for preparing monoclonal-antibody-producing hybridoma cells and cell vaccines for cancer immunotherapy (reviewed in [133]), for cloning organisms such as Dolly [134], and in the treatment of diabetes [135]. Similarly, electrofusion can be obtained between two different GUVs or between GUVs and cells.

Membrane electrofusion can be induced provided that two conditions are met: the membranes need to be in close contact and the membranes need to be destabilized in the contact zone. In electrofusion experiments, GUVs (and/or cells) are most often brought into contact by low-intensity AC electric field, which arranges the GUVs into structures mimicking pearl chains [42]. The pearl-chain formation is a consequence of the GUV movement in the non-homogeneous field because, in a suspension of GUVs, the local field around each GUV is distorted by the presence of other GUVs [44]. Such movement is called dielectrophoresis. If the frequency and the intensity of the AC field are appropriate, the electrostatic interaction forces between individual GUVs are attractive and the GUVs align in a linear fashion with respect to the direction of the applied electric field [42]. Among other methods of establishing contact between the GUVs are the addition of agglutinating agents like PEG [136], or the mechanical manipulation by optical tweezers and microelectrodes [137].

The destabilization of the membranes, as the second condition for electrofusion, is achieved by electroporation of the membranes in the contact zone using strong DC electric pulses. The exact molecular mechanisms of how membrane electroporation facilitates fusion are not completely understood. Sugar *et al.* [138] have proposed a model, which considers that the electric field induces pores spanning across both of the adjacent membranes in the contact zone. Namely, the nucleation of a pore in one of the bilayers could locally increase the electric field and promote nucleation of another pore in the adjacent bilayer. If large numbers of such double-membrane pores are nucleated, these pores could coalesce into larger loop-like and tongue-like cracks. When the electric field is removed, the membrane parts surrounded by loop-like cracks could finally separate to form vesicles. Additionally, unstable membrane undulations induced under an electric field could facilitate local contacts between the adjacent bilayers followed by membrane merging [108-111].

High-speed optical imaging (time resolution of 50 μ s) of the electrofusion process between two GUVs demonstrated that in the absence of salt in the aqueous solutions, several double-membrane pores (fusion necks) typically form in the contact zone during the pulse (Figure 2.9b) [139, 140]. Expansion and subsequent coalescence of these fusion necks lead to the formation of small contact-zone vesicles, which remain trapped in the interior of the fused GUV. On the contrary, no vesicles are observed, if the GUVs are electrofused in the presence of 1 mM NaCl in the external solution, which suggests that a single or very few fusion necks form during the pulse (Figure 2.9c). The expansion of the fusion neck is initially very fast (about 4 cm/s) and after ~ 1 ms slows down as the opening of the neck decreases the membrane tension. The value of the initial velocity implies that



the formation of a single fusion neck can be completed in a few hundred nanoseconds after the onset of the applied electric pulse [139]. Interestingly, when fusion is induced between two GUVs functionalized with synthetic ligand molecules that mimic the action of fusion proteins, the opening of the fusion neck exhibits similar kinetics (Figure 2.9a).

Apart from the influence of ions, electrofusion is also influenced by the physicochemical properties of the membrane. Stoicheva *et al.* have reported that GUVs made from negatively charged lipids are more difficult to fuse than GUVs made of zwitterionic lipids, possibly because of larger repulsive forces between the charged lipids [141]. The inhibiting effect on the electrofusion between GUVs has also been observed in the presence of cadmium ions, presumably because they increase the membrane rigidity, which hinders the opening of the fusion neck [142].

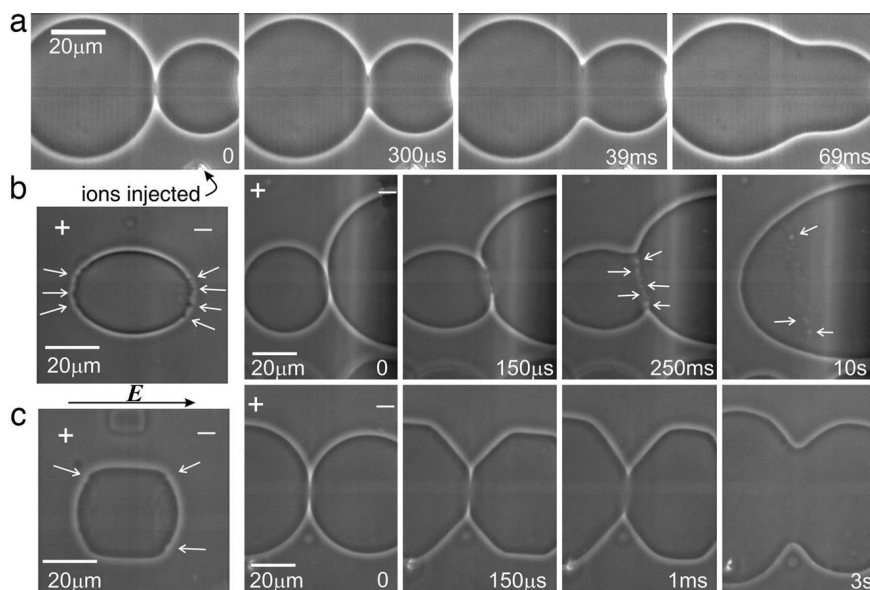


Figure 2.9. Several series of snapshots for the fusion of two vesicles. (a) Fusion of two functionalized GUVs held by micropipettes (only the right pipette tip is visible on the snapshots). A third pipette (bottom right corner) is used to inject a small volume (few tens of nanoliters) of 50 μM solution of EuCl_3 . The first image corresponding to the starting time $t = 0$ represents the last snapshot before the adhesion zone of the vesicles undergoes detectable changes. (b) The behaviour of a single GUV (first image) and a GUV couple (remaining images) when exposed to a 150 μs , 1.8 kV/cm pulse in the absence of salt. (c) Behaviour of a single GUV (first image) and a GUV couple (remaining images) in the presence of 1 mM NaCl in the exterior solution. In this case, the GUV couple was exposed to a 150 μs , 3 kV/cm pulse. The polarity of the electrodes is indicated with a plus (+) or a minus (–) sign. The arrows in the first images indicate porated parts of the membrane, which lead to the leakage of enclosed liquid. For both b and c, the starting time $t = 0$ corresponds to the onset of the pulse. In the last two snapshots of the sequence (b), the fused vesicles contain an array of internal vesicles (bright spots) as indicated by the arrows. Reprinted with permission from [139]. Copyright 2006 National Academy of Sciences.

While high-speed optical microscopy allows imaging of the electrofusion process with a temporal resolution of tens of microseconds, it cannot provide the information on the processes occurring in the microsecond or submicrosecond time-scale after the onset of an electric pulse. Theoretical calculations are useful for revealing more details on U_m and the electroporation kinetics before fusion. Calculations of U_m induced on the membranes of a pair of GUVs in contact have shown that U_m at the contact zone depends on the GUV geometry (spherical or ellipsoidal shape) and the ratio $\chi = \lambda_i/\lambda_e$ between the conductivities of the internal and external aqueous solutions [143, 144]. Let us first consider two spherical GUVs of an equal size. When the membranes become fully charged and U_m reaches the steady state, the absolute value of U_m established at the contact zone is lower than at the poles of the GUV pair facing the electrodes (cf. lines A, B, and C in Figure 2.10a). This suggests that, if the electric pulse is long enough for U_m to reach the steady state, electroporation of the contact zone is accompanied by electroporation of the poles of the GUV pair. However, immediately after the application of an electric pulse, while the membranes are still in the charging phase, U_m strongly depends on χ . If the

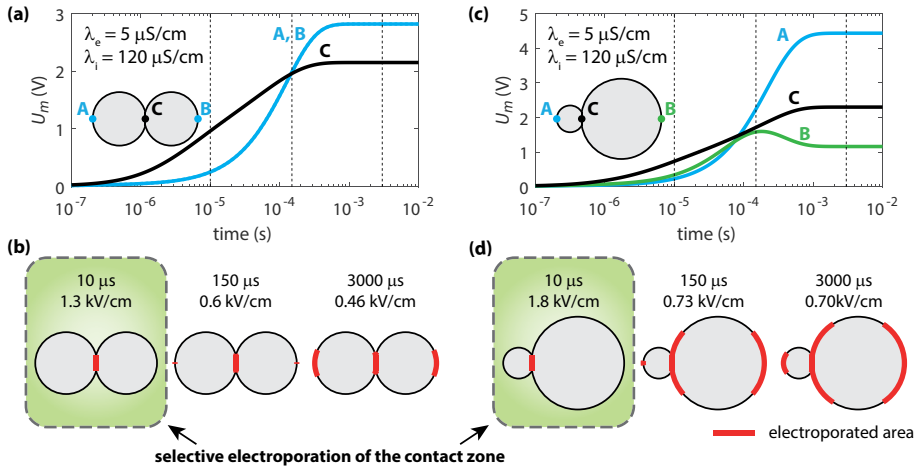


Figure 2.10. Theoretical predictions of selective electroporation of the contact zone in a pair of GUVs. (a) Time course of transmembrane voltage U_m (absolute value) induced in a pair of GUVs with radius of 20 μ m, after the onset of a pulse with amplitude of 1 kV/cm. U_m is shown at three points (A, B, and C) indicated on the sketch inside the graph. Note that U_m at the contact zone (C) surpasses U_m on the poles of the GUV pair (A, B) for times up to ~ 150 μ s. (b) Calculations of the electroporated area for pulses with three different durations (10 μ s, 150 μ s, and 3000 μ s). The amplitude of each pulse was adjusted such that the predicted pore density at the contact zone exceeds 10 pores per μ m². The pore density above 10 pores per μ m² is indicated by thick red lines. (c,d) Same calculations as in (a,b), but for two GUVs with different size (radius 10 μ m and 30 μ m). The results were obtained in the same way as in [145], except that the model parameters were adapted to experimental conditions for GUVs. The membrane capacitance was set to 0.67 μ F/cm², membrane conductivity to 10^{-9} S/m [43], and the radius of the contact zone to 5 μ m. The external and internal conductivities are given in the graphs and correspond to pure sugar solution on the outside and sugar solution containing 1 mM NaCl on the inside of the GUVs.

internal conductivity is lower than the external conductivity ($\chi < 1$), the highest U_m always establishes at the poles of the GUV pair (not shown). On the contrary, if the internal conductivity is higher than the external ($\chi > 1$), the highest U_m transiently establishes at the contact zone (Figure 2.10a). This indicates that if $\chi > 1$ and if the pulse duration is short enough, it is possible to achieve selective electroporation of the contact zone, which is exactly the condition required for inducing vesicle electrofusion. This is corroborated by numerical calculations of the density of pores, which form along the membrane, as predicted by a theoretical model of electroporation (Figure 2.10b) [146]. Similar results can be observed if the GUVs in contact are spherical but of a different size (Figure 2.10c,d) [145], or if the GUVs have ellipsoidal shapes caused by electrodeformation [147]. The theoretical results indicate that selective electroporation of the contact zone can be obtained for a range of pulse durations, but this range depends on the size and shape of the GUVs, and the ratio as well as the absolute values of the internal and external conductivities. Under low-conductivity conditions in which GUVs are typically electrofused, a pulse duration in the order of 10 μ s would be appropriate (Figure 2.10). The theoretical predictions of course have practical significance only if such short pulses are sufficient to induce electrofusion. Indeed, experiments on cells have demonstrated that the application of 20 pulses as short as 50 ns can induce electrofusion [145]. In addition, the formation of the fusion neck could indeed occur within hundreds of nanoseconds [139], as discussed above. Overall, the results suggest that by appropriately tuning the pulse duration, it is possible to induce electrofusion between GUVs while preventing any leakage from the vesicle interior, regardless of the GUV size and shape. This is relevant, for example, when studying biochemical reactions by electrofusing GUVs.

2.2.4 Approaching towards more realistic cell models

GUVs have provided unique opportunities to investigate the fundamental mechanisms of electroporation and electrofusion of cells, and the pulse-induced molecular transmembrane transport. However, several profound phenomena observed on GUVs show discrepancies compared to the observations seen on living cells. (i) Macropores have never been visualised in living cells [90]. (ii) The membrane of a GUV typically reseals and retains its impermeability within hundreds of milliseconds after pulse application [69], whereas cell membrane resealing often takes place for few minutes [148]. (iii) Lipids loss can be observed in GUVs [80], whereas cells can osmotically swell or shrink after pulse application [149, 150]. (iv) A profound difference is also observed in the mechanism of DNA transport across the electroporated membrane. DNA enters the GUV during the pulse via an electrophoretic mechanism [151], whereas in cells the DNA forms a complex with the cell membrane and most likely translocates the membrane via an endocytotic mechanism [152].

As shown above, the GUV is a simplified model of the cell. However, a GUV can be easily modified in its composition, implying the possibilities of extending this model

closer towards a real cell, by increasing the GUV's complexity [153]. Cell membranes contain an asymmetric composition of a variety of lipids and cholesterol, coexisting in different lipid phases. The lipid bilayer serves as a matrix for membrane proteins, which constitute about half of the mass of a typical cell membrane [154, 155]. Furthermore, cell membranes are under an intrinsic tension due to cytoskeleton attachments [156]. The intracellular and extracellular milieus contain high concentrations of salt (about 150 mM), together with dissolved proteins and nucleic acids [154]. The cytoplasm is a crowded, compartmentalised environment with numerous membrane-bound organelles [155]. As the science of implementing these complex systems into the GUV improves, the mechanisms of pulse-induced effects on real cells can be elucidated further. Below we discuss the possibilities for extending the GUV as a model for the real cell.

The first method to increase the complexity of the GUV, as already discussed above, is to adjust the membrane composition and study GUVs containing lipid mixtures [116], cholesterol [60, 68], or GUVs made from natural lipid extract [114]. Additionally, methods of GUV preparation under physiological conditions (≥ 140 mM) have been developed [23, 157-161]. The techniques of GUV preparation have exceeded even further, enabling the preparation of much more complex GUV structures [3]. On the one hand, a complex membrane structure can be controlled by embedding membrane proteins [17, 18, 162, 163] and preparing controlled asymmetric membranes [164, 165]. On the other hand, biomaterials can be encapsulated by the GUVs, such as the actin cytoskeleton [166-169], enzymes [170] and gel-like materials mimicking the cytoplasm [171, 172]. Lira *et al.* have already shown that agarose encapsulated inside a GUV strongly affects both the electrodeformation and the pore dynamics, while maintaining the lateral diffusion of the lipids [173]. Therefore, it can be concluded that the electroporation mechanism is strongly influenced by the inner part of the GUVs. Simultaneously, this system is a great way to immobilize the GUV for a long-time study on, for example, the diffusive response of membrane proteins due to an electrical pulse [174]. From results on living cells, it is also expected that the cytoskeleton plays an important role in both the resealing of the membrane [175, 176] and in the gene electrotransfer through the membrane [152, 177-179]. Adding the cytoskeleton motors (dynein, kinesin and myosin) could possibly also reveal the mechanisms by which the genetic material is transported from the cell membrane to the nucleus [152, 179].

2.3 FUTURE PERSPECTIVE

It is necessary to explore more realistic cell models in the electroporation of vesicles, which account for the complex, heterogeneous structure of the cell. Pioneering studies have been carried out to understand the basic principles of simple GUVs in electric fields, revealing the response of the membrane solely. More complex GUV systems are desired to elucidate more realistic mechanisms of electroporation of a living cell. Systematic investigation of GUVs with incorporated membrane proteins, cytoskeleton network, and dense gel-like



aqueous core would reveal more insights on how these sub-cellular structures influence cell electroporation. While cell electroporation has been widely used in biomedical and technological applications, the exact mechanisms that contribute to the experimentally observed increased permeability of cell membranes are not yet fully elucidated [180]. There are many open questions, including: Why the resealing of cell membranes after electroporation generally takes orders of magnitude more time than in model membrane systems (minutes or even hours in cells versus up to hundreds of milliseconds in GUVs)? Can the increase in the cell membrane permeability after electroporation be attributed solely to lipid pores formed during exposure to electric pulses, or does lipid peroxidation present a contributing/alternative mechanism [181, 182]? How are the membrane proteins affected by the electric field and how do they participate in the increased cell membrane permeability [176, 183]? What are the molecular mechanisms of the transmembrane transport of small drugs and large macromolecules such as DNA and how is the transport influenced by the resting potential of the cell membrane [184, 185]? Why is the translocation of DNA across the cell membrane different in GUVs than in cells and what is the role of cytoskeleton in DNA translocation [151, 177, 186]? Answering these questions through controlled experiments on more complex model GUV systems would improve our understanding of cell electroporation and consequently help optimise current electroporation-based treatments (e.g. gene electrotransfer), as well as develop new ways to exploit cell electroporation for various applications in medicine, food processing, and environmental applications.

Further, studying complex GUVs in electric field could have implications in single-cell diagnostics. By increasing the complexity of a GUV, also the mechanical properties can be correlated to their intra-cellular components via electrodeformation measurements. Single-cell diagnostics have already shown that some diseases alter the mechanical properties [187], e.g. cancer cells have a lower stiffness than healthy cells [188] and even the Young's modulus of different tumour cells can be discriminated [189]. By gaining a comprehensive understanding of how different intra-cellular components contribute to the mechanical properties of living cells through a bottom-up approach, the diagnostics can be further improved. Additionally, it would open up the field to use electric fields as a contactless diagnostic tool to measure the changes in mechanical properties of cells and distinguish important biological factors associated with disease progression (such as pathological, genetic, and epigenetic factors).

To develop successful applications for the characterization and screening on the single GUV or cell level, microfluidic concepts provide unprecedented options. Furthermore, exposing GUVs or cells to an electric field in a microfluidic device offers the benefit of remote and contactless manipulation without the need of sophisticated and expensive micromanipulators. In particular, when the microfluidic design contains the posts to trap individual cells/vesicles together with integrated electrodes in close proximity to the traps, it is possible to simultaneously expose numerous cells/GUVs to the electric field, while analysing each cell/GUV separately. The possibility of trapping individual cells and GUVs

has already shown great potential in inducing controlled pairwise cell-cell electrofusion [190]. Similar concepts can be further designed to induce pairwise electrofusion between cells and GUVs. For example, by embedding selected membrane proteins into the GUV membrane and/or DNA or even micro/nanomachines inside the GUV, cell-GUV electrofusion could provide a platform for a controlled delivery of selected material into living cells and analyse its influence on cell properties and functions [137, 191].

Elucidating electroporation of GUVs in micro/nanofluidic devices would also provide important insights into fundamental electroporation mechanisms. Presence of nanostructures, such as nanochannels, nanopores, or nanowires, strongly influences the local electric field distribution and consequently, the spatial distribution of the pores formed in the GUV/cell membrane [192-194]. Fabricating nanostructures with well-defined geometries and performing electroporation of GUVs with increasing complexity next to such nanostructures would improve the theoretical knowledge of electroporation and further optimize the design of electroporation protocols. For instance, when cells are electroporated next to a nanochannel, DNA can be delivered directly into the cytoplasm [192], whereas in conventional bulk electroporation, the DNA first forms a complex with the cell membrane and then most likely translocates across the membrane via endocytotic mechanisms [152, 195].

In this review, we have focused on the following topics: electrodeformation, electroporation, and electrofusion of vesicles, highlighting both fundamental and application results. These model systems of the cell have provided unique opportunities to bridge the gap between the soft matter physics and the reality of the soft living matter. The fundamental understanding of the mechanical properties of vesicles (GUVs, LUVs, and SUVs) is an essential step towards advancing our fundamental knowledge about the complex behaviour of cell membranes in an electric field. In addition, this fundamental knowledge can inspire us to develop novel liposome approaches for practical biomedical applications.

2.4 REFERENCES

1. Pezzulo, G., and Levin, M., Top-down models in biology: explanation and control of complex living systems above the molecular level. *Journal of The Royal Society Interface*, 2016. 13(124).
2. Ross, J., and Arkin, A.P., Complex Systems: From chemistry to systems biology. *Proceedings of the National Academy of Sciences*, 2009. 106(16): p. 6433-6434.
3. Lagny, T.J., and Bassereau, P., Bioinspired membrane-based systems for a physical approach of cell organization and dynamics: usefulness and limitations. *Interface Focus*, 2015. 5(4).
4. Szathmary, E., Life: In search of the simplest cell. *Nature*, 2005. 433(7025): p. 469-470.



5. Liu, A.P., and Fletcher, D.A., Biology under construction: in vitro reconstitution of cellular function. *Nat Rev Mol Cell Biol*, 2009. 10(9): p. 644-650.
6. Sens, P., L. Johannes, and Bassereau, P., Biophysical approaches to protein-induced membrane deformations in trafficking. *Current Opinion in Cell Biology*, 2008. 20(4): p. 476-482.
7. Schwille, P., *Bottom-Up Synthetic Biology: Engineering in a Tinkerer's World*. Science, 2011. 333(6047): p. 1252-1254.
8. Luisi, P.L., and Stano, P., *The Minimal Cell: The Biophysics of Cell Compartment and the Origin of Cell Functionality*. 2010: Springer Science & Business Media.
9. Menger, F.M., and Keiper, J.S., Chemistry and physics of giant vesicles as biomembrane models. *Current Opinion in Chemical Biology*, 1998. 2(6): p. 726-732.
10. Mozafari, M.R., Nanoliposomes: Preparation and Analysis, in *Liposomes*, V. Weissig, Editor. 2010, Humana Press. p. 29-50.
11. Walde, P., Cosentino, K., Engel, H., and Stano, P., Giant Vesicles: Preparations and Applications. *ChemBioChem*, 2010. 11(7): p. 848-865.
12. Swaay, D.v., and, deMello, A., Microfluidic methods for forming liposomes. 2013. 13(5): p. 752-767.
13. Jesorka, A., and Orwar, O., Liposomes: technologies and analytical applications. *Annu. Rev. Anal. Chem.*, 2008. 1: p. 801-832.
14. Dimova, R., Aranda, S., Bezlyepkina, N., Nikolov, V., Riske, K.A., and Lipowsky, R., A practical guide to giant vesicles. Probing the membrane nanoregime via optical microscopy. *Journal of Physics: Condensed Matter*, 2006. 18(28): p. S1151.
15. Menger, F.M., and Angelova, M.I., Giant Vesicles: Imitating the Cytological Processes of Cell Membranes. *Accounts of Chemical Research*, 1998. 31(12): p. 789-797.
16. Bucher, P., Fischer, A., Luisi, P.L., Oberholzer, T., and Walde, P., Giant Vesicles as Biochemical Compartments: The Use of Microinjection Techniques. *Langmuir*, 1998. 14(10): p. 2712-2721.
17. Girard, P., Pécrciaux, J., Lenoir, G., Falson, P., Rigaud, J.-L., and Bassereau. P., A New Method for the Reconstitution of Membrane Proteins into Giant Unilamellar Vesicles. *Biophysical Journal*, 2004. 87(1): p. 419-429.
18. Davidson, M., Karlsson, M., Sinclair, J., Sott, K., and Orwar, O., Nanotube-Vesicle Networks with Functionalized Membranes and Interiors. *Journal of the American Chemical Society*, 2003. 125(2): p. 374-378.

19. Rigaud, J.-L., B. Pitard, and D. Levy, Reconstitution of membrane proteins into liposomes: application to energy-transducing membrane proteins. *Biochimica et Biophysica Acta (BBA) - Bioenergetics*, 1995. 1231(3): p. 223-246.
20. Sachse, R., Dondapati, S.K., Fenz, S.F., Schmidt, T., and Kubick, S., Membrane protein synthesis in cell-free systems: From bio-mimetic systems to bio-membranes. *FEBS Letters*, 2014. 588(17): p. 2774-2781.
21. Soga, H., Fujii, S., Yomo, T., Kato, Y., Watanabe, H., and Matsuura, T., In Vitro Membrane Protein Synthesis Inside Cell-Sized Vesicles Reveals the Dependence of Membrane Protein Integration on Vesicle Volume. *ACS Synthetic Biology*, 2014. 3(6): p. 372-379.
22. Helfrich, M.R., Mangeney-Slavin, L.K., Long, M.S., Djoko, K.Y., and Keating, C.D., Aqueous Phase Separation in Giant Vesicles. *Journal of the American Chemical Society*, 2002. 124(45): p. 13374-13375.
23. Yamashita, Y., Oka, M., Tanaka, T., and Yamazaki, M., A new method for the preparation of giant liposomes in high salt concentrations and growth of protein microcrystals in them. *Biochimica et Biophysica Acta (BBA) - Biomembranes*, 2002. 1561(2): p. 129-134.
24. Fischer, A., A. Franco, and T. Oberholzer, Giant vesicles as microreactors for enzymatic mRNA synthesis. *ChemBioChem*, 2002. 3(5): p. 409-417.
25. Michel, M., Winterhalter, M., Darbois, L., Hemmerle, J., Voegel, J.C., Schaaf, P., and Ball, V., Giant Liposome Microreactors for Controlled Production of Calcium Phosphate Crystals. *Langmuir*, 2004. 20(15): p. 6127-6133.
26. Noireaux, V., and Libchaber, A., A vesicle bioreactor as a step toward an artificial cell assembly. *Proceedings of the National Academy of Sciences of the United States of America*, 2004. 101(51): p. 17669-17674.
27. Chiu, D.T., Wilson, C.F., Ryttsén, F., Strömberg, A., Farre, C., Karlsson, A., Nordholm, S., Gaggar, A., Modi, B.P., Moscho, A., Garza-López, R.A., Orwar, O., and Zare, R.N., Chemical Transformations in Individual Ultrasmall Biomimetic Containers. *Science*, 1999. 283(5409): p. 1892-1895.
28. Long, M.S., Jones, C.D., Helfrich, M.R., Mangeney-Slavin, L.K., and Keating, C.D., Dynamic microcompartmentation in synthetic cells. *Proceedings of the National Academy of Sciences*, 2005. 102(17): p. 5920-5925.
29. Allen, T.M., and Cullis, P.R., Liposomal drug delivery systems: From concept to clinical applications. *Advanced Drug Delivery Reviews*, 2013. 65(1): p. 36-48.
30. Sercombe, L., Veerati, T., Moheimani, F., Wu, S.Y., Sood, A.K., and Hua, S., Advances and Challenges of Liposome Assisted Drug Delivery. *Frontiers in Pharmacology*, 2015.



6(286).

31. Yarmush, M.L., Golberg, A., Serša, G., Kotnik, T., and Miklavčič, D., Electroporation-based technologies for medicine: Principles, applications, and challenges. *Annual Review of Biomedical Engineering*, 2014. 16(1): p. 295-320.

32. Mahnič-Kalamiza, S., E. Vorobiev, and D. Miklavčič, Electroporation in food processing and biorefinery. *The Journal of Membrane Biology*, 2014. 247(12): p. 1279-1304.

33. Kotnik, T., Frey, W., Sack, M., Haberl Meglič, S., Peterka, M., and Miklavčič, D., Electroporation-based applications in biotechnology. *Trends in Biotechnology*, 2015. 33(8): p. 480-488.

34. Dimitrov, D.S., Electroporation and electrofusion of membranes. *Handbook of Biological Physics*, 1995. 1(C): p. 851-901.

35. Strömberg, A., Karlsson, A., Ryttsén, F., Davidson, M., Chiu, D.T., and Orwar, O., Microfluidic Device for Combinatorial Fusion of Liposomes and Cells. *Analytical Chemistry*, 2001. 73(1): p. 126-130.

36. Dimova, R., Bezlyepkina, N., Jordo, M.D., Knorr, R.L., Riske, K.A., Staykova, M., and Vlahovska, P.M., Yamamoto, T., Yang, P., and Lipowsky, R., Vesicles in electric fields: Some novel aspects of membrane behavior. *Soft Matter*, 2009. 5(17): p. 3201-3212.

37. Dimova, R., Riske, K.A., Aranda, S., Bezlyepkina, N., Knorr, R.L., and Lipowsky, R., Giant vesicles in electric fields. *Soft Matter*, 2007. 3(7): p. 817-827.

38. Portet, T., Mauroy, C., Démary, V., Houles, T., Escoffre J.-M., Dean, D.S., and Rols, M.-P., Destabilizing Giant Vesicles with Electric Fields: An Overview of Current Applications. *The Journal of Membrane Biology*, 2012. 245(9): p. 555-564.

39. Vlahovska, P.M., Voltage-morphology coupling in biomimetic membranes: dynamics of giant vesicles in applied electric fields. *Soft Matter*, 2015. 11(37): p. 7232-6.

40. Pauly, H., and Schwan, H.P., Impedance of a suspension of ball-shaped particles with a shell; a model for the dielectric behavior of cell suspensions and protein solutions. *Zeitschrift fur Naturforschung. Teil B, Chemie, Biochemie, Biophysik, Biologie und verwandte Gebiete*, 1959. 14B(2): p. 125-131.

41. Schwan, H.P., and Sher, L.D., Alternative-Current Field-Induced Forces and Their Biological Implications. *Journal of The Electrochemical Society*, 1969. 116(1): p. 22C-26C.

42. Zimmermann, U., Electric field-mediated fusion and related electrical phenomena. *Biochimica et Biophysica Acta (BBA) - Reviews on Biomembranes*, 1982. 694(3): p. 227-277.

43. Chan, K.L., Gascoyne, P.R.C., Becker, F.F., and Pethig, R., Electrorotation of liposomes:

verification of dielectric multi-shell model for cells. *Biochimica Et Biophysica Acta-Lipids and Lipid Metabolism*, 1997. 1349(2): p. 182-196.

44. Voldman, J., Electrical forces for microscale cell manipulation. *Annual Review of Biomedical Engineering*, 2006. 8: p. 425-454.

45. Kotnik, T., and Pucihar, G., Induced transmembrane voltage – theory, modeling, and experiments, in *Advanced Electroporation Techniques in Biology and Medicine*, A.G. Pakhomov, D. Miklavčič, and M.S. Markov, Editors. 2010, CRC Press, Boca Raton. p. 51-70.

46. Salipante, P.F., Knorr, R.L., Dimova, R., and Vlahovska, P.M., Electrodeformation method for measuring the capacitance of bilayer membranes. *Soft Matter*, 2012. 8(14): p. 3810-3816.

47. Riske, K.A., and Dimova, R., Electro-Deformation and Poration of Giant Vesicles Viewed with High Temporal Resolution. *Biophysical Journal*, 2005. 88(2): p. 1143-1155.

48. Kotnik, T., and Miklavcic, D., Analytical description of transmembrane voltage induced by electric fields on spheroidal cells. *Biophysical Journal*, 2000. 79(2): p. 670-679.

49. Hibino, M., Shigemori, M., Itoh, H., Nagayama, K., and Kinosita, K., Membrane conductance of an electroporated cell analyzed by submicrosecond imaging of transmembrane potential. *Biophysical Journal*, 1991. 59(1): p. 209-220.

50. Kotnik, T., and Miklavčič, D., Second-order model of membrane electric field induced by alternating external electric fields. *IEEE Transactions on Biomedical Engineering*, 2000. 47(8): p. 1074-1081.

51. Taupin, C., Dvolaitzky, M., and Sauterey, C., Osmotic pressure-induced pores in phospholipid vesicles. *Biochemistry*, 1975. 14(21): p. 4771-4775.

52. Abidor, I.G., Arakelyan, V.B., Chernomordik, L.V., Chizmadzhev, Y.A., Pastushenko, V.F., and Tarasevich, M.R., Electric breakdown of bilayer lipid membranes I. The main experimental facts and their qualitative discussion. *Bioelectrochemistry and Bioenergetics*, 1979. 6(1): p. 37-52.

53. Powell, K.T., and Weaver, J.C., Transient aqueous pores in bilayer membranes: A statistical theory. *Bioelectrochemistry and Bioenergetics*, 1986. 15(2): p. 211-227.

54. Needham, D., and Hochmuth, R.M., Electro-mechanical permeabilization of lipid vesicles. Role of membrane tension and compressibility. *Biophysical Journal*, 1989. 55(5): p. 1001-1009.

55. Lewis, T.J., A model for bilayer membrane electroporation based on resultant electromechanical stress. *IEEE Transactions on Dielectrics and Electrical Insulation*, 2003. 10(5): p. 769-777.



56. Vasilkoski, Z., Esser, A.T., Gowrishankar, T.R., and Weaver, J.C., Membrane electroporation: The absolute rate equation and nanosecond time scale pore creation. *Physical Review E*, 2006. 74(2): p. 021904.
57. Glaser, R.W., Leikin, S.L., Chernomordik, L.V., Pastushenko, V.F., and Sokirko, A.I., Reversible electrical breakdown of lipid bilayers: formation and evolution of pores. *Biochimica et Biophysica Acta (BBA) - Biomembranes*, 1988. 940(2): p. 275-287.
58. Neu, J.C., Smith, K.C., and Krassowska, W., Electrical energy required to form large conducting pores. *Bioelectrochemistry*, 2003. 60(1-2): p. 107-114.
59. Brochard-Wyart, F., de Gennes, P.G., and Sandre, O., Transient pores in stretched vesicles: role of leak-out. *Physica A: Statistical Mechanics and its Applications*, 2000. 278(1-2): p. 32-51.
60. Portet, T., and Dimova, R., A New Method for Measuring Edge Tensions and Stability of Lipid Bilayers: Effect of Membrane Composition. *Biophysical Journal*, 2010. 99(10): p. 3264-3273.
61. Gurtovenko, A.A., Anwar, J., and Vattulainen, I., Defect-mediated trafficking across cell membranes: Insights from in silico modeling. *Chemical Reviews*, 2010. 110(10): p. 6077-6103.
62. Levine, Z.A., and Vernier, P.T., Life cycle of an electropore: Field-dependent and field-independent steps in pore creation and annihilation. *The Journal of Membrane Biology*, 2010. 236(1): p. 27-36.
63. Kandasamy, S.K., and Larson, R.G., Cation and anion transport through hydrophilic pores in lipid bilayers. *The Journal of Chemical Physics*, 2006. 125(7): p. 074901.
64. Böckmann, R.A., Leikin, S.L., Chernomordik, L.V., Pastushenko, V.F., and Sokirko, A.I., Kinetics, Statistics, and Energetics of Lipid Membrane Electroporation Studied by Molecular Dynamics Simulations. *Biophysical Journal*, 2008. 95(4): p. 1837-1850.
65. Rems, L., Lipid Pores: Molecular and Continuum Models, in *Handbook of Electroporation*, D. Miklavcic, Editor. 2016, Springer International Publishing. p. 1-21.
66. Tokman, M., Lee, J.H., Levine, Z.A., Ho, M.-C., Colvin, M.E., and Vernier, P.T., Electric Field-Driven Water Dipoles: Nanoscale Architecture of Electroporation. *PLOS ONE*, 2013. 8(4): p. e61111.
67. Neu, J.C., and Krassowska, W., Asymptotic model of electroporation. *Physical Review E*, 1999. 59(3): p. 3471-3482.
68. Mauroy, C., Rico-Lattes, I., Teissie, J., and Rols, M.-P., Electric Destabilization of Supramolecular Lipid Vesicles Subjected to Fast Electric Pulses. *Langmuir*, 2015. 31(44): p. 12215-12222.

69. Tekle, E., Astumian, R.D., Friauf, W.A., and Chock, P.B., Asymmetric pore distribution and loss of membrane lipid in electroporated DOPC vesicles. *Biophysical Journal*, 2001. 81(2): p. 960-968.
70. Ziegler, M.J., and Vernier, P.T., Interface Water Dynamics and Porating Electric Fields for Phospholipid Bilayers. *The Journal of Physical Chemistry B*, 2008. 112(43): p. 13588-13596.
71. Majhi, A.K., Kanchi, S., Venkataraman, V., Ayappa, K.G., and Maiti, P.K., Estimation of activation energy for electroporation and pore growth rate in liquid crystalline and gel phases of lipid bilayers using molecular dynamics simulations. *Soft Matter*, 2015. 11(44): p. 8632-8640.
72. Polak, A., Tarek, M., Tomšič, M., Valant, J., Ulrih, N.P., Jamnik, A., Kramer, P., and Miklavčič, D., Electroporation of archaeal lipid membranes using MD simulations. *Bioelectrochemistry*, 2014. 100(0): p. 18-26.
73. Polak, A., Bonhenry, D., Dehez, F., Kramar, P., Miklavčič, D., and Tarek, M., On the Electroporation Thresholds of Lipid Bilayers: Molecular Dynamics Simulation Investigations. *The Journal of Membrane Biology*, 2013. 246(11): p. 843-850.
74. Gurtovenko, A.A., and Lyulina, A.S., Electroporation of Asymmetric Phospholipid Membranes. *The Journal of Physical Chemistry B*, 2014. 118(33): p. 9909-9918.
75. Bennett, W.F.D., Sapay, N., and Tieleman, D.P., Atomistic Simulations of Pore Formation and Closure in Lipid Bilayers. *Biophysical Journal*, 2014. 106(1): p. 210-219.
76. Hu, Y., Sinha, S.K., and Patel, S., Investigating hydrophilic pores in model lipid bilayers using molecular simulations: Correlating bilayer properties with pore-formation thermodynamics. *Langmuir*, 2015. 31(24): p. 6615-6631.
77. Riske, K.A., and Dimova, R., Electric Pulses Induce Cylindrical Deformations on Giant Vesicles in Salt Solutions. *Biophysical Journal*, 2006. 91(5): p. 1778-1786.
78. Sadik, M.M., Li, J., Shan, J.W., Shreiber, D.I., and Lin, H., Vesicle deformation and poration under strong dc electric fields. *Physical Review E*, 2011. 83(6): p. 066316.
79. Salipante, P.F., and Vlahovska, P.M., Vesicle deformation in DC electric pulses. *Soft Matter*, 2014. 10(19): p. 3386-3393.
80. Portet, T., Camps i Febrer, F., Escoffre, J.-M., Favard, C., Rols, M.-P., and Dean, D.S., Visualization of Membrane Loss during the Shrinkage of Giant Vesicles under Electropulsation. *Biophysical Journal*, 2009. 96(10): p. 4109-4121.
81. Helfrich, W., and Servuss, R.M., Undulations, steric interaction and cohesion of fluid membranes. *Il Nuovo Cimento D*, 1984. 3(1): p. 137-151.



82. Evans, E., and Rawicz, W., Entropy-driven tension and bending elasticity in condensed-fluid membranes. *Physical Review Letters*, 1990. 64(17): p. 2094-2097.
83. Hyuga, H., Kinosita Jr, K., and Wakabayashi, N., Steady-state deformation of a vesicle in alternating electric fields. *Bioelectrochemistry and Bioenergetics*, 1993. 32(1): p. 15-25.
84. Vlahovska, P.M., Gracià, R.S., Aranda-Espinoza, S., and Dimova, R., Electrohydrodynamic Model of Vesicle Deformation in Alternating Electric Fields. *Biophysical Journal*, 2009. 96(12): p. 4789-4803.
85. Peterlin, P., Frequency-dependent electrodeformation of giant phospholipid vesicles in AC electric field. *Journal of Biological Physics*, 2010. 36(4): p. 339-354.
86. Nganguia, H., and Young, Y.N., Equilibrium electrodeformation of a spheroidal vesicle in an ac electric field. *Physical Review E*, 2013. 88(5): p. 052718.
87. Kummrow, M., and Helfrich, W., Deformation of giant lipid vesicles by electric fields. *Phys Rev A*, 1991. 44(12): p. 8356-8360.
88. Aranda, S., Riske, K.A., Lipowsky, R., and Dimova, R., Morphological Transitions of Vesicles Induced by Alternating Electric Fields. *Biophysical Journal*, 2008. 95(2): p. L19-L21.
89. Gracia, R.S., Bezlyepkina, N., Knorr, R.L., Lipowsky, R., and Dimova, R., Effect of cholesterol on the rigidity of saturated and unsaturated membranes: fluctuation and electrodeformation analysis of giant vesicles. *Soft Matter*, 2010. 6(7): p. 1472-1482.
90. Kinosita, K., Hibino, M., Itoh, H., Shigemori, M., Hirano, K.i., Kirino, Y., and Hayakawa, T., Events of membrane electroporation visualized on a time scale from microsecond to seconds, in *Guide to Electroporation and Electrofusion*, D.C.C.M.C.A.S.E. Sowers, Editor. 1992, Academic Press: San Diego. p. 29-46.
91. Hyuga, H., Kinosita, K., and Wakabayashi, N., Deformation of vesicles under the influence of strong electric fields. *Japanese Journal of Applied Physics*, 1991. 30(5R): p. 1141.
92. Hyuga, H., Kinosita, K., and Wakabayashi, N., Deformation of vesicles under the influence of strong electric fields II. *Japanese Journal of Applied Physics*, 1991. 30(6R): p. 1333.
93. Schwalbe, J.T., Vlahovska, P.M., and Miksis, M.J., Vesicle electrohydrodynamics. *Physical Review E*, 2011. 83(4): p. 046309.
94. McConnell, L.C., Vlahovska, P.M., and Miksis, M.J., Vesicle dynamics in uniform electric fields: squaring and breathing. *Soft Matter*, 2015. 11(24): p. 4840-4846.
95. McConnell, L.C., Miksis, M.J., and Vlahovska, P.M., Continuum modeling of the

electric-field-induced tension in deforming lipid vesicles. *The Journal of Chemical Physics*, 2015. 143(24): p. 243132.

96. Kolahdouz, E.M., and Salac, D., Dynamics of three-dimensional vesicles in dc electric fields. *Physical Review E*, 2015. 92(1): p. 012302.

97. Kolahdouz, E., and Salac, D., Electrohydrodynamics of Three-Dimensional Vesicles: A Numerical Approach. *SIAM Journal on Scientific Computing*, 2015. 37(3): p. B473-B494.

98. Yu, M., Lira, R.B., Riske, K.A., Dimova, R., and Lin, H., Ellipsoidal Relaxation of Deformed Vesicles. *Physical Review Letters*, 2015. 115(12): p. 128303.

99. Evans, E., Heinrich, V., Ludwig, F., and Rawicz, W., Dynamic Tension Spectroscopy and Strength of Biomembranes. *Biophysical Journal*, 2003. 85(4): p. 2342-2350.

100. Sandre, O., Moreaux, L., and Brochard-Wyart, F., Dynamics of transient pores in stretched vesicles. *Proceedings of the National Academy of Sciences*, 1999. 96(19): p. 10591-10596.

101. Olbrich, K., Rawicz, W., Needham, D., and Evans, E., Water Permeability and Mechanical Strength of Polyunsaturated Lipid Bilayers. *Biophysical Journal*, 2000. 79(1): p. 321-327.

102. Leontiadou, H., Mark, A.E., and Marrink, S.J., Molecular Dynamics Simulations of Hydrophilic Pores in Lipid Bilayers. *Biophysical Journal*, 2004. 86(4): p. 2156-2164.

103. Levadny, V., Tsuboi, T.-a., Belaya, M., and Yamazaki, M., Rate Constant of Tension-Induced Pore Formation in Lipid Membranes. *Langmuir*, 2013. 29(12): p. 3848-3852.

104. McConnell, L.C., Miksis, M.J., and Vlahovska, P.M., Vesicle electrohydrodynamics in DC electric fields. *IMA Journal of Applied Mathematics*, 2013. 78(4): p. 797-817.

105. Mauroy, C., Portet, T., Winterhalder, M., Bellard, E., Blache, M.C., Teissie, J., Zumbusch, A., and Rols, M.-P., Giant lipid vesicles under electric field pulses assessed by non invasive imaging. *Bioelectrochemistry*, 2012. 87: p. 253-259.

106. Antonova, K., Vitkova, V., and Meyer, C., Membrane tubulation from giant lipid vesicles in alternating electric fields. *Physical Review E*, 2016. 93(1).

107. Sens, P., and Isambert, H., Undulation instability of lipid membranes under an electric field. *Physical review letters*, 2002. 88(12): p. 128102.

108. Lacoste, D., Menon, G.I., Bazant, M.Z., and Joanny, J.F., Electrostatic and electrokinetic contributions to the elastic moduli of a driven membrane. *The European Physical Journal E*, 2009. 28(3): p. 243-264.

109. Ziebert, F., Bazant, M.Z., and Lacoste, D., Effective zero-thickness model for



a conductive membrane driven by an electric field. *Physical Review E*, 2010. 81(3): p. 031912.

110. Schwalbe, J.T., Vlahovska, P.M., and Miksis, M.J., Lipid membrane instability driven by capacitive charging. *Physics of Fluids*, 2011. 23(4): p. 041701.

111. Seiwert, J., Miksis, M.J., and Vlahovska, P.M., Stability of biomimetic membranes in DC electric fields. *Journal of Fluid Mechanics*, 2012. 706: p. 58-70.

112. Nagle, J.F., and Tristram-Nagle, S., Structure of lipid bilayers. *Biochimica et Biophysica Acta (BBA) - Reviews on Biomembranes*, 2000. 1469(3): p. 159-195.

113. Veatch, S.L., and Keller, S.L., Organization in Lipid Membranes Containing Cholesterol. *Physical Review Letters*, 2002. 89(26): p. 268101.

114. Riske, K.A., Knorr, R.L., and Dimova, R., Bursting of charged multicomponent vesicles subjected to electric pulses. *Soft Matter*, 2009. 5(10): p. 1983-1986.

115. Knorr, R.L., Staykova, M., Gracia, R.S., and Dimova, R., Wrinkling and electroporation of giant vesicles in the gel phase. *Soft Matter*, 2010. 6(9): p. 1990-1996.

116. Liu, Z.-W., Zeng, X.-A., Sun, D.-W., and Han, Z., Effects of pulsed electric fields on the permeabilization of calcein-filled soybean lecithin vesicles. *Journal of Food Engineering*, 2014. 131: p. 26-32.

117. van Uitert, I., Le Gac, S., and van den Berg, A., Determination of the electroporation onset of bilayer lipid membranes as a novel approach to establish ternary phase diagrams: example of the l- α -PC/SM/cholesterol system. *Soft Matter*, 2010. 6(18): p. 4420-4429.

118. Hung, W.-C., Lee, M.-T., Chen, F.-Y., and Huang, H.W., The Condensing Effect of Cholesterol in Lipid Bilayers. *Biophysical Journal*, 2007. 92(11): p. 3960-3967.

119. Pan, J., Mills, T.T., Tristram-Nagle, S., and Nagle, J.F., Cholesterol perturbs lipid bilayers nonuniversally. *Physical review letters*, 2008. 100(19): p. 198103.

120. Pan, J., Tristram-Nagle, S., Kučerka, N., and Nagle, J.F., Temperature Dependence of Structure, Bending Rigidity, and Bilayer Interactions of Dioleoylphosphatidylcholine Bilayers. *Biophysical Journal*. 94(1): p. 117-124.

121. Casciola, M., Bonhenry, D., Liberti, M., Apollonio, F., and Tarek, M., A molecular dynamic study of cholesterol rich lipid membranes: comparison of electroporation protocols. *Bioelectrochemistry*, 2014. 100: p. 11-17.

122. Fernández, M.L., Marshall, G., Sagués, F., and Reigada, R., Structural and Kinetic Molecular Dynamics Study of Electroporation in Cholesterol-Containing Bilayers. *The Journal of Physical Chemistry B*, 2010. 114(20): p. 6855-6865.

123. Reigada, R., Electroporation of heterogeneous lipid membranes. *Biochimica et Biophysica Acta (BBA) - Biomembranes*, 2014. 1838(3): p. 814-821.
124. Ogle, B.M., Cascalho, M., and Platt, J.L., Biological implications of cell fusion. *Nature Reviews Molecular Cell Biology*, 2005. 6(7): p. 567-575.
125. Chen, E.H., Grote, E., Mohler, W., and Vignery, A., Cell-cell fusion. *FEBS Letters*, 2007. 581(11): p. 2181-2193.
126. Noubissi, F.K., and Ogle, B.M., Cancer Cell Fusion: Mechanisms Slowly Unravel. *International Journal of Molecular Sciences*, 2016. 17(9).
127. Jahn, R., and Südhof, T.C., Membrane Fusion and Exocytosis. *Annual Review of Biochemistry*, 1999. 68(1): p. 863-911.
128. Martens, S. and H.T. McMahon, Mechanisms of membrane fusion: disparate players and common principles. *Nature Reviews Molecular Cell Biology*, 2008. 9(7): p. 543-556.
129. Chernomordik, L.V., and Kozlov, M.M., Mechanics of membrane fusion. *Nature Structural & Molecular Biology*, 2008. 15(7): p. 675-683.
130. Köhler, G., and Milstein, C., Continuous cultures of fused cells secreting antibody of predefined specificity. *Nature*, 1975. 256(5517): p. 495-497.
131. Golestani, R., Pourfathollah, A.A., and Moazzeni S.M., Cephalin as an Efficient Fusogen in Hybridoma Technology: Can It Replace Poly Ethylene Glycol? *Hybridoma*, 2007. 26(5): p. 296-301.
132. Kulin, S., Kishore, R., Helmerson, K., and Locascio, L., Optical Manipulation and Fusion of Liposomes as Microreactors. *Langmuir*, 2003. 19(20): p. 8206-8210.
133. Kanduđer, M., and Ušaj, M., Cell electrofusion: past and future perspectives for antibody production and cancer cell vaccines. *Expert Opinion on Drug Delivery*, 2014. 11(12): p. 1885-1898.
134. Campbell, K.H.S., McWhir, J., Ritchie, W.A., and Wilmut, I., Sheep cloned by nuclear transfer from a cultured cell line. *Nature*, 1996. 380(6569): p. 64-66.
135. Yanai, G., Hayashi, T., Zhi, Q., Yang, K.-C., Shirouzu, Y., Shimabukuro, T., Hiura, A., Inoue, K., and Sumi, S., Electrofusion of Mesenchymal Stem Cells and Islet Cells for Diabetes Therapy: A Rat Model. *PLoS ONE*, 2013. 8(5): p. e64499.
136. Teissié, J., Rols, M.P., and Blangero, C., Electrofusion of Mammalian Cells and Giant Unilamellar Vesicles, in *Electroporation and Electrofusion in Cell Biology*, E. Neumann, A.E. Sowers, and C.A. Jordan, Editors. 1989, Springer US: Boston, MA. p. 203-214.
137. Strömberg, A., Ryttsén, F., Chiu, D.T., Davidson, M., Eriksson, P.S., Wilson, C.F.,



Orwar, O., and Zare, R.N., Manipulating the genetic identity and biochemical surface properties of individual cells with electric-field-induced fusion. *Proceedings of the National Academy of Sciences*, 2000. 97(1): p. 7-11.

138. Sugar, I.P., Förster, W., and Neumann, E., Model of cell electrofusion: Membrane electroporation, pore coalescence and percolation. *Biophysical Chemistry*, 1987. 26(2-3): p. 321-335.

139. Haluska, C.K., Riske, K.A., Marchi-Artzner, V., Lehn, J.-M., Lipowsky, R., and Dimova, R., Time scales of membrane fusion revealed by direct imaging of vesicle fusion with high temporal resolution. *Proceedings of the National Academy of Sciences*, 2006. 103(43): p. 15841-15846.

140. Riske, K.A., Bezlyepkina, N., Lipowsky, R., and Dimova, R., Electrofusion of model lipid membranes viewed with high-temporal resolution. *Biophysical Reviews and Letters*, 2006. 01(04): p. 387-400.

141. Stoicheva, N.G., and Hui, S.W., Electrofusion of cell-size liposomes. *Biochimica et Biophysica Acta (BBA) - Biomembranes*, 1994. 1195(1): p. 31-38.

142. Yang, P., Lipowsky, R., and Dimova, R., Nanoparticle Formation in Giant Vesicles: Synthesis in Biomimetic Compartments. *Small*, 2009. 5(18): p. 2033-2037.

143. Washizu, M., and Tschannat, B., Cell membrane voltage during electrical cell fusion calculated by re-expansion method. *Journal of Electrostatics*, 2007. 65(9): p. 555-561.

144. Tschannat, B., Numerical analysis of DC-field-induced transmembrane potential of spheroidal cells in axisymmetric orientations. *IEEE Transactions on Dielectrics and Electrical Insulation*, 2013. 20(5): p. 1567-1576.

145. Rems, L., Ušaj, M., Kandušer, M., Reberšek, M., Miklavčič, D., and Pucihar, G., Cell electrofusion using nanosecond electric pulses. *Scientific Reports*, 2013. 3: p. 3382.

146. DeBruin, K.A., and Krassowska, W., Modeling Electroporation in a Single Cell. I. Effects of Field Strength and Rest Potential. *Biophysical Journal*, 1999. 77(3): p. 1213-1224.

147. Liu, L., Mao, Z., Zhang, J., Liu, N., and Liu, Q.H., The Influence of Vesicle Shape and Medium Conductivity on Possible Electrofusion under a Pulsed Electric Field. *PLOS ONE*, 2016. 11(7): p. e0158739.

148. Rols, M.P. and Teissié, J., Electroporation of mammalian cells. Quantitative analysis of the phenomenon. *Biophysical Journal*, 1990. 58(5): p. 1089-1098.

149. Kinoshita, K., and Tsong, T.Y., Formation and resealing of pores of controlled sizes in human erythrocyte membrane. *Nature*, 1977. 268(5619): p. 438-441.

150. Nesin, O.M., Pakhomova, O.N., Xiao, S., Pakhomov, A.G., Manipulation of cell

volume and membrane pore comparison following single cell permeabilization with 60- and 600-ns electric pulses. *Biochimica et Biophysica Acta (BBA) - Biomembranes*, 2011. 1808(3): p. 792-801.

151. Portet, T., Favard, C., Teissie, J., Dean, D.S., and Rols, M.-P., Insights into the mechanisms of electromediated gene delivery and application to the loading of giant vesicles with negatively charged macromolecules. *Soft Matter*, 2011. 7(8): p. 3872-3881.

152. Rosazza, C., Meglic, S.H., Zumbusch, A., and Rols, M.-P., Miklavcic D., Gene Electrotransfer: A Mechanistic Perspective. *Current Gene Therapy*, 2016. 16(2): p. 98-129.

153. Fenz, S.F., and Sengupta, K., Giant vesicles as cell models. *Integrative Biology*, 2012. 4(9): p. 982-995.

154. Alberts, B., Johnson, A., Lewis, J., Raff, M., Roberts, K., and Walter, P., *Molecular biology of the cell*. 5th ed. 2008, New York: Garland Science, Taylor & Francis Group.

155. Lodish, H., Berk, A., Zipursky, S.L., Matsudaira, P., Baltimore, D., and Darnell, J., *Molecular cell biology*. 4th ed. Vol. 29. 2001, New York: W. H. Freeman and Company.

156. Diz-Muñoz, A., Fletcher, D.A., and Weiner, O.D., Use the force: membrane tension as an organizer of cell shape and motility. *Trends in Cell Biology*, 2013. 23(2): p. 47-53.

157. Estes, D.J., and Mayer, M., Giant liposomes in physiological buffer using electroformation in a flow chamber. *Biochimica et Biophysica Acta (BBA) - Biomembranes*, 2005. 1712(2): p. 152-160.

158. Pavlič, J.I., Genova, J., Popkirov, G., Kralj-Iglič, V., Iglič, A., and Mitov, M.D., Mechanoformation of neutral giant phospholipid vesicles in high ionic strength solution. *Chemistry and Physics of Lipids*, 2011. 164(8): p. 727-731.

159. Montes, L.R., Alonso, A., Goñi, F.M., and Bagatolli, L.A., Giant Unilamellar Vesicles Electroformed from Native Membranes and Organic Lipid Mixtures under Physiological Conditions. *Biophysical Journal*, 2007. 93(10): p. 3548-3554.

160. Akashi, K., Miyata, H., Itoh, H., and Kinoshita, K., Preparation of giant liposomes in physiological conditions and their characterization under an optical microscope. *Biophysical Journal*, 1996. 71(6): p. 3242-3250.

161. Pott, T., Bouvrais, H., and Méléard, P., Giant unilamellar vesicle formation under physiologically relevant conditions. *Chemistry and Physics of Lipids*, 2008. 154(2): p. 115-119.

162. Deshpande, S., Caspi, Y., Meijering, A.E.C., and Dekker, C., Octanol-assisted liposome assembly on chip. *Nature Communications*, 2016. 7: p. 10447.

163. Varnier, A., Kermarrec, F., Blesneac, I., Moreau, C., Liguori, L., Lenormand, J.L., and



Picollet-D'hahan, N., A Simple Method for the Reconstitution of Membrane Proteins into Giant Unilamellar Vesicles. *Journal of Membrane Biology*, 2010. 233(1): p. 85-92.

164. Pautot, S., Frisken, B.J., and Weitz, D.A., Engineering asymmetric vesicles. *Proceedings of the National Academy of Sciences*, 2003. 100(19): p. 10718-10721.

165. Chiantia, S., Schwille, P., Klymchenko, A.S., and London, E., Asymmetric GUVs Prepared by M β CD-Mediated Lipid Exchange: An FCS Study. *Biophysical Journal*, 2011. 100(1): p. L1-L3.

166. Limozin, L., and Sackmann, E., Polymorphism of Cross-Linked Actin Networks in Giant Vesicles. *Physical Review Letters*, 2002. 89(16): p. 168103.

167. Pontani, L.-L., van der Gucht, J., Salbreux, G., Heuvingh, J., Joanny, J.-F., and Sykes, C., Reconstitution of an Actin Cortex Inside a Liposome. *Biophysical Journal*, 2009. 96(1): p. 192-198.

168. Limozin, L., Roth, A., and Sackmann, E., Microviscoelastic Moduli of Biomimetic Cell Envelopes. *Physical Review Letters*, 2005. 95(17): p. 178101.

169. Häckl, W., Bärmann, M., and Sackmann, E., Shape Changes of Self-Assembled Actin Bilayer Composite Membranes. *Physical Review Letters*, 1998. 80(8): p. 1786-1789.

170. Walde, P., Enzymatic reactions in liposomes. *Current Opinion in Colloid & Interface Science*, 1996. 1(5): p. 638-644.

171. Viallat, A., Dalous, J., and Abkarian, M., Giant Lipid Vesicles Filled with a Gel: Shape Instability Induced by Osmotic Shrinkage. *Biophysical Journal*, 2004. 86(4): p. 2179-2187.

172. Osinkina, L., Markström, M., Orwar, O., and Jesorka, A., A Method for Heat-Stimulated Compression of Poly(N-isopropyl acrylamide) Hydrogels Inside Single Giant Unilamellar Vesicles. *Langmuir*, 2010. 26(1): p. 1-4.

173. Lira, Rafael B., Dimova, R., and Riske, K.A., Giant Unilamellar Vesicles Formed by Hybrid Films of Agarose and Lipids Display Altered Mechanical Properties. *Biophysical Journal*, 2014. 107(7): p. 1609-1619.

174. Lira, R.B., Steinkühler, J., Knorr, R.L., Dimova, R., and Riske, K.A., Posing for a picture: vesicle immobilization in agarose gel. *Scientific Reports*, 2016. 6: p. 25254.

175. Rols, M.-P., and Teissié, J., Experimental evidence for the involvement of the cytoskeleton in mammalian cell electroporation. *Biochimica et Biophysica Acta (BBA) - Biomembranes*, 1992. 1111(1): p. 45-50.

176. Teissie, J., and Rols, M.-P., Manipulation of Cell Cytoskeleton Affects the Lifetime of Cell Membrane Electroporation. *Annals of the New York Academy of Sciences*, 1994. 720(1): p. 98-110.

177. Rosazza, C., Escoffre, J.-M., Zumbusch, A., and Rols, M.-P., The actin cytoskeleton has an active role in the electrotransfer of plasmid DNA in mammalian cells. *Molecular therapy : the journal of the American Society of Gene Therapy*, 2011. 19(5): p. 913-921.
178. Rosazza, C., Buntz, A., Rieß, T., Wöll, D., Zumbusch, A., and Rols, M.-P., Intracellular Tracking of Single-plasmid DNA Particles After Delivery by Electroporation. *Molecular Therapy*, 2013. 21(12): p. 2217-2226.
179. Vaughan, E.E., and Dean, D.A., Intracellular Trafficking of Plasmids during Transfection Is Mediated by Microtubules. *Molecular Therapy*, 2006. 13(2): p. 422-428.
180. Rems, L., and Miklavčič, D., Tutorial: Electroporation of cells in complex materials and tissue. *Journal of Applied Physics*, 2016. 119(20): p. 201101.
181. Maccarrone, M., Bladergroen, M.R., Rosato, N., and Agro, A.F., Role of lipid peroxidation in electroporation-induced cell permeability. *Biochemical and Biophysical Research Communications*, 1995. 209(2): p. 417-425.
182. Leguèbe, M., Silve, A., Mir, L.M., and Poinard, C., Conducting and permeable states of cell membrane submitted to high voltage pulses: Mathematical and numerical studies validated by the experiments. *Journal of Theoretical Biology*, 2014. 360: p. 83-94.
183. Teissié, J., and Tsong, T.Y., Evidence of voltage-induced channel opening in Na/K ATPase of human erythrocyte membrane. *The Journal of Membrane Biology*, 1980. 55(2): p. 133-140.
184. Gabriel, B., and Teissié, J., Direct observation in the millisecond time range of fluorescent molecule asymmetrical interaction with the electroporeabilized cell membrane. *Biophysical Journal*, 1997. 73(5): p. 2630-2637.
185. Tekle, E., Oubrahim, H., Dzekunov, S.M., Kolb, J.F., Schoenbach, K.H., and Chock, P.B., Selective Field Effects on Intracellular Vacuoles and Vesicle Membranes with Nanosecond Electric Pulses. *Biophysical Journal*, 2005. 89(1): p. 274-284.
186. Golzio, M., Teissié, J., and Rols, M.-P., Direct visualization at the single-cell level of electrically mediated gene delivery. *Proceedings of the National Academy of Sciences*, 2002. 99(3): p. 1292-1297.
187. Nematbakhsh, Y., and Lim, C.T., Cell biomechanics and its applications in human disease diagnosis. *Acta Mechanica Sinica*, 2015. 31(2): p. 268-273.
188. Dahl, J.B., Lin, J.-M.G., Muller, S.J., and Kumar, S., Microfluidic strategies for understanding the mechanics of cells and cell-mimetic systems. *Annual review of chemical and biomolecular engineering*, 2015. 6: p. 293-317.
189. Chivukula, V.K., Krog, B.L., Nauseef, J.T., Henry, M.D., and Vigmostad, S.C., Alterations in cancer cell mechanical properties after fluid shear stress exposure: A



micropipette aspiration study. *Cell Health and Cytoskeleton*, 2015. 7: p. 25-35.

190. Hu, N., Yang, J., Joo, S.W., Banerjee, A.N., and Qian, S., Cell electrofusion in microfluidic devices: A review. *Sensors and Actuators B: Chemical*, 2013. 178: p. 63-85.

191. Saito, A.C., Ogura, T., Fujiwara, K., Murata, S., and Nomura, Si.-M., Introducing Micrometer-Sized Artificial Objects into Live Cells: A Method for Cell–Giant Unilamellar Vesicle Electrofusion. *PLoS ONE*, 2014. 9(9): p. e106853.

192. Boukany, P.E., Morss, A., Liao, W.C., Henslee, B., Jung, H., Zhang, X., Yu, B., Wang, X., Wu, Y., Li, L., Gao, K., Hu, X., Zhao, X., Hemminger, O., Lu, W., Lafyatis G.P., and Lee, L.J., Nanochannel electroporation delivers precise amounts of biomolecules into living cells. *Nature Nanotechnology*, 2011. 6(11): p. 747-754.

193. Liu, C., Xie, X., Zhao, W., Liu, N., Maraccini, P.A., Sassoubre, L.M., Boehm, A.B., and Cui, Y., Conducting nanosponge electroporation for affordable and high-efficiency disinfection of bacteria and viruses in water. *Nano Letters*, 2013. 13(9): p. 4288-4293.

194. Xie, X., Xu, A.M., Leal-Ortiz, S., Cao, Y., Garner, C.C., and Melosh, N.A., Nanostraw–Electroporation System for Highly Efficient Intracellular Delivery and Transfection. *ACS Nano*, 2013. 7(5): p. 4351-4358.

195. Rosazza, C., Deschout, H., Buntz, A., Braeckmans, K., Rols, M.-P., and Zumbusch, A., Endocytosis and Endosomal Trafficking of DNA After Gene Electrotransfer In Vitro. *Molecular Therapy. Nucleic Acids*, 2016. 5(2): p. e286.



3

The role of gel-phase domains in electroporation of vesicles

Transient permeabilisation of the cell membrane is a critical step to introduce drugs or DNA into living cells, yet challenging for both biological research and therapeutic applications. To achieve this, electroporation (or electropermeabilisation) has become a widely used method due to its simplicity to deliver almost any biomolecule to any cell type. Although, this method demonstrates promise in the field of drug/gene delivery, the underlying physical mechanisms of the response of the heterogeneous cell membrane to strong electric pulses is still unknown. In this study, we have investigated the role of gel-phase lipids in the electroporation of binary giant unilamellar vesicles (GUVs), composed from DPPC (gel-phase) and DPhPC (fluid-phase) lipids (molar ratio 8:2 and 2:8). We have observed that the exposure to electric pulses leads to expel of fluid-phase lipids and concomitant decrease in GUV size, whereas the gel-phase domains become buckled. Based on experiments on pure fluid-phase and gel-phase GUVs, we have found that fluid-phase lipids can be expelled by electrical forces and the highly viscous gel-phase lipids cannot. Moreover, our analyses suggest that pore formation occurs primarily in fluid-phase domains and that the pore size is similar in all GUVs containing fluid-phase lipids, irrespective of the gel-phase percentage.



3.1 INTRODUCTION

Every living cell is enclosed by the cell membrane, which provides a protective barrier and governs the cell permeability to the extracellular environment. The cell membrane consists mainly of lipids, that self-assemble based on hydrophobic and hydrophilic interactions. In order to permeabilise the lipid bilayer for drug delivery, these interactions must be overcome. By applying a direct current (DC) pulse the membrane can be permeabilised transiently, due to the transmembrane voltage that builds up on the membrane during the pulse [1]. Transient pores are formed when the transmembrane voltage exceeds a critical value, typically between 0.2 and 1 V [2, 3]. This approach, referred to as electroporation or electropermeabilisation, is used for both living cells and lipid vesicles to enhance the transmembrane transport of drugs, genetic material, and other (bio)molecules in the field of medicine, food processing, and environmental applications [4-7]. Despite the wide use of this technique, the cascade of mechanisms that are operative during the electric pulse is still not fully understood.

To reveal the electroporation mechanisms, electroporation is studied using simplified model systems such as giant unilamellar vesicles (GUVs) [8-10], planar lipid bilayers [11] and different theoretical methods including molecular dynamics (MD) simulations [12-14]. GUVs provide the benefit of isolating the function of the membrane from the complex intracellular components involved in a cell, while resembling the size of the cell and curvature of the cell membrane. Additionally, the composition of the membrane is controllable, for example the GUVs can be prepared from lipids with different phase-states. Depending on their molecular structure, the lipids can be either in the fluid-phase state, containing high mobility and low order, or in the gel-phase state, which contain a low mobility and are tightly packed [15]. Experiments on GUVs have revealed that electroporation depends strongly on the phase-state of the lipids. It has been shown that electroporation of fluid-phase GUVs is associated with formation of micrometre-sized pores (macropores) and lipid loss [16-18]. Compared to fluid-phase GUVs, Knorr *et al.* [19] have shown that gel-phase GUVs electroporate at considerably higher critical transmembrane voltage of about 10 V, which they have attributed to a higher bending rigidity and thickness of the gel-phase membrane. Furthermore, they have observed irreversible cracks in electroporated gel-phase GUVs, in contrast to the reversible macropores in fluid-phase GUVs. Mauroy *et al.* [20] have demonstrated that the phase state plays the decisive role in the increased critical transmembrane voltage of gel-phase GUVs with respect to fluid-phase GUVs, and not the carbon chain length, due to the large cohesion of the gel-phase lipids. This increased critical transmembrane voltage for electroporation of gel-phase lipids is supported by MD simulations [12].

Most of the studies discussed above have been performed on membranes consisting of single-phase lipids. However, the cell membrane is composed of various types of lipids which can coexist in different phases, organised in domains [21, 22]. Studies investigating electroporation of multiphase membranes are scarce. Liu *et al.* [23] have performed

experiments on large unilamellar vesicles (diameter $\sim 1 \mu\text{m}$) with fluid-phase and gel-phase lipids and have demonstrated that the critical transmembrane voltage increases by increasing the amount of gel-phase lipids in the vesicles. Reigada [13] and Van Uitert [11] have studied heterogeneous lipid membranes consisting of fluid-ordered and fluid-disordered phases by MD simulations and resistance measurements on lipid bilayers, respectively. By mixing cholesterol into a binary lipid bilayer, the two lipids can organize into fluid-ordered (containing the majority of the cholesterol) and fluid-disordered domains [24]. Both studies [11, 13] have shown that the fluid-ordered domains increase the critical transmembrane voltage. In addition, the MD simulations have given the molecular insight that the pores are preferentially formed in the fluid-disordered domains [13]. These results are supported by Sengel and Wallace [25] with experiments on droplet-interface bilayers.

In this study we focus on the role of gel-phase domains in electroporation, by mixing gel-phase and fluid-phase lipids in GUVs with a radius between 10 and 30 μm . DPhPC (1,2-diphytanoyl-*sn*-glycero-3-phosphocholine) and DPPC (1,2-dipalmitoyl-*sn*-glycero-3-phosphocholine) are used as the fluid-phase and the gel-phase lipids at room temperature, respectively. These two lipids contain the same head group and differ in their carbon chain: DPhPC has methyl groups (fluid-phase) and DPPC has a linear chain (gel-phase). GUVs with four different lipid compositions have been prepared, going from pure fluid to pure gel-phase GUVs with two intermediate binary phase mixtures. All GUVs have been exposed to multiple electric pulses of increasing electric field strength, and their responses have been imaged using bright-field microscopy.

3.2 RESULTS

The responses of the GUVs have been studied before, during and after the electric field application. The interior of the GUVs consists of 200 mM sucrose, whereas the exterior consists of 200 mM glucose to create a difference in both the density and the refractive index. Consequently, the density difference has enabled the GUVs to sediment to the bottom of the glass slide, and the mismatch in refractive index has enabled the imaging of the GUVs. The setup is shown in Figure 3.1A-C. Unless noted otherwise, each GUV has been exposed to multiple 500 μs -long rectangular electric pulses with increasing amplitude, so each subsequent pulse results in a higher electric field strength in between the electrodes. The time interval between the pulses is approximately 5 minutes, to minimize the effect of the former pulse. Therefore, these pulses are referred to as individual 500 μs pulses. Nevertheless, it should be noted that the effects of consecutive pulses could be accumulating during the experiment. The response of the GUV is captured by imaging at approximately 10 to 25 frames per second. The contour of the GUV before, during and after the electric pulse application has been tracked, extracting the area and the perimeter of the GUV with a pixel count, as depicted in Figure 3.1D. These properties have been



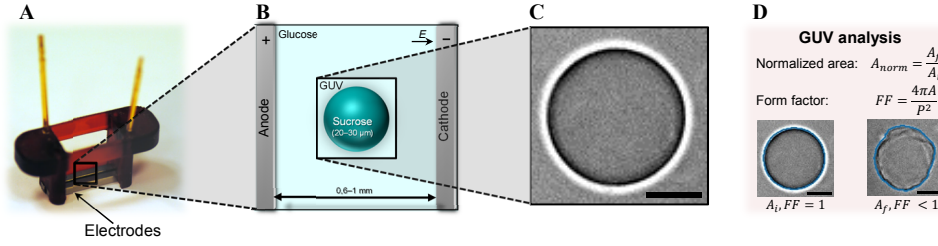


Figure 3.1. The experimental setup and analysis for the electroporation of the GUVs. (A) A picture of the electroporation setup. (B) A schematic of the sucrose-filled GUV in the glucose environment, in between the electrodes with a distance ranging between 0.6 and 1 mm. The drawing is not to scale. (C) Bright field image of a sucrose-filled GUV in a glucose environment. (D) The analysis of the GUVs: the contour is tracked, after which the area, A , and the perimeter, P , are determined. From these, the normalised area and the form factor are calculated. The form factor is 1 for a circular GUV, and less than one for a non-circular GUV. The scale bar is 10 μm .

used to determine the shrinkage of the GUV induced by each applied pulse, by calculating the normalised area $A_{norm} = A_f / A_i$ before (A_i) and after (A_f) the application of the pulse. In addition, the shape of the GUV has been determined based on the form factor (FF):

$$FF = \frac{4\pi A}{P^2} \quad (3.1)$$

where A represents the area of the GUV, and P the perimeter. The form factor is 1 for a circular shape, and less than 1 when the shape is non-circular. Apart from the area loss and form factor, loss of contrast after the electric pulses has been used to indicate electroporation of the membrane.

3.2.1 Fluid-phase and gel-phase GUVs

In order to understand the role of lipid phase-state on the response of GUVs to electric pulses, we have first studied the response of pure fluid-phase and pure gel-phase GUVs. In agreement with previous observations on fluid-phase egg phosphatidylcholine and DOPC (1,2-dioleoyl-*sn*-glycero-3-phosphocholine) GUVs [16, 26], the fluid-phase DPhPC GUVs have exhibited shrinkage as a consequence of the electric pulses (Figure 3.2A). The GUVs have decreased in size up to $\sim 30\%$ when reaching the highest electric field tested ($\sim 400 \text{ V/mm}$). The gel-phase DPPC GUVs also exhibited a slight shrinkage at higher electric field ($\geq 600 \text{ V/mm}$), confirming that the gel-phase GUVs are more stable than fluid-phase GUVs, as observed previously [19, 23]. However, a difference in the shrinkage mechanism for the fluid-phase and the gel-phase GUVs can be seen from the change in the form factor. The form factor of the fluid-phase GUVs remains around one, indicating that the GUVs remain spherical (Figure 3.2B). This is due to the simultaneous loss of the surface area and the interior volume. To visualise the shrinkage mechanism of the fluid-

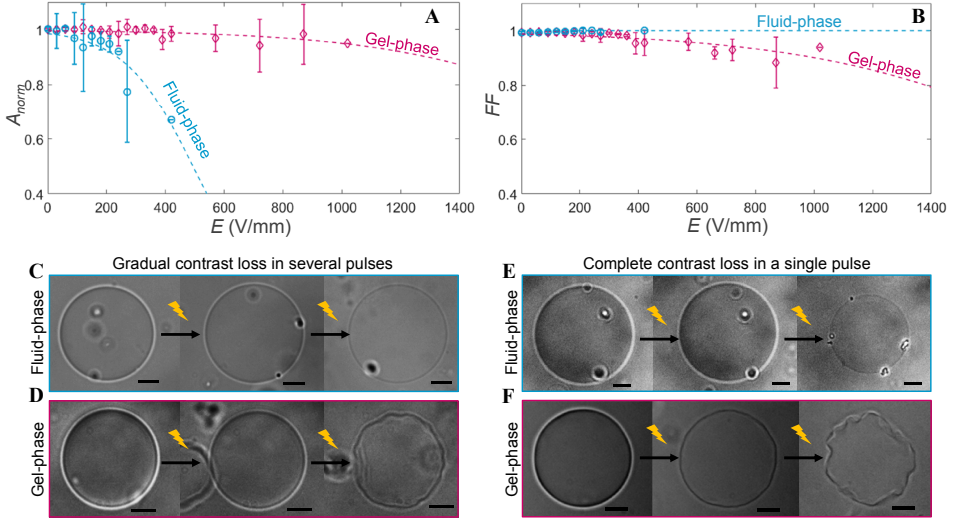


Figure 3.2. The response of the fluid-phase (in blue) and gel-phase (in pink) GUVs to the electric field. (A) and (B) show, respectively, the averaged normalised area and form factor plotted versus the electric field of the pulse. The fluid-phase data is averaged over 11 different GUVs, with radii between 11 and 28 μ m. The gel-phase data is averaged over 12 different GUVs, with radii between 10 and 22 μ m. The error bars in the plots represent the standard deviation. The dotted lines represent the least-squares fit with a sigmoid curve. (C) and (D) are snapshots of the fluid-phase and gel-phase GUVs showing the gradual contrast loss. (C) from left to right: before pulse application, more than 100 seconds after the tenth pulse at 52 V/mm and after the twenty-fourth pulse at 372 V/mm. (D) from left to right: before pulse application, more than 100 seconds after the fourth pulse at 74 V/mm and after the twentieth pulse at 100 V/mm. (E) and (F) are snapshots of the fluid-phase and gel-phase GUVs showing the complete contrast after one of the pulses. (E) from left to right: before pulse application, more than 100 seconds after the second pulse at 89 V/mm and after the third pulse at 97 V/mm. (F) from left to right: before pulse application, more than 100 seconds after the third pulse at 595 V/mm and after the fourth pulse at 744 V/mm. The scale bar in all images is 10 μ m.

phase GUVs, confocal measurements have been conducted. In addition to exposing the GUVs to multiple 500 μ s pulses, the GUVs were also exposed to multiple 5 ms pulses of 0.33 Hz to compare the shrinkage mechanism to the former study of Portet *et al.* [16]. It is found that the DPhPC fluid-phase GUVs exhibit shrinkage due to either small vesicles formation and/or tubulation (Figure 3.3), as observed previously [16] although less pronounced. The vesicle formation is the dominant phenomenon. After expulsion, both the small vesicles and tubules remain attached to the GUV. No reabsorption of neither the vesicles nor the tubules is observed on the time scale of the experiments (2 min). This shrinkage mechanism is in this work referred to as lipid loss or lipid expel, despite the fact that the formed daughter vesicles and tubules remain attached to the mother GUV. On the contrary to the fluid-phase GUVs, gel-phase GUVs have shown no apparent loss of lipids (Figure S3.2.1). Moreover, the form factor of the gel-phase GUVs has dropped below one, showing that these GUVs have lost their spherical shape. On the application of pulses with

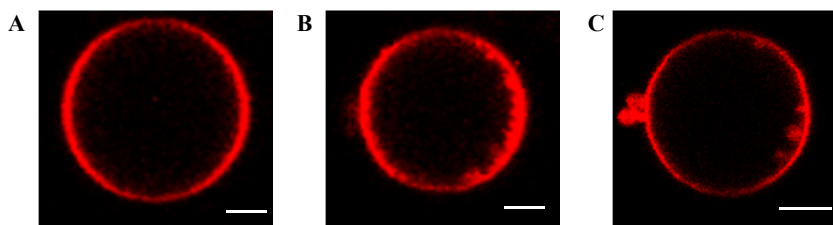


Figure 3.3. (A) A DPhPC GUV before pulse application and two representative examples of the shrinkage mechanism of the DPhPC GUVs (B) showing tubule formation (C) and vesicle formation. In these examples, the GUVs have been exposed to 2-8 pulses, duration 5 ms, amplitude ~ 90 V/mm. The majority of the GUVs have exhibited vesicle formation. The scale bar in all images is $5\ \mu\text{m}$, the cathode is on the left side and the anode on the right side of the GUVs.

an electric field strength ≥ 400 V/mm, the gel-phase GUVs have deformed permanently into asymmetrical shapes, here referred to as buckling. This buckling behaviour of the gel-phase GUVs demonstrates that these GUVs have lost part of their interior volume while conserving their lipids.

To assess the permeability of the GUVs after pulse application, the contrast loss of the GUVs is studied. Two different contrast loss regimes can be observed. About 50% of the tested fluid-phase GUVs have expressed a gradual contrast loss throughout the whole experiment, where consecutive pulses of increasing amplitude have been applied (Figure 3.2C). At higher fields (≥ 100 V/mm), the cumulative contrast loss is accompanied by shrinkage of the GUVs. These GUVs have shrank rapidly (within ~ 100 ms during/after the pulse) by up to few percent. These results are similar as reported before on other fluid-phase GUVs like DOPC [26]. Similarly, gradual contrast loss is observed of about 50% of the gel-phase GUVs at lower electric fields, followed by gradual buckling at higher fields (Figure 3.2D). However, in about 50% of the tested fluid-phase GUVs, we have also observed a complete drop in contrast after one individual pulse with a sufficient amplitude. The complete contrast loss after this pulse takes place for tens of seconds, and is in half of these cases accompanied by more profound (up to $\sim 30\%$) decrease in the GUV size (Figure 3.2E and Movie S3.1.1). Therefore, it appears that an electric pulse can lead to both a short term and a long term permeability of the fluid-phase GUVs. The gel-phase GUVs also display long term ($\sim 50\%$ of the gel-phase GUVs) permeability of the membrane after an individual pulse, similarly to the fluid-phase GUVs. In gel-phase GUVs, the contrast loss is accompanied by buckling of the GUV instead of lipid loss (Figure 3.2F and Movie S3.1.2).

In addition to the duration of the membrane permeability after the pulse application, the movies also provide the dynamics of the GUVs immediately after the pulse and during the relaxation. Similarly to earlier studies, elliptical deformations and macropores have been observed in fluid-phase GUVs. For the gel-phase GUVs first reversible electroporation is observed and at higher electric fields folds and cracks have been seen immediately after the pulse application, similar as reported by Knorr *et al.* [19]. However, our gel-phase

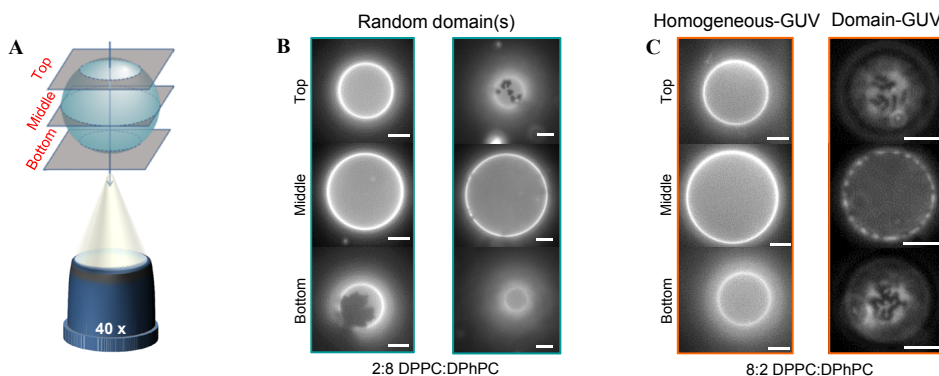


Figure 3.4. The fluorescence images of the binary GUVs before electroporation. (A) A schematic drawing of the three different focal planes (bottom, middle and top planes) of the GUVs, not drawn to scale. (B) Two examples of the 2:8 DPPC:DPhPC GUVs, showing different gel-phase domains. The GUVs are visualised by use of fluorescence microscopy, where the dark parts represent the gel-phase domains, and the bright parts the fluid-phase or mixed domains. (C) The two different categories of the 8:2 DPPC:DPhPC GUVs. Left: a homogeneous-GUV, showing no visible domains. Right: a domain-GUV, showing a uniform distribution of dark gel-phase domains on the surface of the GUV. The scale bar is 10 μm .

GUVs slowly relax back into a buckled shape after approximately 170 seconds (Movie S3.1.3). These slow responses have not been reported in former studies, possibly because of the duration of their experiments.

3.2.2 Binary GUVs containing fluid-phase and gel-phase lipids

To assess the influence of gel-phase domains in a fluid-phase membrane on the GUV response we have prepared binary GUVs with two different molar ratios of DPPC:DPhPC, (i) 2:8 and (ii) 8:2. The mixing behaviour of the lipids in the GUV membrane has been determined by imaging GUVs in three different focal planes using fluorescence microscopy, as schematically depicted in Figure 3.4A. The GUVs are fluorescently labelled with 1,2-dioleoyl-*sn*-glycero-3-phosphoethanolamine-N-(lissamine rhodamine B sulfonyl) (ammonium salt) (DOPE-RhoB) lipids, which preferentially organise in the fluid-phase domains; therefore the fluid-phase and gel-phase domains can be visualised as bright and dark patches, respectively, in the fluorescence images. The phase-separation of the two phases is governed by the cooling rate of the GUVs from a temperature above the transition temperature of the gel-phase lipids, where the GUVs are in a one-phase state, to a temperature below the transition temperature, where two coexisting phases can be formed [27, 28]. During the cooling of the GUVs the gel-phase domains nucleate and grow as a function of cooling rate, resulting in phase-separation [29]. The size, shape and number of domains are dependent on the ratio of the two lipids [27], the cooling down rate [29] and the membrane tension [30]. Based on the mixing behaviour, these binary GUVs have been divided into three different categories: (1) the 2:8 DPPC:DPhPC GUVs,

which exhibit few gel-phase domains distributed stochastically in the size and number (Figure 3.4B), (2) the 8:2 DPPC:DPhPC GUVs where no gel-phase domains were visible, which suggests that the lipids are homogeneously mixed, referred to as homogeneous-GUVs (Figure 3.4C), and (3) the 8:2 DPPC:DPhPC GUVs showing phase separation by displaying gel-phase domains, called domain-GUVs (Figure 3.4C). These three categories provide the opportunity to study the influence of the distribution of the gel-phase domains on the GUV response to the electric field. It must be noted that the domains are stable throughout the whole experiment, also after pulse application.

The 2:8 DPPC:DPhPC GUVs enable to capture the role of small, stochastically distributed gel-phase domains on the response of the GUVs to an electric pulse. Similarly to the pure fluid-phase GUVs, these 2:8 DPPC:DPhPC GUVs show a shrinkage in size at an electric field above ~ 150 V/mm (Figure 3.5A). At higher fields (~ 400 V/mm) the form factor drops, indicating the 20% of DPPC lipids cause a small buckling effect (Figure 3.5B). The fluorescence images after pulse application reveal that the buckled patches are located at the gel-phase domains (Figure 3.5C and D). Nevertheless, no correlation is found between the gel-phase domains distribution and either the area loss or the form factor, due to the stochastic distribution of the gel-phase domains. The captured movies also reveal some of the dynamics of the 2:8 DPPC:DPhPC GUVs. Pores have been observed for seven

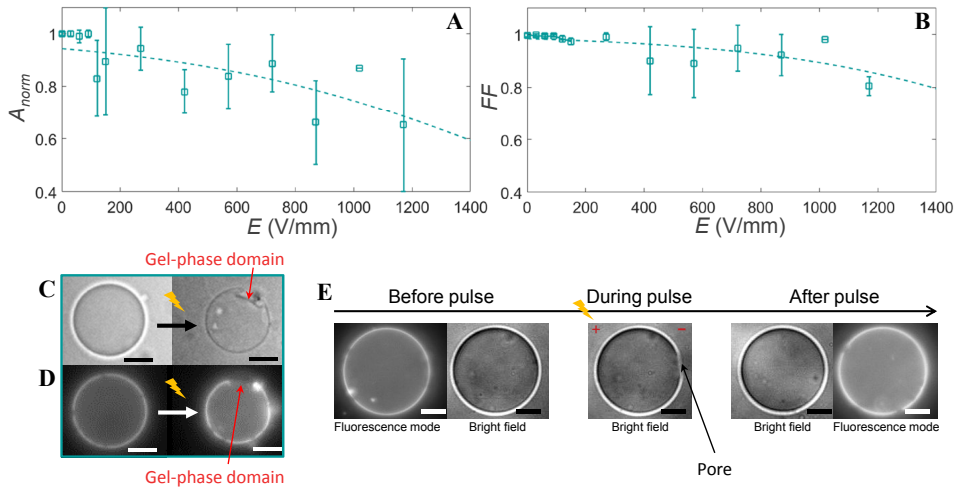


Figure 3.5. The normalised area and the form factor of the 2:8 DPPC:DPhPC GUVs. (A) The averaged normalised area and (B) the form factor of the 2:8 DPPC:DPhPC GUVs. The data is averaged over 13 different GUVs, with radii between 11 and 26 μm . The dotted lines represent the least-squares fit with a sigmoid curve. The error bars in the plots represent the standard deviation. (C) Images of a GUV before and more than 100 seconds after the second pulse at 445 V/mm pulse. (D) Fluorescence images of the same GUV. The fluorescence image after the pulse shows that the buckled patch is located at the gel-phase domain (the dark patch). (E) Bright field and fluorescence images of a GUV before the pulse, during the pulse when a macropore is observed, and after the third pulse at 29 V/mm. The fluorescence images are only captured before and after the pulse. The scale bar is 10 μm .

GUVs out of the thirteen captured GUVs, as shown in the snapshots in Figure 3.5E and in Movie S3.1.4. These pores are found both on the cathode and the anode side. Due to the limited temporal resolution, the pores are only visible for approximately one single frame. Therefore, only the presence of pores can be confirmed and the maximum pore size cannot be determined. These pores are similar to earlier reported pores in fluid-phase GUVs [31, 32] and are referred to as macropores. In addition, all captured GUVs have exhibited complete contrast loss after one of the individual pulses. This indicates that the electric field causes long term defects in the binary membrane.

The 8:2 DPPC:DPhPC GUVs have been divided into two different categories, the homogeneous-GUVs and the domain-GUVs, to reveal the influence of the mixing behaviour of the two lipids on the GUV response. The homogeneous-GUVs have shown a similar size decrease as the pure gel-phase GUVs (Figure 3.6A), whereas the domain-GUVs have displayed size decrease at a lower electric field. The same holds for the drop in the form factor of the homogeneous- and the domain-GUVs (Figure 3.6B). This indicates that the lipids in the homogeneous-GUVs are predominantly in the gel-phase. Despite the different electric field strengths required, the buckling behaviour of both types of GUVs appears similar (Figure 3.6C). The dynamics of the domain-GUVs and the homogeneous-GUVs show differences in their response to the electric pulse. As the homogeneous-

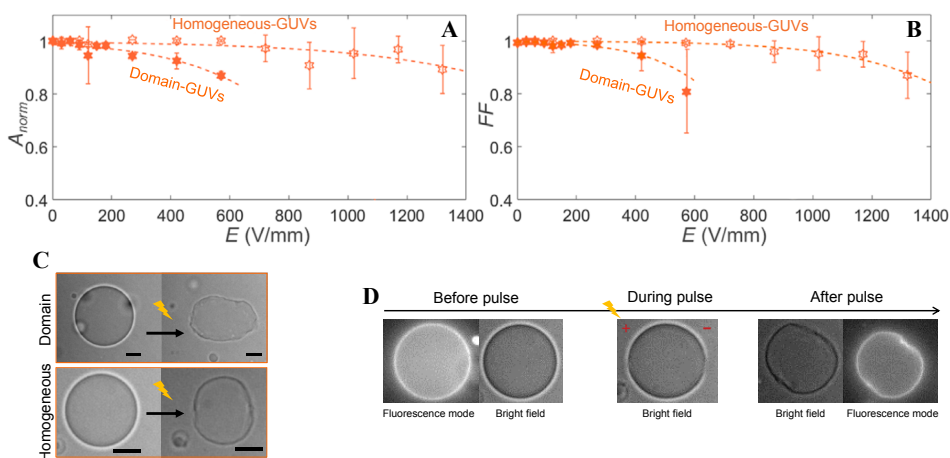


Figure 3.6. The response of the 8:2 DPPC:DPhPC GUVs to increasing electric pulses. (A) The averaged normalised area and (B) the form factor of the homogeneous- and domain-GUVs. The data is averaged over 13 different GUVs, with radii between 11 and 28 μm , where 7 GUVs contain domains (radius between 11 and 28 μm) and 6 GUVs have fully mixed phases (radius between 14 and 22 μm). The dotted lines represent the least-squares fit with a sigmoid curve. (C) The images of the domain- and the homogeneous-GUVs before and more than 100 seconds after the first pulse at 445 V/mm (domain-GUV) or the third pulse at 890 V/mm (homogeneous-GUV), respectively. (D) Bright field and fluorescence images of the homogeneous-GUV shown in (C) before the pulse, during the pulse when a macropore is observed, and after the pulse. The fluorescence images are only captured before and after the pulse. The scale bar is 10 μm .

GUVs relax back into a quasi-spherical, buckled shape, the domain-GUVs can also relax back into a quasi-elliptical, buckled shape (Movie S3.1.5 and S3.1.6). For two of the six homogeneous-GUVs macropores have been observed both on the anode and the cathode side (Figure 3.6D and Movie S3.1.5). The lack of observation of macropores for the remaining GUVs may be caused by the limited temporal resolution of the measurements. Finally, about $\sim 80\%$ of the homogeneous-GUVs and $\sim 70\%$ of the domain-GUVs exhibit complete contrast loss after one of the individual pulses.

3.3 DISCUSSION

The binary GUVs exhibit a complex behaviour with characteristics of both fluid-phase and gel-phase lipids. The shrinkage of these GUVs is associated with tubulation and/or vesicle formation observed for the fluid-phase GUVs and the buckling at higher electric fields is related to the gel-phase lipids. In order to explain this mixed behaviour of the binary GUVs, we will first shed light on why fluid-phase GUVs expel lipids and gel-phase GUVs do not. Consequently, this understanding of the pure-phases will enable us to provide a mechanistic insight into the response of the binary GUVs to the electric pulses.

The decrease in size of the fluid-phase GUVs is due to loss of membrane lipids via formation of small membrane vesicles and/or tubules. Tubulation has been observed when exposing GUVs to both DC and AC electric field [16, 33]. The mechanisms of this lipid loss are not well understood yet. During the pulse, the electric stress builds up due to the ions accumulated on both sides of the membrane. Small curvatures in the bilayer lead to a locally unbalanced electric stress and membrane shape undulations because of the different surface charge densities on each side of a curved membrane [34]. This unbalanced stress is directly proportional to the membrane surface tension induced by the electric field, which is given by [33-36]

$$\sigma_{el} \approx 0.5C_m \Psi_m^2 \quad (3.2)$$

where C_m is the membrane capacitance and Ψ_m is the transmembrane voltage. For a spherical GUV, the maximum Ψ_m can be calculated as [37]

$$\Psi_m = 1.5RE(1 - e^{-t/\tau}) \quad (3.3)$$

where R is the radius of the GUV, E is the applied electric field strength, t is the duration of the electric field, and τ is the characteristic membrane charging time given by

$$\tau \approx RC_m \left(\frac{1}{\lambda_e} + \frac{1}{\lambda_i} \right) \quad (3.4)$$

where λ_e and λ_i are the external and the internal conductivities of the liquids, respectively.

Antonova *et al.* [33] recently have proposed a model, which considers that the electrical tension σ_{el} exerts a force tending to form a small membrane bud and elongate it into a membrane tubule, analogous to the force required to mechanically pull a membrane tubule (tether) from a GUV. This is based on their experimental findings of tubule growth in phosphatidylcholine GUVs subjected to non-electroporative AC fields (1 – 2 kHz) with a strength beyond ~ 15 V/mm. They have estimated the force which triggers the tubule formation as [33]:

$$F_{el} = 2\pi\sqrt{2k_c\sigma_{el}} \quad (3.5)$$

where k_c is the bending elasticity modulus. In order for a tubule to grow, this F_{el} needs to be compared to the opposing force due to the viscous dissipation accompanying the tubule formation. This dissipation is produced by the slipping motion between the two leaflets of the lipid bilayer and by the surface stress due to the extensional flow of the membrane from the GUV body to the tubule [38, 39]:

$$F_v = 2\pi\eta_{eff}V_t \quad (3.6)$$

where η_{eff} represents the effective viscosity, which includes the membrane surface viscosity and the intermonolayer slip coefficient, and V_t represents the velocity of tubule elongation [39]. The estimates of the electrical (F_{el}) and viscous (F_v) forces can shed light on why lipid loss cannot be observed in gel-phase GUVs. As the surface viscosity of gel-phase lipids is about six orders of magnitude higher than the viscosity of fluid-phase lipids [40], we expect that these lipids cannot be removed by the electric field due to the high viscous forces of the gel-phase lipids, whereas the fluid-phase lipids can be removed in the form of tubulation and vesicle formation.

The electrical and viscous forces from above indicate that the binary GUVs mainly expel their fluid-phase lipids and keep their gel-phase lipids. This is supported by the observations that buckling takes place at higher electric fields for the 2:8 DPPC:DPhPC GUVs, after which many of the fluid-phase lipids are already removed by the electric field. Moreover, the expel of fluid-phase lipids is supported by the dynamics of the domain-GUVs. Such GUV can be elongated during the pulse. Yet, during the relaxation, after the fluid-phase lipids have been removed, the GUV appears more rigid and thus remains permanently elliptically shaped (Movie S3.1.5 and S3.1.6). This phenomenon is observed for a domain-GUV, though such behaviour is not observed for the homogeneous-GUVs.

Both the 2:8 and the 8:2 DPPC:DPhPC GUVs have revealed macropores, even for the homogeneous-GUVs. As the pores are similar to the ones observed in the pure fluid-phase GUVs, these pores indicate that the pore formation takes place in the fluid-phase domains. This is corroborated by MD simulations [13] and experiments on droplet-interface bilayers [25], that have shown a preferential pore formation in the fluid-phase domains for heterogeneous systems. Additionally, the macropores in the 8:2 DPPC:DPhPC GUVs

show that large (observable) pores can be formed, despite the high concentration of DPPC lipids. During the exposure of a GUV to an electric pulse the pressure inside the GUV increases due to an increase in the surface tension of the membrane. As soon as the pores are formed, the built-up surface tension can be released both by the expansion of pores in the membrane and the efflux of the internal liquid through the expanding pores [31, 41]. Hence, by determining the efflux, we can gain insight on the sizes of the pores. For simplicity, we assume that the majority of the efflux is transported through a single pore. This is supported by former research, where a single macro-pore has been observed [16–18] in electroporated GUVs. Under this assumption the efflux Q can be directly related to the pore radius r [41, 42]:

$$Q = \frac{2\sigma}{3\eta_0 R} r^3 \quad (3.7)$$

where η_0 is the liquid viscosity, σ is the membrane surface tension. From our experiments we can extract the efflux from the observed area loss $A = \pi R^2$ of the GUV as follows:

$$Q = -\frac{dV}{dt} = -4A \frac{d}{dt} \left(\sqrt{\frac{A}{\pi}} \right) = -\sqrt{\frac{4A}{\pi}} \frac{dA}{dt} \quad (3.8)$$

where V is the volume of the GUV, where it is assumed that the GUV is spherical. Based on these geometrical conditions, the efflux for some example GUVs is calculated from the fitted area loss (Table 3.1 and supplementary Figure S3.3.1). The efflux for the pure fluid-phase GUVs ($Q > 1000 \mu\text{m}^3/\text{s}$) is considerably higher than for the pure gel-phase GUVs ($Q < 200 \mu\text{m}^3/\text{s}$). Our estimations of the fluxes and the correlation to the formed pore sizes are very rough, based on the assumptions of equation (3.7) and the geometrical conditions in equation (3.8). Nevertheless, this large difference in the fluxes for the fluid-phase and gel-phase GUVs indicate that the formed pores in the fluid-phase GUVs are considerably larger than the formed pores in the gel-phase GUVs. This agrees with the observations of macropores for the binary systems. All binary GUVs have shown similar flux to the pure fluid-phase GUVs, independent of the DPPC percentage and its mixing behaviour. This indicates that the pores in binary GUVs have comparable pore sizes as in pure fluid-phase GUVs. Contrary to the expectations, the homogeneous-GUVs, where no phase separation is observed and which appear to have predominantly gel-phase properties, show similar pore sizes as the pure fluid-phase GUVs. This might be due to small fluid-phase domains in these GUVs, that cannot be resolved with fluorescence microscopy. Consequently, based on the experimental observations of macropores and the approximation of the effluxes, it can be concluded that the permeabilisation of the heterogeneous membranes is mainly determined by the presence of fluid-phase domains.

For the 8:2 DPPC:DPhPC GUVs, the homogeneous-GUVs have displayed a higher electrical stability than the domain-GUVs. This increased stability may be due to the predominant gel-phase of the lipids in the homogeneous-GUVs [27]. The domain-GUVs, on the other hand, also contain fluid-phase domains. Consequently, the lipid loss takes

Table 3.1. The estimated values of Q for the different GUVs.

Pure DPhPC GUVs	2:8 DPPC:DPhPC GUVs	8:2 DPPC:DPhPC GUVs	Pure DPPC GUVs
$Q > 1000 \mu\text{m}^3/\text{s}$	$Q > 1000 \mu\text{m}^3/\text{s}$	$Q > 1000 \mu\text{m}^3/\text{s}$	$Q < 200 \mu\text{m}^3/\text{s}$

place at a lower electric field, due to the presence of fluid-phase domains. However, it must be noted that the different mixing behaviour could also be a consequence of a different membrane tension of the GUVs [30]. These two parameters, gel-phase lipid ratio and membrane tension, are poorly controlled due to the used method for the preparation of the GUVs and can both cause an increased stability of the GUVs.

Finally, we need to comment on the slow post-pulse shrinkage of the fluid-phase GUVs. This slow post-pulse shrinkage is always observed in combination with a complete contrast loss after one of the individual pulses. Therefore, this shrinkage effect is linked to long-lived defects caused by the electric pulse. Polak *et al.* [14] have already shown that the properties of the carbon-chain determine the electrical stability of the membrane. In this research we have used DPhPC lipids, which contain methyl-branched carbon-chains. These lipids are known to have slower lateral diffusion than the often used unsaturated DOPC [43]. It is plausible that this nature of the DPhPC lipids slows down the resealing of the created pores. The slow contrast loss indicates the presence of an influx of glucose molecules, whereas the shrinkage indicates an efflux of the inner liquid. Therefore, it can be concluded that during the resealing of the membrane both an influx and efflux are present, where the net flux is directed outward. It seems plausible that the post-pulse shrinkage of the GUVs can be caused by the shear stress on the membrane due to this efflux, which is driven through the pores by the post-pulse membrane tension.

3.4 CONCLUSION

To elucidate the role of gel-phase lipids in electroporation of the cell membrane, we have studied GUVs composed of DPPC and DPhPC lipids, as well as GUVs composed of binary mixtures of both lipids. Our observations show that pure fluid-phase GUV shrink after application of an electroporative electric pulse due to the formation of vesicles and/or tubules. On the contrary, pure gel-phase GUVs buckle permanently upon electroporation without any detectable lipid loss. The electric field can act to expel the lipids from fluid-phase GUVs in the form of tubules and vesicles, but not from gel-phase GUVs, due to the much higher surface viscosity of the gel-phase lipids. Likewise, it is observed that the fluid-phase lipids are removed by the electric field from the binary GUVs, while the remaining gel-phase lipids induce buckling of the GUVs. The critical electric field required to observe lipid loss increases with increasing percentage of DPPC lipids. Moreover, both binary systems have revealed macropore formation. Finally, we have analysed the post-



pulse efflux from the GUVs, to estimate the sizes of the experimentally observed pores. The estimates suggest that the pores are comparable to the pores of the pure fluid-phase GUVs, showing the ability to form large pores despite a high percentage of gel-phase lipids.

These results provide an insight on the role of the different domains in the membrane of living cells during electroporation. On the one hand, the gel-phase lipids can provide an increased electrical stability to the membrane, depending on the mixing behaviour of the two phases. On the other hand, it seems that the transport across the cell membrane is mainly determined by the fluid-phase domains and is not considerably affected by the presence of gel-phase domains.

3.5 METHODS

3.5.1 GUV preparation

The GUVs were prepared from 1,2-diphytanoyl-*sn*-glycero-3-phosphocholine (DPhPC), 1,2-dipalmitoyl-*sn*-glycero-3-phosphocholine (DPPC) and 1,2-dioleoyl-*sn*-glycero-3-phosphoethanolamine-N-(lissamine rhodamine B sulfonyl) (ammonium salt) (DOPE-RhoB), all purchased from Avanti Polar Lipids, Inc. All lipids were dissolved in chloroform (Sigma Aldrich), 1 mg/ml, prior to use. Afterwards, the lipids were mixed in the correct ratio: 99% vol DPPC or DPhPC and 1% vol DOPE-RhoB for the pure phases and for the mixtures 79.5% vol DPPC or DPhPC, 19.5% vol DPhPC or DPPC and 1% vol DOPE-RhoB.

The GUVs were prepared by use of the electrosweeling technique. The lipid mixtures were deposited on two indium tin oxide (ITO) slides (Sigma Aldrich), 20 μ L lipid solution on each slide. The slides were placed in a teflon holder facing each other with a 1.5 mm distance, submerged in 1 mL of 200 mM sucrose (Amresco). It was assured that the swelling took place above the transition temperature of the lipids (for pure DPhPC at room temperature, for all lipid mixtures that contained DPPC at 57 °C). An alternating field was applied of 1 V and 10 Hz for 1 hour, and subsequently changed to 1.5 V and 5 Hz for 2 hours, based on the procedure of Knorr *et al.* [19]. After the swelling, the GUV solution was gradually cooled down (~ 0.5 °C /min). It was assumed that the low cooling rate assures that the lipids organise in the energetically most favoured formation [30]. Afterwards, the GUV solution was diluted for at least 10 times with 200 mM glucose (Sigma Aldrich). By using the sucrose interior and a glucose exterior of the GUVs, a contrast difference was observed. Only GUVs with a proper contrast difference and a spherical shape were selected for these experiments, to assure that the membranes were defect free. Additionally, the spherical shape of GUVs indicated that all GUVs in our experiments had a nonzero initial tension. Finally, we have observed GUVs that have shown membrane fluctuations long after the pulse and occasionally even disintegrated. Since these responses were long after the pulse, we have assumed that these phenomena may be induced by different causes, these GUVs have been excluded from the analysis.

3.5.2 Microscopy

All microscopy bright field experiments were conducted with the inverted fluorescence microscope (Zeiss Axio Observer.Z1) and captured by the Andor iXon3 camera, using a 40x oil immersion objective (Ph3, Plan-Neofluar, 40x/1.30 Oil). The contrast of the images was enhanced by optimising the aperture diaphragm before imaging and adjusting the histogram during processing of the images. The fluorescent images were captured by using the Texas Red filter (45 TR, EX BP 560/40, BS FT 585, EM BP 630/75). The confocal experiments were conducted on the Zeiss LSM 710 inverted confocal microscope, using a 40x oil immersion objective (Fluar, 40x/1.30 oil, M27) and the HeNe-laser (543 nm) to image the GUVs.

3.5.3 Electroporation setup

For the electroporation experiments, custom-made stainless steel electrodes were used with two fixed distances of 0.6 and 1 mm (Figure 3.1A-C). Prior to the experiments, the electrodes were submerged in 1 mL of 200 mM glucose solution. 20 μ L of freshly prepared GUVs was deposited in between the electrodes. Subsequently, electric pulses with duration of 500 μ s were applied. The pulse length was comparable to the characteristic time in which the transmembrane voltage builds on the GUV membrane in our experimental conditions. This charging time τ is estimated using equation (3.4) with a membrane capacitance of 0.5-0.6 μ F/cm² [44] and 0.45 μ F/cm² [19] for the fluid-phase and gel-phase lipids, respectively, and 4.5 μ S/cm [33] and 6 μ S/cm [33] for the external and the internal conductivity, respectively; for a GUV with typical radius of 20 μ m τ is about 300 μ s (fluid-phase GUV) or 250 μ s (gel-phase GUV). The time interval between application of individual pulses was approximately 5 minutes, to minimize the effect of the former pulse. With each subsequent pulse, the pulse amplitude was gradually increased in steps by 10 to 150 V/mm. Before, during, and after application of each pulse, a time lapse of the response of the GUVs was captured by imaging at approximately 10 to 25 frames per second. For each applied pulse, a separate movie was recorded. After the pulse application, the GUVs were imaged until relaxed back to stable shape, which meant that the fluid-phase lipids were not floppy at the end of the time lapse. To capture the mechanism of lipid loss, electroporation experiments at the confocal microscope were conducted. The pulse specifications were identical to the bright field experiments, and the images were taken at 1.6 frames per second. In addition, we applied multiple 5 ms pulses of 0.33 Hz to compare the lipid loss mechanism to former research [16]. The joule heating (less than 0.06 K) and evaporation in order to increase the exterior osmotic pressure (in the order of 20 mOsm) during the experiments are negligible, details can be found in supplementary Sections S3.4 and S3.5. All the data is available from the corresponding author.



3.5.4 Data analysis

The area A and perimeter P of the GUVs were tracked by a custom-made Matlab script, as shown in Figure 3.1D, by use of an edge detection. The perimeter and the area of the GUV were determined by a pixel count for most frames of the movie. Subsequently, the area was normalised over the area prior to the given pulse ($A_{norm} = A_f / A_i$). Additionally, the form factor of the GUVs during the movie was calculated ($FF = 4\pi A / P^2$). Subsequently, the final area and form factor (at time ~ 5 min after pulse application) were plotted as a function of electric field per GUV. Afterwards, the mean of both factors of all GUVs was calculated with a bin size of the electric fields of 30 V/mm. Due to the non-spherical and asymmetrical shape of the GUVs after exposure to multiple pulses, the normalised area and the form factor were plotted against the applied electric field and not the induced transmembrane voltage.

3.6 REFERENCES

1. Pakhomov, A.G., Miklavcic, D., and Markov, M.S., *Advanced Electroporation Techniques in Biology and Medicine*. 2010: CRC Press.
2. Towhidi, L., Kotnik, T., Pucihar, G., Firoozabadi, S.M.P., Mozdarani, H. and Miklavčič, D., Variability of the Minimal Transmembrane Voltage Resulting in Detectable Membrane Electroporation. *Electromagnetic Biology and Medicine*, 2008. 27(4): p. 372-385.
3. Teissie, J., Golzio, M., and Rols, M.P., Mechanisms of cell membrane electropermeabilization: A minireview of our present (lack of ?) knowledge. *Biochimica et Biophysica Acta (BBA) - General Subjects*, 2005. 1724(3): p. 270-280.
4. Yarmush, M.L., Golberg, A., Serša, G., Kotnik, T., and Miklavčič, D., Electroporation-Based Technologies for Medicine: Principles, Applications, and Challenges. *Annual Review of Biomedical Engineering*, Vol 16, 2014. 16: p. 295-320.
5. Mahnič-Kalamiza, S., Vorobiev, E., and Miklavčič, D., Electroporation in food processing and biorefinery. *The Journal of Membrane Biology*, 2014. 247(12): p. 1279-1304.
6. Kotnik, T., Frey, W., Sack, M., Meglič, S.H., Peterka, M., and Miklavčič, D., Electroporation-based applications in biotechnology. *Trends in Biotechnology*, 2015. 33(8): p. 480-488.
7. Perrier, D.L., Rems, L., and Boukany, P.E., Lipid vesicles in pulsed electric fields: Fundamental principles of the membrane response and its biomedical applications. *Advances in Colloid and Interface Science*, 2017.
8. Dimova, R., Riske, K.A., Aranda, S., Bezlyepkina, N., Knorr, R.L., and Lipowsky, R., Giant vesicles in electric fields. *Soft Matter*, 2007. 3(7): p. 817-827.

9. Dimova, R., Bezlyepkina, N., Jordö, M.D., Knorr, R.L., Riske, K.A., Staykova, M., Vlahovska, P.M., Yamamoto, T., Yang, P., and Lipowsky, R., Vesicles in electric fields: Some novel aspects of membrane behavior. *Soft Matter*, 2009. 5(17): p. 3201-3212.
10. Portet, T., Mauroy, C., Démary, V., Houles, T., Escoffre, J.-M., Dean D.S., and Rols, M.-P., Destabilizing Giant Vesicles with Electric Fields: An Overview of Current Applications. *The Journal of Membrane Biology*, 2012. 245(9): p. 555-564.
11. van Uitert, I., Le Gac, S., and van den Berg, A., Determination of the electroporation onset of bilayer lipid membranes as a novel approach to establish ternary phase diagrams: example of the 1- α -PC/SM/cholesterol system. *Soft Matter*, 2010. 6(18): p. 4420-4429.
12. Majhi, A.K., Kanchi, S., Venkataraman, V., Ayappa, K.G., and Maiti, P.K., Estimation of activation energy for electroporation and pore growth rate in liquid crystalline and gel phases of lipid bilayers using molecular dynamics simulations. *Soft Matter*, 2015. 11(44): p. 8632-8640.
13. Reigada, R., Electroporation of heterogeneous lipid membranes. *Biochimica et Biophysica Acta (BBA) - Biomembranes*, 2014. 1838(3): p. 814-821.
14. Polak, A., Bonhenry, D., Dehez, F., Kramar, P., Miklavčič, D., and Tarek, M., On the Electroporation Thresholds of Lipid Bilayers: Molecular Dynamics Simulation Investigations. *The Journal of Membrane Biology*, 2013. 246(11): p. 843-850.
15. Nagle, J.F., and Tristram-Nagle, S., Structure of lipid bilayers. *Biochimica et Biophysica Acta (BBA) - Reviews on Biomembranes*, 2000. 1469(3): p. 159-195.
16. Portet, T., Camps i Febrer, F., Escoffre, J.-M., Favard, C., Rols, M.-P., and Dean, D.S., Visualization of Membrane Loss during the Shrinkage of Giant Vesicles under Electropulsation. *Biophysical Journal*, 2009. 96(10): p. 4109-4121.
17. Tekle, E., Astumian, R.D., Friauf, W.A., and Chock, P.B., Asymmetric pore distribution and loss of membrane lipid in electroporated DOPC vesicles. *Biophysical Journal*, 2001. 81(2): p. 960-968.
18. Kinoshita Jr, K., Hibino, M., Itoh, H., Shigemori, M., Hirano, K'i., Kirino, Y., and Hayakawa, T., 3 - Events of Membrane Electroporation Visualized on a Time Scale from Microsecond to Seconds A2 - Chang, Donald C, in *Guide to Electroporation and Electrofusion*, B.M. Chassy, J.A. Saunders, and A.E. Sowers, Editors. 1992, Academic Press: San Diego. p. 29-46.
19. Knorr, R.L., Staykova, M., Gracia, R.S., and Dimova, R., Wrinkling and electroporation of giant vesicles in the gel phase. *Soft Matter*, 2010. 6(9): p. 1990-1996.
20. Mauroy, C., Rico-Lattes, I., Teissié, J., and Rols, M.-P., Electric Destabilization of Supramolecular Lipid Vesicles Subjected to Fast Electric Pulses. *Langmuir*, 2015. 31(44):



p. 12215-12222.

21. Laude, A.J., and Prior, I.A., Plasma membrane microdomains: Organization, function and trafficking (Review). *Molecular Membrane Biology*, 2004. 21(3): p. 193-205.

22. Mouritsen, O.G., and Bagatolli, L.A., Lipid domains in model membranes: a brief historical perspective. *Essays In Biochemistry*, 2015. 57: p. 1-19.

23. Liu, Z.-W., Han, Z., Zeng, X.-A., Sun, D.-W., and Aadil, R.M., Effects of vesicle components on the electro-permeability of lipid bilayers of vesicles induced by pulsed electric fields (PEF) treatment. *Journal of Food Engineering*, 2016. 179: p. 88-97.

24. Veatch, S.L., and Keller, S.L., Organization in Lipid Membranes Containing Cholesterol. *Physical Review Letters*, 2002. 89(26): p. 268101.

25. Sengel, J.T., and Wallace, M.I., Imaging the dynamics of individual electropores. *Proceedings of the National Academy of Sciences*, 2016. 113(19): p. 5281-5286.

26. Mauroy, C., Portet, T., Winterhalder, M., Bellard, E., Blache, M.-C., Teissié, J., Zumbusch, A., and Rols, M.-P., Giant lipid vesicles under electric field pulses assessed by non invasive imaging. *Bioelectrochemistry*, 2012. 87: p. 253-259.

27. Sakuma, Y., Imai, M., Yanagisawa, M., and Komura, S., Adhesion of binary giant vesicles containing negative spontaneous curvature lipids induced by phase separation. *The European Physical Journal E*, 2008. 25(4): p. 403-413.

28. Jørgensen, K., and Mouritsen, O.G., Phase separation dynamics and lateral organization of two-component lipid membranes. *Biophysical Journal*, 1995. 69(3): p. 942-954.

29. Chen, D., and Santore, M.M., 1,2-Dipalmitoyl-*sn*-glycero-3-phosphocholine (DPPC)-Rich Domain Formation in Binary Phospholipid Vesicle Membranes: Two-Dimensional Nucleation and Growth. *Langmuir*, 2014. 30(31): p. 9484-9493.

30. Chen, D., and Santore, M.M., Large effect of membrane tension on the fluid–solid phase transitions of two-component phosphatidylcholine vesicles. *Proceedings of the National Academy of Sciences*, 2014. 111(1): p. 179-184.

31. Portet, T., and Dimova, R., A New Method for Measuring Edge Tensions and Stability of Lipid Bilayers: Effect of Membrane Composition. *Biophysical Journal*, 2010. 99(10): p. 3264-3273.

32. Riske, K.A., and Dimova, R., Electro-Deformation and Poration of Giant Vesicles Viewed with High Temporal Resolution. *Biophysical Journal*, 2005. 88(2): p. 1143-1155.

33. Antonova, K., Vitkova, V., and Meyer, C., Membrane tubulation from giant lipid vesicles in alternating electric fields. *Physical Review E*, 2016. 93(1).

34. Sens, P., and Isambert, H., Undulation instability of lipid membranes under an electric field. *Physical review letters*, 2002. 88(12): p. 128102.
35. Needham, D., and Hochmuth, R.M., Electro-mechanical permeabilization of lipid vesicles. Role of membrane tension and compressibility. *Biophysical Journal*, 1989. 55(5): p. 1001-1009.
36. Vlahovska, P.M., Voltage-morphology coupling in biomimetic membranes: dynamics of giant vesicles in applied electric fields. *Soft Matter*, 2015. 11(37): p. 7232-6.
37. Kotnik, T., and Pucihar, G., Induced transmembrane voltage-theory, modeling, and experiments. *Advanced electroporation techniques in biology and medicine*, 2010: p. 51-70.
38. Evans, E., and Yeung, A., Hidden dynamics in rapid changes of bilayer shape. *Chemistry and Physics of Lipids*, 1994. 73(1): p. 39-56.
39. Hochmuth, F.M., Shao, J.Y., Dai, J., and Sheetz, M.P., Deformation and flow of membrane into tethers extracted from neuronal growth cones. *Biophysical Journal*, 1996. 70(1): p. 358-369.
40. Evans, E., and Needham, D., Surface-Density Transitions, Surface Elasticity and Rigidity, and Rupture Strength of Lipid Bilayer Membranes, in *Physics of Amphiphilic Layers: Proceedings of the Workshop, Les Houches, France February 10-19, 1987*, J. Meunier, D. Langevin, and N. Boccarda, Editors. 1987, Springer Berlin Heidelberg: Berlin, Heidelberg. p. 38-57.
41. Brochard-Wyart, F., de Gennes, P.G., and Sandre, O., Transient pores in stretched vesicles: role of leak-out. *Physica A: Statistical Mechanics and its Applications*, 2000. 278(1-2): p. 32-51.
42. Happel, J., and Brenner, H., *Low Reynolds number hydrodynamics: with special applications to particulate media*. Vol. 1. 2012: Springer Science & Business Media.
43. Griffin, K.R., *Structure and fluidity of lipid membranes on polymer supports*. The University of Arizona.
44. Ridi, A., Scalas, E., Robello, M., and Gliozzi, A., Linear response of a fluctuating lipid bilayer. *Thin Solid Films*, 1998. 327: p. 796-799.



S 3 APPENDIX

S 3.1 Movie captions

Supplementary Movie S3.1.1. The response of a DPhPC fluid-phase GUV to the third pulse of 500 μs at 97 V/mm. The GUV is imaged in the bright field. The movie is speed up 5.4 times. Observation period: 208 seconds. The bright spots on the GUV surface are possibly small vesicles that have been present from the start (before applying pulses). No increase in the GUV surface area is observed, for which it is assumed that these small vesicles do not influence the surface area of the GUV.

Supplementary Movie S3.1.2. Electroporation of a DPPC gel-phase GUV during the third 500 μs pulse at 595 V/mm. The GUV is imaged in the bright field. The movie is speed up 2.5 times. Observation period: 153 seconds.

Supplementary Movie S3.1.3. Buckling of a DPPC gel-phase GUV during the fourth 500 μs pulse at 744 V/mm. The GUV is imaged in the bright field. The movie is speed up 3.8 times. Observation period: 262 seconds.

Supplementary Movie S3.1.4. The response of a binary GUV with 20 mol% DPPC and 80 mol% DPhPC lipids to the third 500 μs pulse at 29 V/mm. Before and after the pulse, the GUV is imaged in the fluorescence mode to capture the response of the domains. During pulse application, the GUV is imaged in the bright field. The movie is speed up 6.3 times.

Supplementary Movie S3.1.5. The response of the homogeneous-GUV with 80 mol% DPPC and 20 mol% DPhPC lipids to the fourth 500 μs pulse at 890 V/mm. Before and after the pulse, the GUV is imaged in the fluorescence mode to capture the response of the domains. During pulse application, the GUV is imaged in the bright field. The movie is speed up 3.4 times.

Supplementary Movie S3.1.6. The response of the domain-GUV with 80 mol% DPPC and 20 mol% DPhPC lipids to the first 500 μs pulse at 445 V/mm. Before and after the pulse, the GUV is imaged in the fluorescence mode to capture the response of the domains. During pulse application, the GUV is imaged in the bright field. The movie is speed up 2.2 times.

S 3.2 Lipid loss in DPhPC fluid-phase GUVs and buckling DPPC gel-phase GUVs

To demonstrate lipid loss in fluid-phase GUVs and lack thereof in gel-phase GUVs, confocal images of the pure fluid-phase and pure gel-phase GUVs are captured after an individual 500 μ s pulse (Figure S3.2.1A and B). Tubular and vesicular protrusions are observed in a DPhPC fluid-phase GUV, whereas neither tubulation nor vesicle formation is observed for a DPPC gel-phase GUV.

We have exposed the GUVs to multiple 5 ms pulses following Portet *et al.* [1]. As observed before, the lipid loss and associated shrinkage in the fluid-phase GUVs is shown to be more pronounced when multiple 5 ms pulses are applied, compared to the individual 500 μ s pulses (Figure S3.2.1C). The DPPC gel-phase GUVs do not demonstrate lipid loss, despite the longer pulse duration, whereas a buckling effect has been observed for these pulse parameters (Figure S1.1D). These results give an additional argument that the viscosity of the gel-phase lipids hinders lipid expel in gel-phase GUVs.

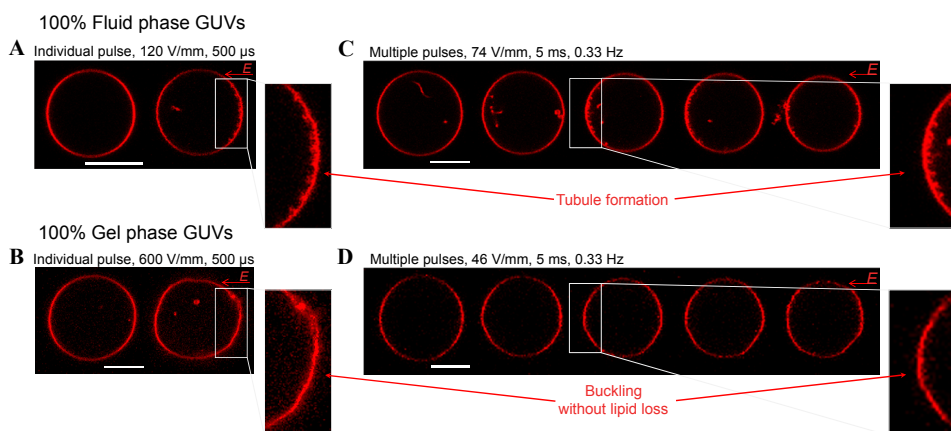


Figure S3.2.1. Confocal images of the pure fluid-phase and gel-phase GUVs exposed to electric pulses. (A) A pure fluid-phase GUV exposed to an individual 500 μ s pulse of 120 V/mm. The lipids in the middle of the GUV have already been detected prior to pulse application, and thus are not indicating lipid expel. The tubules on the right side of the GUV are caused by the electric pulse, indicating lipid expel. (B) A pure gel-phase GUV exposed to an individual 500 μ s pulse of 600 V/mm. The lipids in the middle of the GUV have already been detected prior to pulse application, and thus are not indicating lipid expel. (C) A pure fluid-phase GUV exposed to multiple 5 ms pulses, to enhance the lipid loss effect. (D) A pure gel-phase GUV exposed to multiple 5 ms pulses, to enhance the lipid loss effect. This shows that indeed no tubules nor vesicles are formed due to the pulse, even during the application of longer electric pulses. The scale bar in all images is 10 μ m.

S 3.3 Calculation of the efflux for the GUVs exposed to the electric pulses

The effluxes for the GUVs are calculated from the change in area during the electroporation experiments. The area of the GUVs is captured and tracked over time. This data is fitted, in order to calculate the flux of the GUVs as a function of time, as shown in Figure S3.3.1 (A-D).

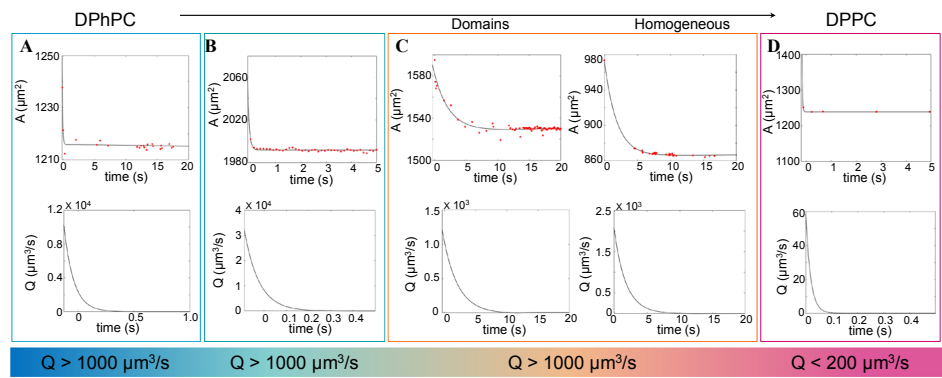


Figure S3.3.1. The absolute area of the different GUVs as a function of time: (A) pure fluid-phase lipids (R-square: 0.95), (B) 2:8 DPPC:DPhPC (R-square: 0.96), (C) 8:2 DPPC:DPhPC (domain-GUVs R-square: 0.93 and homogeneous-GUVs R-square: 0.98), and (D) pure gel-phase lipids (R-square: 0.98). The data from the experiments are depicted in red dots and the solid black lines represent the fitted area and subsequently the calculated flux from the fitted area.

S 3.4 Joule heating during electroporation of vesicles

To ensure that the gel-phase GUVs remained in gel phase during the experiments and did not undergo phase transition due to the Joule heating from the pulse application, we calculate the maximum temperature increase during application of a 500 μ s pulse. Considering that the delivered heat Q equals the work done by the electric field W

$$Q = c_m m \Delta T \quad (\text{S3.1})$$

$$W = J E \Delta t = \lambda_e E^2 t_{\text{pulse}} \quad (\text{S3.2})$$

$$\Delta T = \frac{W}{c_m m} = \frac{E^2 \lambda_e}{c_m \rho} t_{\text{pulse}} \quad (\text{S3.3})$$

where ΔT is the temperature rise (in kelvins), c_m is the heat capacity of the sample, m is the mass of the sample, J is the electric current density, E is the electric field intensity, t_{pulse} is the pulse duration, λ_e is the electrical conductivity of sample, and ρ is the density of the sample.

For an electric field of 1000 V/mm (the maximum electric field used in experiments):

$$\Delta T = \frac{E^2 \lambda_e}{c_m \rho} t_{\text{pulse}} = \frac{(10^6 \text{ V/m})^2 \times 5 \cdot 10^{-4} \text{ S/m}}{4200 \frac{\text{J}}{\text{kgK}} \times 1000 \text{ kg/m}^3} \times 5 \cdot 10^{-4} \text{ s} = 0$$

The heat capacity and density are taken for water. The electrical conductivity of 200 mM glucose solution is taken from Riske and Dimova [2]. The calculated temperature increase is too low to have any effect on the lipids.

S 3.5 Evaporation of the exterior liquid during experiments

Some of the fluid-phase DPhPC GUVs have exhibited a slow (on the timescale of several seconds) and profound ($\sim 20\%$) size decrease after the pulse application, which has not been reported before for GUVs prepared from other fluid-phase lipids, such as egg phosphatidylcholine or DOPC [1-4]. We have checked whether this phenomenon can be due to an increase in the exterior osmotic pressure caused by the evaporation of the exterior liquid.

The evaporation of the exterior liquid during the experiments has been determined by a control experiment. The imaging chamber has been filled with 1.1 ml of 200 mM glucose

solution and placed under the microscope, similarly as during the experiments. The weight of the glucose solution has been determined every hour for three hours, to find the total weight loss of the glucose solution. It must be noted that most experiments have taken less than two hours; however, in order to ensure that no side effects of evaporation have been imaged, we have monitored the evaporation for three hours. In one hour, approximately 3.5% volume has been evaporated, and thus approximately 10% of the total volume has been evaporated in three hours. The 10% evaporated volume can increase the exterior osmotic pressure by ~ 10 mOsm. We do not expect such small increase in the osmotic pressure to considerably affect our results, since an osmotic difference of ~ 20 mOsm (being higher in the exterior with respect to the interior) is often used before in electroporation experiments on fluid-phase GUVs [1, 3]. Furthermore, GUVs can exhibit a similar slow size decrease, if they have been immediately exposed to a single high-intensity electric pulse, before any considerable evaporation can take place (not shown). Therefore, we attribute this slow size decrease, not reported before for other fluid-phase lipids, to the nature of the DPhPC lipids.

S 3.6 References

1. Portet, T., Camps i Febrer, F., Escoffre, J.-M., Favard, C., Rols, M.-P., and Dean, D.S., Visualization of Membrane Loss during the Shrinkage of Giant Vesicles under Electropulsation. *Biophysical Journal*, 2009. 96(10): p. 4109-4121.
2. Riske, K.A., and Dimova, R., Electro-Deformation and Poration of Giant Vesicles Viewed with High Temporal Resolution. *Biophysical Journal*, 2005. 88(2): p. 1143-1155.
3. Mauroy, C., Portet, T., Winterhalder, M., Bellard, E., Blache, M.-C., Teissié, J., Zumbusch, A., and Rols, M.-P., Giant lipid vesicles under electric field pulses assessed by non invasive imaging. *Bioelectrochemistry*, 2012. 87: p. 253-259.
4. Portet, T., and Dimova, R., A New Method for Measuring Edge Tensions and Stability of Lipid Bilayers: Effect of Membrane Composition. *Biophysical Journal*, 2010. 99(10): p. 3264-3273.

4. UNRAVELLING THE RESPONSE OF A BIOMIMETIC ACTIN CORTEX TO ELECTRIC PULSES IN VESICLES



4

Unraveling the response of a biomimetic actin cortex to electric pulses in vesicles

The role of a biomimetic actin cortex was investigated during the application of electric pulses that induce electroporation or electropermeabilization, using giant unilamellar vesicles (GUVs) as a model system. The actin cortex, a subadjacently attached interconnected network of actin filaments, regulates the shape and mechanical properties of membranes in living cells as well, and is a major factor influencing the mechanical response of the cell to external physical cues. We demonstrate that the presence of the actin shell inhibits the formation of macropores in the electroporated GUVs. Additionally, experiments on the uptake of dye molecules after electroporation show that the actin network slows down the resealing process of the permeabilized membrane. We further analyze the stability of the actin network inside the GUVs exposed to high electric pulses. We find disruption of the actin layer that is likely due to the electrophoretic forces acting on the actin filaments during the permeabilization of the GUVs. Our findings on the GUVs containing a biomimetic cortex provide a step towards understanding the discrepancies between the electroporation mechanism of a living cell and its simplified model of the empty GUV.



4.1 INTRODUCTION

The plasma membrane is a selective barrier that separates the intracellular environment from the cell exterior and regulates the transport of molecules of different sizes in or out of the cell. The membrane consists of a lipid bilayer with numerous anchored and embedded inclusions, providing the membrane with both fluidic and elastic properties; additionally, an inter-connected network of actin filaments, called the actin cortex, lies immediately underneath the plasma membrane. The cortical skeleton is strongly bound to the lipid bilayer via diverse linkers, maintaining the global shape of the cell [1-3], and controlling the lateral organization of the plasma membrane [4, 5]. The bi-directional interplay between the membrane and actin cortex strongly influences any mechanical response of the cell to external stimuli during diverse biological processes, ranging from cell migration and differentiation to cell division [6].

The actin network also plays an essential role in electroporation, also referred to as electropermeabilization, of cells. This is a membrane permeabilization technique used for the delivery of a wide range of molecules ranging from small molecules such as drugs to large molecules, such as DNA, into the cell. Applying direct current (DC) electric pulses to a cell builds up an induced transmembrane voltage, which can permeabilize the cell membrane above a critical transmembrane voltage ($\sim 0.2 - 1$ V) [7, 8]. The kinetics of the electroporation mechanisms in cells appears to consist of five consecutive steps: (i) nucleation of defects in the membrane, (ii) expansion of these defects, (iii) stabilization of the permeabilized state, (iv) resealing of the permeated membrane, (v) the recovery of structural changes in the membrane while the membrane is already resealed, also called the “memory” of the cell [8]. It has been shown that cells can remain permeabilized from minutes up to hours after pulsation [9-11]. This long resealing process is considerably slower than that observed for bare lipid bilayers (less than one second) [12-14]. Additionally, it was reported in electrofusion experiments that the permeabilized area in cells does not diffuse laterally [15]. Based on the evidence from the electroporation and the electrofusion experiments, it has been suggested that the actin cortex is involved in the electroporation mechanism [16-18]. The physical properties of such transient permeated lipid structures and the associated intracellular components are the most important factors that enable a successful delivery of biomolecules to the cells [8, 19-21]. Until now, a complete understanding of the effects of the actin cortex on electroporation of a lipid bilayer is lacking.

There have been several studies on the role of the cytoskeleton during electroporation of living cells [17, 18, 22-29]. In these studies, the actin filaments were manipulated either by drugs that cause chemical disruption [17, 18, 22, 26] or stabilization [23] or by genetic engineering [24] of the cytoskeleton. Cell permeabilization was measured in terms of the uptake or release of tracer molecules, like Trypan Blue and Propidium Iodide [17, 18, 22-27]. Depolymerization of the actin in chinese hamster ovary (CHO) cells and human erythrocytes leads to acceleration of the post-pulse membrane resealing, while it does

not considerably affect the initial steps in the permeabilization process [17, 18]. More recently, nanosecond pulses have gained attention due to their ability to permeabilize intracellular membranes [30]. Disruption of the actin cortex in CHO cells appears to make the cells more susceptible to nanosecond electroporation [25]. Moreover, nanosecond electroporation was found to be more damaging to non-adherent cultures such as Jurkat cells than adherent cell cultures such as HeLa cells, possibly because of the less extensive cytoskeletal network of the former [27]. In addition, some biological processes, like apoptosis and necrosis, have been triggered by nanosecond pulses [26, 28], which could involve the pulse-mediated disruption of the actin cytoskeleton [22, 29].

The studies discussed above illustrate how challenging it is to decouple the mechanical interaction between actin filaments and the membrane from other biological processes involving actin, such as apoptosis and necrosis, and to manipulate the cytoskeleton of a living cells without side effects, like cell death. Therefore, simplified cell models like planar lipid bilayer models [31-33] or giant unilamellar vesicles (GUVs) [34-36] have been utilized to study the fundamental mechanisms of pore formation during electroporation. The process of pore formation involves a balance between membrane tension and edge tension. During the pulse, the electric field imposes a Maxwell stress on the membrane, similar to lateral tension [37, 38]. This rising membrane tension eventually drives pore formation [39, 40]. After the pore formation, the growth of the pore can be regulated by the intensity and the duration of electric pulses [11, 41]. On the contrary, the edge tension confers an energy penalty for making a pore in the lipid bilayer and counteracts pore growth. After the electric pulse, this edge tension governs the resealing of the pore [41, 42]. Studies on GUVs have revealed the presence of micrometer sized pores (referred to as macro-pores) during electroporation [12, 40, 43-45]. The resealing time of these pores is typically in the order of 10 ms [40], as opposed to several minutes or even hours in living cells. It has been shown that the dynamics of these pores can be modified by adjusting the edge tension of the lipid bilayer, e.g. by adding cholesterol to increase the edge tension [39, 46]. Moreover, gel-phase lipids have been shown to prevent the formation of macropores due to high surface viscosity [47, 48]. From these studies, it can be concluded that the membrane components are crucial for the dynamics of electroporeabilization in cells.

Although the same physics governs the competition between membrane tension and edge tension during pore formation, GUVs and living cells exhibit drastically different permeabilized membranes. The pores formed in GUVs due to pulse application are in the micrometer range, and reseal within tens of milliseconds. By contrast, the electropores (or permeated membrane) in living cells were reported to be in the order of few nanometers [11, 49, 50] and express a slow resealing process which takes minutes up to hours [49, 51, 52], suggesting that the permeabilization dynamics are influenced by an interplay between the lipid bilayer and the intracellular structures, in addition to other lipid-associated interactions [16, 18].



In this research, we focus on the role of the actin cortex during electroporation of the membrane in order to understand the discrepancy between model membranes and the plasma membrane. To isolate the mechanical role of the actin, we have used a bottom-up approach where we have incorporated a biomimetic actin cortex inside GUVs. We have used a high-speed imaging technique to reveal the pore formation and resealing in response to controlled electric pulses for GUVs, with and without an encapsulated actin network. Additionally, we assessed the uptake of sulforhodamine B dye molecules to study the permeability dynamics after electric pulses. Finally, we use confocal imaging to investigate the structural stability of the encapsulated actin cortex in the electric field.

4.2 MATERIALS AND METHODS

4.2.1 Preparation of the GUVs

The GUVs (with and without actin filaments) were prepared by electrosweeling, based on a procedure utilized by Schäfer *et al.* [53]. The following membrane composition was used for the bright field experiments: 95 mol% 1,2-dioleoyl-*sn*-glycero-3-phospholipine (DOPC) and 5 mol% Ca^{2+} -ionophore (A23187). For the confocal experiments, the membrane was fluorescently labelled using the following membrane composition: 94.5 mol% DOPC, 5 mol% Ca^{2+} -ionophore and 0.5 mol% 1,2-dioleoyl-*sn*-glycero-3-phosphoethanolamine-N-(lissamine rhodamine B sulfonyl) (ammonium salt) (DOPE-RhoB, ex/em 560 nm/583 nm). The lipids were purchased from Avanti Polar Lipids, Inc and the Ca^{2+} -ionophore from Sigma Aldrich, and stored at -20°C . All membrane components were dissolved separately in chloroform at a concentration of 1 mg/mL, stored under nitrogen at -20°C , and mixed prior to the experiments. 10 μL of lipid mixture was deposited on the conductive face of two Indium Tin Oxide (ITO) slides (purchased from Sigma Aldrich) and left under vacuum for more than 2 hours. Afterwards, the ITO slides were inserted in the teflon swelling chamber with the conductive sides facing each other, spaced 1.5 mm apart. 335.6 μL swelling buffer (pH of ~ 8) was inserted in between the ITO slides, consisting of 200 mM sucrose, 2 mM Tris-HCl (Thermo Fischer), 0.17 mM Adenosine 5'-triphosphate disodium salt hydrate (Na_2ATP) and 0.21 mM dithiothreitol (DTT) (both purchased from Sigma Aldrich). In the case of the GUVs with encapsulated filaments, actin monomers from rabbit muscle (Thermo Fischer), purchased as 1 mg of lyophilised powder, was dissolved in 2 mM Tris-HCl (pH 8.0) to get a stock solution of 2 mg/mL and stored at -80°C . For visualization of the filaments, fluorescently labelled actin monomers with Alexa Fluor 488 (Thermo Fischer, ex/em 495 nm/519 nm) was purchased as a solution with a concentration in the range of 3 – 5 mg/mL in a buffer (5 mM Tris (pH 8.1), 0.2 mM DTT, 0.2 mM CaCl_2 , and 0.2 mM ATP) containing 10% (w/v) sucrose. A solution of 7 μM actin monomers, of which 0.5 μM fluorescently labelled, was added to the swelling buffer. An alternating current (AC) was applied at 70 Hz, 2.4 V for 3 hours at room temperature (around 20°C), using the Agilent 33220A 20 MHz Function / Arbitrary Waveform Generator.

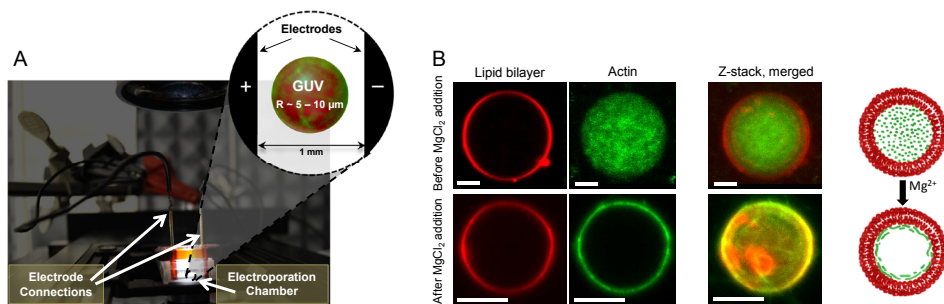


Figure 4.1. (A) The electroporation setup. (A) Photograph of the electroporation setup, with a schematic of the GUV in between the electrodes shown in the inset, not drawn to scale. (B) Confocal fluorescence microscopy images of a GUV (red signal, ex/em 560 nm/583 nm) before and after the addition of 19 mM MgCl_2 , showing that actin polymerizes and accumulates underneath the lipid bilayer membrane (green signal, ex/em 495 nm/519 nm). The scale bar in all images is 5 μm .

4.2.2 Polymerization and binding of actin to the membrane

The polymerization of the actin filaments and their attachment to the membrane were induced by adding Mg^{2+} ions [53], as shown in Figure 4.1B. The GUV solution obtained by electrosweeling was diluted with 1.3 mL glucose buffer of 200 mM glucose and 2 mM Tris-HCl (pH of ~ 8) in order to dilute the actin monomer concentration and the sucrose concentration on the outside of the GUVs. 163 μL of 67.3 mM MgCl_2 solution (pH of ~ 8.5) was then added to increase the MgCl_2 concentration to 6 mM. Subsequently, due to the presence of the Ca^{2+} -ionophore in the membrane, the Mg^{2+} ions are transported into the GUVs to initiate polymerization and bind the actin filaments to the membrane as a cortex, left overnight at room temperature. Prior to the electroporation experiments, the MgCl_2 concentration in the outer solution was increased to 19 mM to ensure a cortex at the membrane for all GUVs. This increase in the MgCl_2 concentration to 19 mM after equilibrating the GUVs at 6 mM overnight has led to the most consistent result with a large majority of GUVs containing an actin network ($> 90\%$) (see Figure S.4.2.1. in the supplementary information). Since the ion concentration has a large impact on the response of the GUVs to electric pulses, altering the deformations of the GUVs [54] and the pore dynamics [55], we fixed the concentration of MgCl_2 at 19 mM. The stability of the GUVs was not affected by the high ion concentration overnight. The absence of actin polymerization on the outside of the GUV during the storage overnight and during the electroporation experiments was confirmed by control experiments of empty GUVs with actin monomers on the outside (see Figure S.4.3.1. in the supplementary information).

4.2.3 Electroporation setup combined with high speed imaging

To image the dynamics of the membrane during an electric pulse, the GUVs were

visualized by an inverted microscope (Zeiss Axio Observer.Z1) equipped with a Phantom v9.1 high-speed camera (10 000 – 15 000 frames per second, fps, Vision Research Inc.), using a 40x oil immersion objective (Ph3, Plan-Neofluar, 40x/1.30), providing a pixel size of 0.3 μm . Prior to the experiments, the imaging chamber was treated with 5 g/L Bovine Serum Albumin (BSA) solution (purchased from Sigma Aldrich) for 20 minutes, to avoid rupture of the GUVs when interacting with the glass bottom of the chamber. Custom made stainless-steel 20 mm-long electrodes with 1 mm distance were submerged in 1 mL glucose buffer with 412.4 μL MgCl_2 and 33 μL of GUV solution was added by carefully pipetting the GUV-solution in between the electrodes using a cut-off pipette tip (Figure 4.1A). We selected the actin-encapsulated GUVs based on the fluorescence signal of the actin, to ensure that the filaments were organized along the GUV membrane as a cortex, as shown in Figure 4.1B. The actin-encapsulated GUVs had a radius between 5 and 10 μm , empty GUVs of similar sizes were selected for the experiments. During the dynamics experiments, consecutive 500 μs pulses with increasing amplitude were applied. The electric pulses induce a transmembrane voltage as follows [56]:

$$\Psi_m = 1.5RE(1 - \exp(-t/\tau)) \quad (4.1)$$

where R , E and t indicate the radius of the GUV, the applied electric field strength and the duration of the pulse, respectively. τ is the charging time of the membrane given by

$$\tau \approx RC_m\left(\frac{1}{\lambda_e} + 1/\lambda_i\right) \quad (4.2)$$

where C_m , λ_e and λ_i are the membrane capacitance, and the internal and external solution conductivity, respectively. In our experiments the pulses were chosen such that the induced transmembrane voltage started from about 1 V, with approximately 1 minute interval between the pulses to minimize the effect of the former pulse. The sucrose-filled GUVs with glucose solution on the outside assure sufficient optical contrast to image the GUVs in bright field, and indicate permeabilization of the membrane by a contrast loss. Consecutive pulses with increasing amplitude were applied until a complete contrast loss of the GUVs was observed.

4.2.4 Electroporation setup for pore dynamics

To assess the resealing of the membrane, the transport of sulforhodamine B through the membrane was monitored. Sulforhodamine B was added to the outer solution at a concentration of 2.5 μM . The same pulse protocol was used as during the high-speed imaging experiments. The molecule transport was captured with a Zeiss LSM 710 inverted confocal microscope, using a 100x oil immersion objective (Ph2, Archoplan, 100x/1.25 Oil). Images were taken at a frequency of around 1.5 Hz to observe the diffusive transport of the dye molecules through the membrane. To obtain the uptake kinetics of

the sulforhodamine B, the intensity of 80% of the inner GUV area was monitored, to exclude the increased intensity of the membrane (Figure 4.4.A). In addition, the intensity of the background was captured. The data was normalized as follows: $I_{uptake} = (I_{dye,t} - I_{dye,0}) / (I_{background,t} - I_{dye,0})$, where I_{uptake} , $I_{dye,t}$, $I_{dye,0}$ and $I_{background,t}$ represent the normalized intensity in the GUV at time t , the intensity in the GUV at time t , the initial intensity prior to the pulse and the intensity of the background, respectively.

4.2.5 Electroporation chamber combined with confocal imaging

The response of the actin cortex to the electric pulses was visualized with a Zeiss LSM 710 inverted confocal microscope, using a 100x oil immersion objective (Ph2, Archoplan, 100x/1.25 Oil) to image both the lipid bilayer and the actin cortex. Two different pulsing protocols were used: (i) consecutive increasing pulses starting from low fields, increasing gradually to higher fields (ranging from 10 – 300 V/mm with steps of approximately 10 V/mm), (ii) immediate high pulses (ranging from 300 – 1000 V/mm with steps of approximately 200 V/mm), where only 2 to 4 pulses were applied of increasing field. In both cases 500 μ s pulses were used, with approximately 1 minute interval between the pulses. The first pulse protocol (i) was used to test the onset of the breakdown of the actin cortex. The second pulse protocol (ii) was used to decouple the breakdown of the actin cortex from the cumulative effect of the multiple consecutive pulses. A z-stack of 7 focal planes, with a range of approximately the diameter of the GUV $\Delta z \sim 4 \mu$ m), of the fluorescence signal of the membrane and the actin was taken before and after the pulses, to record the response of the actin cortex. The z-stack imaging is a slow technique (approximately 5 to 10 seconds time interval in between the z-stacks), so only the GUV size and the actin cortex stability before and after the pulse were extracted.

4.2.6 Data analysis of GUVs response

The bright field images of the GUVs were analyzed by a custom written Matlab script. The contours of the GUVs were detected with the Canny edge detection method and fitted to an ellipse to extract the equatorial a and polar (b , the distance from the center to the poles of a spheroid) radii of the GUVs. For the dynamics studies, these two radii were used to obtain the deformation ratio (a/b) during and after the pulse. Afterwards, the time-dependent deformation was fitted to an exponential decay curve to obtain the relaxation time(s) of the GUVs, similar to the method reported by Riske and Dimova [40] (Figure 4.2).

During the confocal experiments, multiple planes of the GUVs were imaged. The radius of the GUVs was determined from the fluorescent confocal membrane images taken at the equatorial plane of the GUV by a similar detection method as described above. These images were used to reveal the area loss of the GUVs as a function of electric field. In



order to remove spurious effects due to motion of the GUV in and out of the imaging plane (which changed their observed radius), the normalized area (A_{norm}) was calculated at pulse n and corrected for the area loss at the previous pulse ($n - 1$): $A_{norm} = (A_f/A_i)_n (A_f/A_i)_{n-1}$. Here, A_i and A_f represent the initial and the final area of the GUV before (initial) and after (final) the pulse, respectively. $(A_f/A_i)_n$ and $(A_f/A_i)_{n-1}$ are the normalized areas of the GUV at the pulse n and at the preceding pulse ($n - 1$). By multiplying these two factors, the normalized area is corrected for shrinkage due to earlier pulses. Additionally, the intensity of the fluorescence signal of the actin was obtained from confocal z-stacks by determining the mean and average intensity of all planes. Photobleaching of the actin cortex was removed by correcting the data at scan number k with a reference of a separate photobleaching experiment of a GUV without applying any pulses. By normalizing the actin fluorescence intensity from the bleaching experiment, the correction factor for the photobleaching per scan is calculated ($I_{ref,k} = I_{k,ref}/I_{0,ref}$, where $I_{0,ref}$ and $I_{k,ref}$ are the intensities of the image at the start of the photobleaching experiment and at the relevant scan number k , respectively). Consequently, the results of the electroporation experiments were corrected as follows: $I_{norm} = I_k / (I_0 I_{ref,k})$. Again, I_0 and I_k represent the intensities of the image at the start of the experiment and at scan number k , respectively, in this case during an electroporation experiment (see Figure S4.4.1. in the supplementary material).

4.3 RESULTS AND DISCUSSION

4.3.1 The dynamics of the GUVs

To investigate the influence of the actin cortex on the electroporation of GUVs, we captured the dynamics of the GUVs by high speed imaging 10 000 – 15 000 fps) in bright field. The deformations of the GUVs were measured in the terms of the deformation ratio a/b during and after the electric pulse (see the schematic in Figure 4.2). The GUVs are electroporated once the accumulated transmembrane voltage exceeds a threshold voltage. Electroporation can be recognized by the observation of a macropore or the contrast loss due to the exchange of glucose and sucrose molecules between the interior and exterior of the GUV. Below the critical threshold field, where no macropores nor contrast loss were observed, the GUVs exhibited squarelike deformations, as shown in Figure 4.2A. These deformations relax back exponentially with a characteristic relaxation time time (τ_l) in the order of 100 μ s for both the empty and the actin-encapsulated GUVs. Riske and Dimova [54] have shown that the presence of the ions (NaCl, Ca^{2+} or Mg^{2+} acetates) flattens the membrane, which they attributed mainly to the electrophoretic forces of the ions, leading to squarelike deformations.

The conductivity ratio χ is defined as the ratio between the conductivity of the internal λ_{in} and external solution of the vesicle λ_{out} , $\chi = \lambda_{in}/\lambda_{out}$. Depending on this conductivity ratio, vesicles are expected to either deform along the field, referred to as a tubelike shape, (deformation ratio $a/b > 1$, $\chi > 1$) or perpendicular to the field, referred to as a disklike shape,

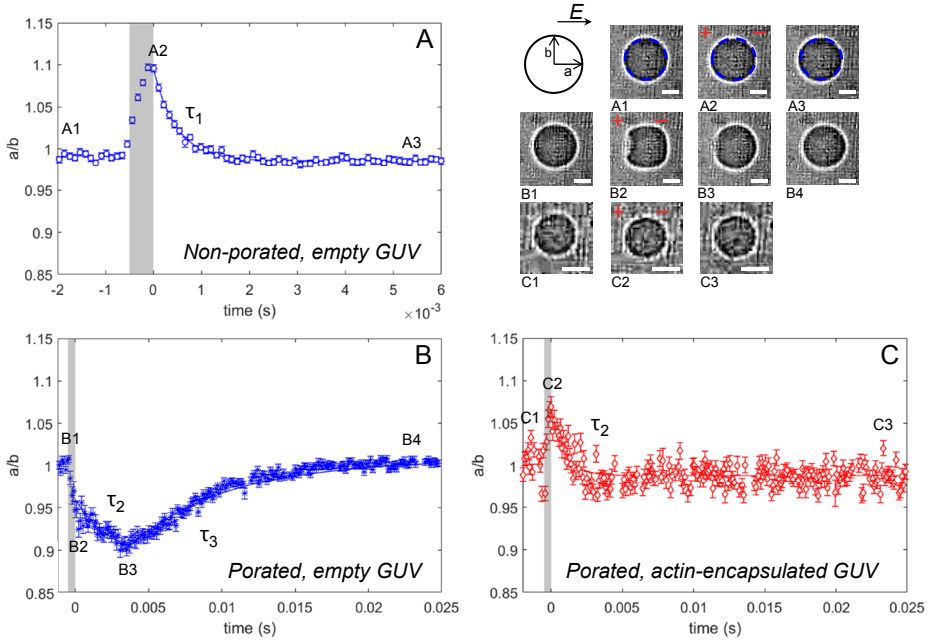


Figure 4.2. The dynamics of GUVs with and without an encapsulated actin shell. (A) The dynamics of a non-porated empty GUV, where deformation and a single relaxation (τ_1) is observed. The blue dotted lines in the snap shots of A1-A3 show the tracking method used to determine radii a and b . (B) The dynamics of a porated empty GUV, where a pore is observed together with a double relaxation (τ_2 and τ_3). (C) The dynamics of a porated actin-encapsulated GUV where no macropore is observed, and only a single relaxation (τ_2). The relaxation times are obtained from exponential fits to the deformation data, as explained in the text. The scale bar in all images is $5 \mu\text{m}$. The definitions of non-porated and porated GUVs are explained in the text.

(deformation ratio $a/b < 1$, $\chi < 1$). We observed both disklike and tubelike deformations during the pulsing experiments of both the empty and the actin-encapsulated GUVs. It must be noted that an ionophore is used to transport Mg^{2+} into the GUVs to initiate actin polymerization and cortex formation after the GUV formation, as discussed in the methods section. Some variation in the conductivity of the inner solution of the GUVs is possible due to our preparation method, which would explain the observations of both disklike and tubelike deformations. Additionally, permeabilizing pulses cause an exchange of the inner and outer solutions, and consequently may alter the conductivities of the two solutions. As these observations are similar for both the empty and actin-encapsulated GUVs, they can be related to the presence of the ionophore and the ion-imbalance of the inner and outer solution.

The response of the empty and the actin-encapsulated GUVs to an electroporative pulse was strikingly different, as shown in Figure 4.2. Macropores were observed for the empty GUVs, as was reported before [40], whereas the actin-encapsulated GUVs exhibited no visible macropores. Additionally, for the empty GUVs we observed a characteristic

4. UNRAVELLING THE RESPONSE OF A BIOMIMETIC ACTIN CORTEX TO ELECTRIC PULSES IN VESICLES

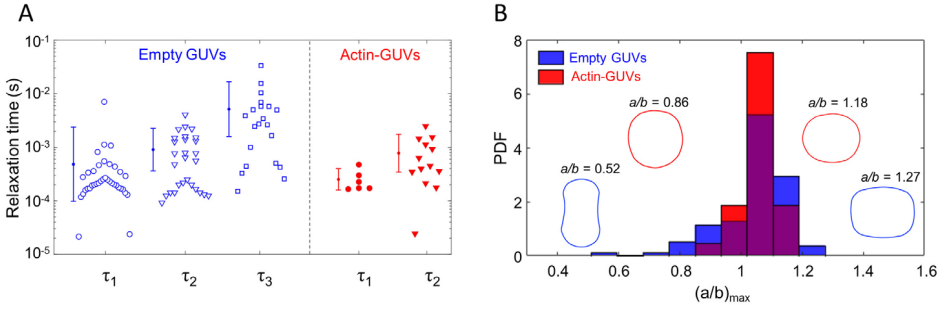


Figure 4.3. The relaxation time and maximum deformation of the GUVs during an electric pulse with and without actin shell. (A) Relaxation times of empty (blue open symbols) and actin-encapsulated (red filled symbols) GUVs in the non-electroporative regime (τ_1) and the electroporative regime (τ_2 and τ_3). (B) The distribution of the maximum deformations of empty (blue) and actin-encapsulated (red) GUVs during all pulses (both electroporative and non-electroporative). The schematics in the histogram represent simplified contours of the corresponding disklike and tubelike deformations, not to scale. The data in both panels is of 16 actin-encapsulated GUVs with an average radius of $\sim 5 \mu\text{m}$ and 10 empty GUVs with an average radius of $\sim 5 \mu\text{m}$. In both cases the experiments have been repeated five times on different days.

relaxation process, where the relaxation of the macropore (with a duration τ_2 of $\sim 1 \text{ ms}$) was followed by a subsequent relaxation (with a duration τ_3 of $\sim 10 \text{ ms}$), as illustrated in Figure 4.2B and Movie S4.1.1. The observation of the latter relaxation time τ_3 (see Figure 4.2B3) did not always occur during macropore formation. This response is similar to earlier reports for empty GUVs composed of egg phosphatidylcholine by Riske and Dimova [40]. They attributed τ_2 to the relaxation time of the macropore in a standalone lipid bilayer ($\tau_{\text{pore}} \sim \eta_s r / (2\gamma)$, where η_s , γ and r are the surface viscosity, the line energy per unit length and the pore radius, respectively) and τ_3 to the relaxation of the membrane due to either the excess surface area of the GUVs or an increase of the excess area during the macroporation [40]. The similarities between the macropores exhibited by our empty GUVs and previous studies show that the ionophore and the Mg^{2+} ions present in the solution have a negligible effect on the GUV dynamics during electroporation.

The distributions of the different relaxation times in the non-porative and porative regimes are shown in Figure 4.3A for both the empty and actin-encapsulated GUVs. In strong contrast to the observations of the macropores and large deformations for the empty GUVs, the actin-encapsulated GUVs show only small deformations during the electroporative pulses and do not exhibit macropores (Figure 4.2C and Movie S4.1.2). Since no macropore was observed for these GUVs, electropermeabilization was determined by the contrast loss of the GUVs. This contrast loss indicates the permeabilization of the membrane, due to the exchange of molecules through the membrane. Due to limited recording time of the high-speed imaging in the experiments (maximum of 2 seconds), no long-term dynamics of the contrast loss was captured. The relaxation time τ_2 , which shows the time-dependent deformation of the actin-encapsulated GUVs in the electroporative regime, is comparable to the relaxation time τ_2 of the empty GUVs (Figure 4.3A). However, the slow dynamics of

the contrast loss after a pulse for the actin-containing GUVs indicates that the membrane remains permeabilized up to minutes, which was not observed for the empty GUVs. Therefore, the pore resealing time of the actin-encapsulated GUVs cannot be deduced from τ_2 , due to the absence of macropores and the slow resealing process which occurs in the presence of the actin cortex. In conclusion, the presence of the actin layer in the GUVs hinders the formation of macropores. Previous studies on living cells have proposed that the formed electropores in the membrane cannot expand beyond the mesh size of the actin network [19, 49]. Possibly, a similar mechanism limits the growth of the pores in the actin-encapsulated GUVs.

As discussed above, we observed both disklike ($a/b < 1$) and tubelike ($a/b > 1$) deformations for the empty and the actin-encapsulated GUVs. The broad distribution of the maximum deformation $(a/b)_{max}$ at the end of the pulse is shown in Figure 4.3B. For both types of GUVs, the majority of the GUVs undergoes tubelike deformation, indicating a higher conductivity of the interior of the GUVs due to the Mg^{2+} transport across the membrane by the ionophore. The deformations of the actin-encapsulated GUVs are significantly smaller than those of the empty GUVs, which can be seen from the more narrow distribution of $(a/b)_{max}$ (shown in red in Figure 4.3B). Experiments on GUVs in alternating current (AC) fields have shown that the extent of membrane deformation depends on the bending rigidity of the membrane [57]. Additionally, in DC field experiments, non-electroporative pulses can be used to study the stiffness of the membrane [58]. In our experiments we focused on pulses around the transmembrane voltage of 1 V, therefore we cannot derive the precise mechanical properties. Nevertheless, the smaller deformations of the GUVs with an encapsulated actin cortex clearly signify an increase in the bending rigidity of the GUVs, consistent with previous research works showing that the presence of an actin cortex leads to an increased bending rigidity [53, 59, 60]. The wide distribution observed for $(a/b)_{max}$ of the GUVs is caused by the preparation technique used for making the actin-encapsulated GUVs. It offers a poor control on the membrane tension of the GUVs (both for the empty and the actin-encapsulated GUVs). Moreover, the actin-encapsulated GUVs likely possess different actin cortex thicknesses, leading to different mechanical properties [53]. In conclusion, our results show that the actin cortex prevents macropore formation and reduces membrane deformation, which may contribute to the differences observed between the response of cells and empty GUVs to electric pulses.

4.3.2 Resealing of the permeabilized membrane

The permeabilization dynamics of the membranes has been determined by the uptake of dye molecules into the GUVs. Due to the relatively slow imaging, only the transport after the pulse could be captured, which is predominantly diffusive [61]. The pulses applied are in the same range where macro-pores were observed for the empty GUVs. An increase in the inner fluorescence of the GUVs immediately after the pulse is defined as electroporation of the membrane. To find the amount and the characteristic time of dye

4. UNRAVELLING THE RESPONSE OF A BIOMIMETIC ACTIN CORTEX TO ELECTRIC PULSES IN VESICLES

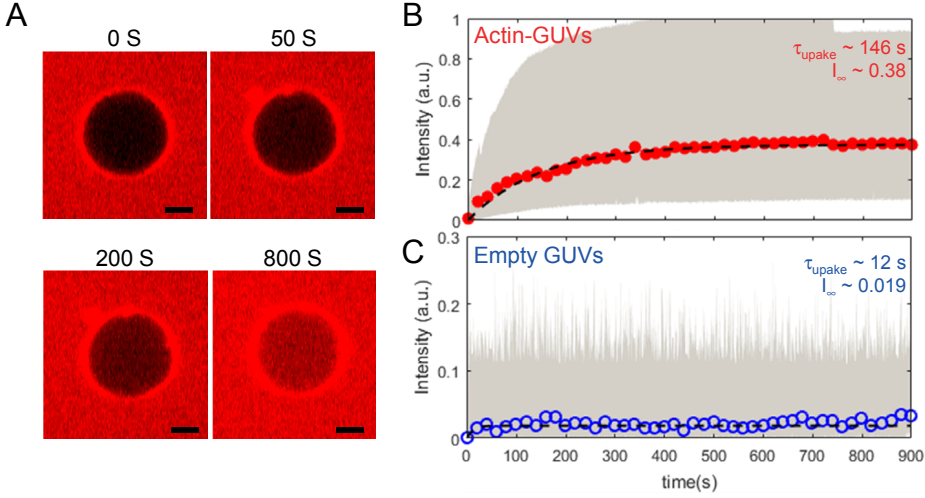


Figure 4.4. The kinetics of the uptake of dye molecules from the outer solution during the resealing of GUVs. (A) Four snapshots of a resealing experiment of an actin-encapsulated GUV, showing the uptake of the dye molecules after a 85 V/mm pulse over time. The scale bar in all images is 5 μm . (B) The average intensity of sulforhodamine B in the actin-GUVs over time of 13 different GUVs with an average radius of $\sim 10 \mu\text{m}$. The GUVs were exposed to electroporative pulses inducing a transmembrane voltage above 1 V. Already one single 500 μs pulse caused considerable uptake of the dye molecules. (C) The average intensity of fluorescent dye in empty GUVs over time of 15 different GUVs. To ensure dye uptake by the GUVs after pulse application, multiple pulses were applied when no visible dye uptake was obtained. Only the pulses where an increase of the dye intensity immediately after the pulse was observed have been selected to calculate the average intensity increase. The dotted lines in both graphs represent the least-squares fit of Equation 4.3 through the averaged data. The highlighted area in gray in both graphs shows the spread of the data points of all experiments. Only every twentieth data point of the averaged data is shown here, to improve the readability of the graph. The fitting parameters, characteristic time of the uptake of dye molecules and the amount uptake, obtained from the fits are shown in the graphs.

molecule uptake after the pulse, which is mainly diffusive, we use the following fitting equation [61]:

$$I_{\text{uptake}} = I_{\infty} + (I_0 - I_{\infty})e^{-t/\tau_{\text{uptake}}} \quad (4.3)$$

where I_{∞} , I_0 and τ_{uptake} represent the final sulforhodamine B intensity of the GUV, the initial sulforhodamine B intensity of the GUV prior to the pulse and the characteristic time of the uptake of the dye molecules. The two fitting parameters I_{∞} and τ_{uptake} for the actin-encapsulated GUVs after a pulse are larger than for the empty GUVs (Figure 4.4). A former study on the dye leakage of GUVs with a high temporal resolution showed that the leakage of dye mainly occurred through macropores [62]. Similarly, we observed macropore formation for the empty GUVs, which was accompanied with $\sim 2\%$ uptake of dye molecules after a single pulse and a characteristic uptake time of approximately 12 seconds. Taken together, these observations indicate that most dye transport occurs during

the pulse and shortly after the pulse. It must be noted that earlier studies have shown a resealing of the membrane in 10 ms [40], which is faster than our temporal resolution. Therefore, the actual characteristic uptake time might be considerably smaller than the determined 12 seconds. Nevertheless, the presence of the ionophore in the membrane may slow down the resealing of the membrane to the approximated 12 seconds. The actin-encapsulated GUVs, on the other hand, do not show any macro-pores and exhibit a longer characteristic uptake time of approximately 146 seconds together with a dye uptake of $\sim 38\%$. Our observations are reminiscent of prior observations of a high and long-lived permeability for lipid membranes associated with an agarose mesh work [62]. In that work, it was proposed that the agarose mesh stabilizes pores formed by an electric pulse. The actin network in our experiments appears to affect the membrane stability similarly, enabling transport through the membrane for a longer duration than of the empty GUVs.

Despite the differences between the biomimetic cortex in our experiments, bundled and inhomogeneously distributed over the membrane, and the actin cortex of a living cell, similarities can be found between the response of our actin-encapsulated GUVs and living cells to electric pulses. The exponential increase in uptake of the actin-encapsulated GUVs appears similar to the exponential uptake of living cells [61]. The presence of an actin network is known to increase the membrane tension [63, 64]. The enhanced tension likely explains the increased permeability of the actin-encapsulated GUVs, compared to the empty GUVs at similar pulses. Additionally, a slow resealing process of the membrane is consistent with observations in electroporated cells, where the role of the actin cortex is the resealing of the permeated structures [17, 18].

4.3.3 Stability of the actin network

To assess the response of the actin network inside the GUV to the electric pulse, the GUV and actin were concurrently visualized by confocal microscopy. The fluorescence signals of the membrane and actin network were used to detect the area of the GUV and the actin intensity, respectively (see Figure S4.5.1 in the supplementary material). In order to determine the coverage of the actin network on the inner membrane surface and any possible lateral inhomogeneities of the shell, a confocal z-stack was taken before and after the pulse. Consecutive pulses of increasing voltage were applied to the GUVs, with at least 1 minute in between the pulses to minimize the effect of the former pulse. Similar to earlier studies [12, 39, 43, 65], the empty GUVs exhibit increasing shrinkage with higher electric pulses (Figure 4.5A). The immediate high pulses reveal the cumulative effect of multiple pulses on the shrinkage of the empty GUVs. A single pulse of 300 V/mm does not induce the same shrinkage as a 300 V/mm pulse preceded by multiple pulses at lower field strength (see Figure 4.5A). Compared to the empty GUVs, the actin-encapsulated GUVs display shrinkage at higher electric fields, i.e. the actin-supported bilayer has a higher electrical stability (Figure 4.5B). This could be caused by the increased surface viscosity of the bilayer due to the presence of the actin layer, as it was recently shown that

4. UNRAVELLING THE RESPONSE OF A BIOMIMETIC ACTIN CORTEX TO ELECTRIC PULSES IN VESICLES

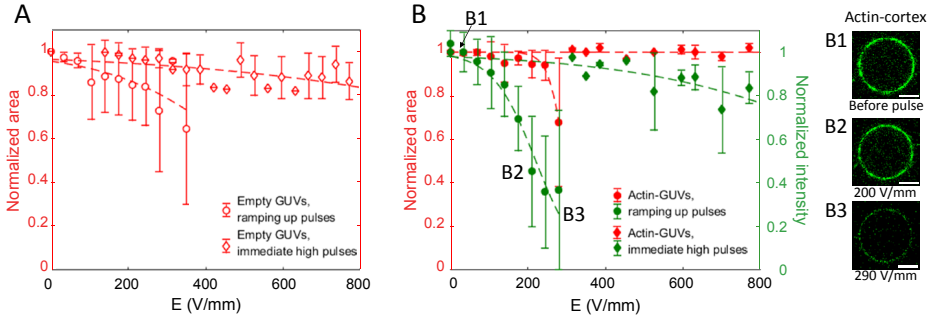


Figure 4.5. The structural stability of the empty and the actin-encapsulated GUVs. (A) The area loss of the empty GUVs as a function of electric field. The average normalized area is shown of 15 empty GUVs in total with an average radius of $\sim 10\ \mu\text{m}$, of which 9 have been exposed to the consecutive ramping up pulses and 5 to immediate high pulses. These experiments have been repeated four times on different days. (B) The area loss of the actin-encapsulated GUVs as a function of the electric field, which is associated with an intensity loss of the actin shell. The average normalized area is shown of 17 actin-encapsulated GUVs in total with an average radius of $\sim 10\ \mu\text{m}$, of which 8 have been exposed to the consecutive ramping up pulses and 9 to immediate high pulses. These experiments have been repeated five times on different days. The confocal images of the actin shell show that the intensity loss can be attributed to shell disruption (B1, B2 and B3). Photobleaching of the fluorescence intensity is observed (shown in Figure S.4.4.1. in the supplementary information) and is corrected as discussed in the Materials and Methods section. The dotted lines in the graphs represent a least-squares fit of a sigmoid curve to guide the eye. The scale bar in all images is $5\ \mu\text{m}$.

the shrinkage of the GUVs depends on the surface viscosity of the bilayer [48].

Strikingly, the increasing pulses also result in a decreasing fluorescence signal of the actin at $\sim 150\ \text{V/mm}$, followed by GUV shrinkage at higher electric pulses ($\sim 200\ \text{V/mm}$), as illustrated in Figure 4.5B and Movie S4.1.3. We observe that the decrease in the fluorescence signal of the actin is associated with a breakdown of the actin network. Additionally, the intensity loss of the actin layer due to the electric pulses appears to be slightly more at the poles, where the GUV is facing the electrodes (Movie S4.1.3). However, this radial dependence is not always observed clearly, perhaps because the GUVs can rotate. After the breakdown of the actin network we did not observe any increase in the intensity in the centre of the GUV (see Section S4.5 and Figure S4.5.1 in the supplementary material). By recording the photobleaching of the actin signal in the absence of the pulse and also the response of GUVs with encapsulated actin network to immediate high pulses, we could confirm that the fluorescence decrease is caused by the breakdown of the network and is not a side effect of bleaching. This notion is further supported by the observation that after the pulse, the actin fluorescence signal progressively decreases for several tens of seconds. This gradual decrease in the signal indicates a slow breakdown of the actin network. In addition, the shrinkage of the actin-encapsulated GUVs at higher electric fields than of the empty GUVs indicates that initially the actin network stabilizes the membrane and that shrinkage only sets in after the breakdown of the network.

Our observations are reminiscent of observations that have been observed for human cell

lines [22] and plant cells [23] exposed to nanosecond pulsed electric fields (nsPEF). The nanosecond pulses affect the actin cytoskeleton, which is attributed to depolymerization of the filaments [22, 23]. For plant cells it was reported that nanosecond pulses induce disassembly of the actin [23, 66]. On the contrary, Pakhomov *et al.* [29] have shown for CHO cells that the depolymerization of the actin cortex is due to osmotic swelling of the cells upon electroporation. However, Tolstykh *et al.* [67] have proposed that additional biological processes are involved in actin depolymerization, involving the depletion of phosphatidylinositol-4,5-bisphosphate (PIP₂) lipids. In the GUV model system, we can exclude biochemical processes and in addition no osmotic swelling was observed in our experiments. The only factors present that might cause actin depolymerization are the mechanical forces, originating from the induced electrical membrane stress during the pulse, as well as the electrophoretic forces acting on the actin filaments as soon as the membrane is permeabilized.

We therefore estimate the magnitude of both these forces, the mechanical and the electrophoretic forces, modelling the actin filaments as semiflexible polymers. For simplicity, we ignore the presence of actin bundles (Figure S4.2.1 in the supplementary information). Assuming a uniform distribution of actin filaments over the membrane surface, the total number of filaments underneath the lipid bilayer can be estimated as [68]:

$$N_f \sim \frac{c_0 \times \frac{4}{3}\pi R^3 \times d}{l} \quad (4.4)$$

where c_0 and d are the initial concentration ($4.2 \times 10^{21} \text{ m}^{-3}$) and size of actin monomers, and l is the average length of filaments. Assuming the filaments have a length in the order of the actin shell thickness (i.e., $l \sim 1 - 4 \text{ } \mu\text{m}$, see Figure S4.6.1 in the supplementary material) and with $R = 10 \text{ } \mu\text{m}$ and $d = 2.5 \text{ nm}$, we estimate the total number of filaments to be $N_f \sim 10^4$. The mesh size of the filament network can be approximated as: $\zeta \sim \sqrt{A/N_f}$ with A being the surface area of the membrane. The amount of stretch imposed on the length of connections in the actin network reads:

$$\Delta\zeta = \zeta_{\text{ellipsoid}} - \zeta_{\text{sphere}} \quad (4.5)$$

As the total enclosed volume of the GUVs is conserved during their deformation into ellipsoidal topologies in the experiments, the equatorial and polar radii become $b = e^{-1/3}R$ and $a = e^{2/3}R$, respectively, where $e = \sqrt{a/b}$ is taken from the example GUV shown in the schematic in Figure 4.2. We choose a value of $e \sim 1.18$, corresponding to the maximum deformation experienced by the GUVs. The total surface area of the GUVs increases during the deformation and hence the concomitant mesh size stretches by $\Delta\zeta \sim 0.8 \text{ nm}$ (if we assume affine deformations for the network). Such an increase in the length of interconnected filaments induces a maximum mechanical force of the order of $f_m \sim 34 \text{ pN}$ for a stretching stiffness of $\sim 43 \text{ pN/nm}$ [69, 70]. This value is markedly smaller than the

force needed for either initiating the depolymerization of a filament network [71] or the rupture of single filaments [72], which is in the range of $\sim 100 - 400$ pN. It is, therefore, unlikely that the mechanical forces generated by in-plane tensions are the only origin of the breakdown of the actin network in our experiments. Other mechanisms, including electrophoretic forces, are expected to be involved.

As soon as the membrane is permeabilized by the electric fields, the membrane tension can relax back through the expansion of the pores and the release of the interior fluid. Additionally, the actin shell is exposed to the electric field and consequently actin filaments experience an electrophoretic force, defined as [73]:

$$f_{\text{electrophoretic}} = \xi_h \mu_B E \quad (4.6)$$

where ξ_h and μ_B represent the hydrodynamic friction coefficient per unit length of a filament close to the surface and the electrophoretic mobility of the actin measured in bulk solution, respectively. By assuming an average length of the actin filaments of $1 - 4$ μm and an interaction of the complete filament with the membrane, due to Mg^{2+} -mediated adhesion, the force per unit length can be converted in the electrophoretic force $f_{\text{electrophoretic}}$. The maximum force experienced by the actin filaments corresponds to a condition in which the filaments are perpendicular to the field. As soon as the GUV is permeabilized and pores are formed, the electric field penetrates into the GUV, with a maximum estimated value of $\sim 0.8 E$ at the poles where the GUV is facing the electrodes (see Figure S4.7.2. in the supplementary material). The fluorescence signal of the actin network drops at approximately 150 V/mm (Figure 4.5.A). At this electric field and considering a hydrodynamic friction of $\zeta = 0.034$ N.s/m² (for cytoplasmic fluid motion perpendicular to the filament length [74]) and an electrophoretic mobility of $\mu_B = 10^{-8}$ m²/(V.s), we predict an electrophoretic force of $f_{\text{electrophoretic}} \sim 160$ pN acting on a single filament for a vesicle size of 10 μm . Compared to the mechanical forces calculated above, these forces appear most plausible to initiate depolymerization of the actin network. Moreover, the disruption of the network mostly occurs above the critical transmembrane voltage (see Figure S4.8.1 in the supplementary material), enabling the electrophoretic forces to affect the actin filaments.

4.4 CONCLUSION

To shed light on the role of the actin cortex on the electroporation of cells, we have prepared GUVs with an encapsulated actin network that forms a biomimetic cortex and exposed them to electric pulses. Time-lapse imaging of the membrane revealed that the increased rigidity of the GUVs due to the rigidification by the actin network [53] inhibits large deformation of the GUVs during the electric pulses. Additionally, we found that the actin layer prevents the formation of large pores, referred to as macropores. Finally, we observed that membrane resealing after pulse application is significantly longer in the

presence of the actin shell than for a bare membrane. Interestingly, time-lapse imaging of actin revealed that, at higher electric fields, the electric pulses cause depolymerization of the actin shell. Based on the estimation of the relevant forces, we suggest that actin shell disruption is predominantly triggered by the electrophoretic forces on the actin filaments during the pulses.

Although our biomimetic cortex is still far from mimicking the actual actin cortex of a living cell, the behaviour of the actin-encapsulated GUVs already show the relevance of modelling the plasma membrane more closely. Our results provide the first step towards understanding the major differences between the electroporation of living cells and GUVs such as (lack of) macropore formation and the resealing dynamics of the defects. Consequently, these actin-supported GUVs enable exploring the behaviour of more complex systems, such as the mechanism of electro-gene transfection.

4.5 REFERENCES

1. Haase, K., and Pelling, A.E., The role of the actin cortex in maintaining cell shape. *Communicative & Integrative Biology*, 2013. 6(6): p. e26714.
2. Salbreux, G., Charras, G., and Paluch, E., Actin cortex mechanics and cellular morphogenesis. *Trends Cell Biol*, 2012. 22(10): p. 536-45.
3. Simon, C., Kusters, R., Caorsi, V., Allard, A., Abou-Ghali, M., Manzi, J., Di Cicco, A., Lévy, D., Lenz, M., Joanny, J.-F., Campillo, C., Plastino, J., Sens, P., and Sykes, C., A direct proof that sole actin dynamics drive membrane deformations. *bioRxiv*, 2018.
4. Heinemann, F., Vogel, S.K., and Schwille, P., Lateral Membrane Diffusion Modulated by a Minimal Actin Cortex. *Biophysical Journal*, 2013. 104(7): p. 1465-1475.
5. Honigsmann, A., Sadeghi, S., Keller, J., Hell, S.W., Eggeling, C., and Vink, R., A Lipid Bound Actin Meshwork Organizes Liquid Phase Separation in Model Membranes. *Biophysical Journal*, 2014. 106(2): p. 634a-634a.
6. Bray, D., and White, J.G., Cortical Flow in Animal-Cells. *Science*, 1988. 239(4842): p. 883-888.
7. Towhidi, L., Kotnik, T., Pucihar, G., Firoozabadi, S.M., Mozdarani, H., Miklavcic, D., Variability of the Minimal Transmembrane Voltage Resulting in Detectable Membrane Electroporation. *Electromagnetic Biology and Medicine*, 2008. 27(4): p. 372-385.
8. Teissie, J., Golzio, M., and Rols, M.-P., Mechanisms of cell membrane electroporation: A minireview of our present (lack of ?) knowledge. *Biochimica et Biophysica Acta (BBA) - General Subjects*, 2005. 1724(3): p. 270-280.
9. Rols, M.-P., and Teissie, J., Electroporation of mammalian cells. *Quantitative*



analysis of the phenomenon. *Biophysical Journal*, 1990. 58(5): p. 1089-1098.

10. Lopez, A., Rols, M.-P., and Teissie, J., ^{31}P NMR analysis of membrane phospholipid organization in viable, reversibly electroporabilized Chinese hamster ovary cells. *Biochemistry*, 1988. 27(4): p. 1222-8.

11. Kinosita, K., Jr., and Tsong, T.Y., Voltage-induced pore formation and hemolysis of human erythrocytes. *Biochim Biophys Acta*, 1977. 471(2): p. 227-42.

12. Tekle, E., Astumian, R.D., Friauf, W.A., and Chock, P.B., Asymmetric pore distribution and loss of membrane lipid in electroporated DOPC vesicles. *Biophysical Journal*, 2001. 81(2): p. 960-968.

13. Benz, R., and Zimmermann, U., Relaxation Studies on Cell-Membranes and Lipid Bilayers in the High Electric-Field Range. *Bioelectrochemistry and Bioenergetics*, 1980. 7(4): p. 723-739.

14. Teissie, J., and Tsong, T.Y., Electric field induced transient pores in phospholipid bilayer vesicles. *Biochemistry*, 1981. 20(6): p. 1548-1554.

15. Sowers, A.E., The long-lived fusogenic state induced in erythrocyte ghosts by electric pulses is not laterally mobile. *Biophysical Journal*, 1987. 52(6): p. 1015-1020.

16. Weaver, J.C., Electroporation Theory, in *Animal Cell Electroporation and Electrofusion Protocols*, J.A. Nickoloff, Editor. 1995, Humana Press: Totowa, NJ. p. 3-28.

17. Rols, M.-P., and Teissie, J., Experimental evidence for the involvement of the cytoskeleton in mammalian cell electroporabilization. *Biochimica et Biophysica Acta (BBA) - Biomembranes*, 1992. 1111(1): p. 45-50.

18. Teissie, J., and Rols, M.-P., Manipulation of Cell Cytoskeleton Affects the Lifetime of Cell Membrane Electroporabilization. *Annals of the New York Academy of Sciences*, 1994. 720(1): p. 98-110.

19. Weaver, J.C., and Chizmadzhev, Y.A., Theory of electroporation: A review. *Bioelectrochemistry and Bioenergetics*, 1996. 41(2): p. 135-160.

20. Rosazza, C., Buntz, A., Rieß, T., Wöll, D., Zumbusch, A., and Rols, M.-P., Intracellular Tracking of Single-plasmid DNA Particles After Delivery by Electroporation. *Molecular Therapy*, 2013. 21(12): p. 2217-2226.

21. Rosazza, C., Meglic, S.H., Zumbusch, A., Rols, M.-P., and Miklavcic, D., Gene Electrotransfer: A Mechanistic Perspective. *Current Gene Therapy*, 2016. 16(2): p. 98-129.

22. Stacey, M., Fox, P., Buescher, S., and Kolb, J., Nanosecond pulsed electric field induced cytoskeleton, nuclear membrane and telomere damage adversely impact cell survival. *Bioelectrochemistry*, 2011. 82(2): p. 131-134.

23. Berghofer, T., Eing, C., Flickinger, B., Hohenberger, P., Wegner, L.H., Frey, W., and Nick, P., Nanosecond electric pulses trigger actin responses in plant cells. *Biochemical and Biophysical Research Communications*, 2009. 387(3): p. 590-595.
24. Hohenberger, P., Eing, C., Straessner, R., Durst, S., Frey, W., and Nick, P., Plant actin controls membrane permeability. *Biochimica Et Biophysica Acta-Biomembranes*, 2011. 1808(9): p. 2304-2312.
25. Thompson, G.L., Roth, C., Tolstykh, G., Kuipers, M., and Ibey, B.L., Disruption of the Actin Cortex Contributes to Susceptibility of Mammalian Cells to Nanosecond Pulsed Electric Fields. *Bioelectromagnetics*, 2014. 35(4): p. 262-272.
26. Xiao, D.Y., Tang, L., Zeng, C., Wang, J., Luo, X., Yao, C., and Sun, C., Effect of actin cytoskeleton disruption on electric pulse-induced apoptosis and electroporation in tumour cells. *Cell Biology International*, 2011. 35(2): p. 99-104.
27. Stacey, M., Stickley, J., Fox, P., Statler, V., Schoenbach, K., Beebe, S.J., and Buescher, S., Differential effects in cells exposed to ultra-short, high intensity electric fields: cell survival, DNA damage, and cell cycle analysis. *Mutation Research-Genetic Toxicology and Environmental Mutagenesis*, 2003. 542(1-2): p. 65-75.
28. Mahlke, M.A., Navara, C., and Ibey, B.L., Effects of Nanosecond Pulsed Electrical Fields (nsPEFs) on the Cell Cycle of CHO and Jurkat Cells. *Optical Interactions with Tissue and Cells Xxv; and Terahertz for Biomedical Applications*, 2014. 8941.
29. Pakhomov, A.G., Xiao, S., Pakhomova, O.N., Semenov, I., Kuipers, M.A., and Ibey, B.L., Disassembly of actin structures by nanosecond pulsed electric field is a downstream effect of cell swelling. *Bioelectrochemistry*, 2014. 100: p. 88-95.
30. Chopinet, L., and Rols, M.-P., Nanosecond electric pulses: A mini-review of the present state of the art. *Bioelectrochemistry*, 2015. 103: p. 2-6.
31. Abidor, I.G., Arakelyan, V.B., Chernomordik, L.V., Chizmadzhev, Y.A., Pastushenko, V.F., and Tarasevich, M.P., Electric breakdown of bilayer lipid membranes: I. The main experimental facts and their qualitative discussion. *Journal of Electroanalytical Chemistry and Interfacial Electrochemistry*, 1979. 104(0): p. 37-52.
32. van Uitert, I., Le Gac, S., and van den Berg, A., Determination of the electroporation onset of bilayer lipid membranes as a novel approach to establish ternary phase diagrams: example of the 1- α -PC/SM/cholesterol system. *Soft Matter*, 2010. 6(18): p. 4420-4429.
33. Sengel, J.T., and Wallace, M.I., Imaging the dynamics of individual electropores. *Proceedings of the National Academy of Sciences*, 2016. 113(19): p. 5281-5286.
34. Dimova, R., Riske, K.A., Aranda, S., Bezlyepkina, N., Knorr, R.L., and Lipowsky, R., Giant vesicles in electric fields. *Soft Matter*, 2007. 3(7): p. 817-827.



35. Dimova, R., Bezlyepkina, N., Jordö, M.D., Knorr, R.L., Riske, K.A., Staykova, M., Vlahovska, P.M., Yamamoto, T., Yang, P., and Lipowsky, R., Vesicles in electric fields: Some novel aspects of membrane behavior. *Soft Matter*, 2009. 5(17): p. 3201-3212.
36. Portet, T., Mauroy, C., Démery, V., Houles, T., Escoffre, J.M., Dean, D.S., and Rols, M.-P., Destabilizing Giant Vesicles with Electric Fields: An Overview of Current Applications. *The Journal of Membrane Biology*, 2012. 245(9): p. 555-564.
37. Powell, K.T., and Weaver, J.C., Transient aqueous pores in bilayer membranes: A statistical theory. *Bioelectrochemistry and Bioenergetics*, 1986. 15(2): p. 211-227.
38. Needham, D., and Hochmuth, R.M., Electro-mechanical permeabilization of lipid vesicles. Role of membrane tension and compressibility. *Biophysical Journal*, 1989. 55(5): p. 1001-1009.
39. Portet, T., and Dimova, R., A New Method for Measuring Edge Tensions and Stability of Lipid Bilayers: Effect of Membrane Composition. *Biophysical Journal*, 2010. 99(10): p. 3264-3273.
40. Riske, K.A., and Dimova, R., Electro-Deformation and Poration of Giant Vesicles Viewed with High Temporal Resolution. *Biophysical Journal*, 2005. 88(2): p. 1143-1155.
41. Isambert, H., Understanding the Electroporation of Cells and Artificial Bilayer Membranes. *Physical Review Letters*, 1998. 80(15): p. 3404-3407.
42. Smith, K.C., Neu, J.C., and Krassowska, W., Model of Creation and Evolution of Stable Electropores for DNA Delivery. *Biophysical Journal*, 2004. 86(5): p. 2813-2826.
43. Portet, T., Camps i Febrer, F., Escoffre, J.M., Favard, C., Rols, M.P., and Dean, D.S., Visualization of Membrane Loss during the Shrinkage of Giant Vesicles under Electropulsation. *Biophysical Journal*, 2009. 96(10): p. 4109-4121.
44. Sadik, M.M., Li, J., Shan, J.W., Shreiber, D.I., and Lin, H., Vesicle deformation and poration under strong dc electric fields. *Physical Review E*, 2011. 83(6): p. 066316.
45. Kinoshita Jr, K., Hibino, M., Itoh, H., Shigemori, M., Hirano, K., Kirino, Y., and Hayakawa, H., 3 - Events of Membrane Electroporation Visualized on a Time Scale from Microsecond to Seconds A2 - Chang, Donald C, in *Guide to Electroporation and Electrofusion*, B.M. Chassy, J.A. Saunders, and A.E. Sowers, Editors. 1992, Academic Press: San Diego. p. 29-46.
46. Moroz, J.D., and Nelson, P., Dynamically stabilized pores in bilayer membranes. *Biophysical Journal*, 1997. 72(5): p. 2211-2216.
47. Knorr, R.L., Staykova, M., Gracià, R.S., and Dimova, R., Wrinkling and electroporation of giant vesicles in the gel phase. *Soft Matter*, 2010. 6(9): p. 1990-1996.

48. Perrier, D.L., Rems, L., Kreutzer, M.T., and Boukany, P.E., The role of gel-phase domains in electroporation of vesicles. *Scientific Reports*, 2018. 8.
49. Chang, D.C., and Reese, T.S., Changes in membrane structure induced by electroporation as revealed by rapid-freezing electron microscopy. *Biophysical Journal*, 1990. 58(1): p. 1-12.
50. Dimitrov, D.S., and Sowers, A.E., Membrane electroporation — fast molecular exchange by electroosmosis. *Biochimica et Biophysica Acta (BBA) - Biomembranes*, 1990. 1022(3): p. 381-392.
51. Weaver, J.C., Harrison, G.I., Bliss, J.G., Mourant, J.R., and Powell, K.T., Electroporation - High-Frequency of Occurrence of a Transient High-Permeability State in Erythrocytes and Intact Yeast. *Febs Letters*, 1988. 229(1): p. 30-34.
52. Tekle, E., Astumian, R.D., and Chock, P.B., Selective and asymmetric molecular transport across electroporated cell membranes. *Proceedings of the National Academy of Sciences*, 1994. 91(24): p. 11512-11516.
53. Schäfer, E., Vache, M., Kliesch, T.-T. and Janshoff, A., Mechanical response of adherent giant liposomes to indentation with a conical AFM-tip. *Soft Matter*, 2015. 11(22): p. 4487-4495.
54. Riske, K.A., and Dimova, R., Electric Pulses Induce Cylindrical Deformations on Giant Vesicles in Salt Solutions. *Biophysical Journal*, 2006. 91(5): p. 1778-1786.
55. Riske, K.A., Knorr, R.L., and Dimova, R., Bursting of charged multicomponent vesicles subjected to electric pulses. *Soft Matter*, 2009. 5(10): p. 1983-1986.
56. Kotnik, T., and Pucihar, G., Induced transmembrane voltage – theory, modeling, and experiments, in *Advanced Electroporation Techniques in Biology and Medicine*, A.G. Pakhomov, D. Miklavčič, and M.S. Markov, Editors. 2010, CRC Press, Boca Raton. p. 51-70.
57. Gracia, R.S., Bezlyepkina, N., Knorr, R.L., Lipowsky, R., and Dimova, R., Effect of cholesterol on the rigidity of saturated and unsaturated membranes: fluctuation and electrodeformation analysis of giant vesicles. *Soft Matter*, 2010. 6(7): p. 1472-1482.
58. Yu, M., Lira, R.B., Riske, K.A., Dimova, R., and Lin, H., Ellipsoidal Relaxation of Deformed Vesicles. *Physical Review Letters*, 2015. 115(12): p. 128303.
59. Guevorkian, K., Manzi, J., Pontani, L.L., Brochard-Wyart, F., and Sykes, C., Mechanics of Biomimetic Liposomes Encapsulating an Actin Shell. *Biophys J*, 2015. 109(12): p. 2471-9.
60. Hackl, W., Barmann, M., and Sackmann, E., Shape changes of self-assembled actin bilayer composite membranes. *Physical Review Letters*, 1998. 80(8): p. 1786-1789.



61. Pucihar, G., Kotnik, T., Miklavcic, D., and Teissié, J., Kinetics of Transmembrane Transport of Small Molecules into Electroporabilized Cells. *Biophysical Journal*, 2008. 95(6): p. 2837-2848.
62. Lira, R.B., Dimova, R., and Riske, K.A., Giant Unilamellar Vesicles Formed by Hybrid Films of Agarose and Lipids Display Altered Mechanical Properties. *Biophysical Journal*, 2014. 107(7): p. 1609-1619.
63. Diz-Muñoz, A., Fletcher, D.A., and Weiner, O.D., Use the force: membrane tension as an organizer of cell shape and motility. *Trends in Cell Biology*, 2013. 23(2): p. 47-53.
64. Pontes, B., Viana, N.B., Salgado, L.T., Farina, M., Moura Neto, V., and Nussenzveig, H.M., Cell Cytoskeleton and Tether Extraction. *Biophysical Journal*, 2011. 101(1): p. 43-52.
65. Mauroy, C., Portet, T., Winterhalder, M., Bellard, E., Blache, M.C., Teissié, J., Zumbusch, A., and Rols, M.-P., Giant lipid vesicles under electric field pulses assessed by non invasive imaging. *Bioelectrochemistry*, 2012. 87: p. 253-259.
66. Hochmuth, F.M., Shao, J.Y., Dai, J., and Sheetz, M.P., Deformation and flow of membrane into tethers extracted from neuronal growth cones. *Biophysical Journal*, 1996. 70(1): p. 358-369.
67. Tolstykh, G.P., Thompson, G.L., Beier, H.T., Steelman, Z.A., and Ibey, B.L., nsPEF-induced PIP2 depletion, PLC activity and actin cytoskeletal cortex remodeling are responsible for post-exposure cellular swelling and blebbing. *Biochemistry and Biophysics Reports*, 2017. 9: p. 36-41.
68. Pontani, L.L., van der Gucht, J., Salbreux, G., Heuvingh, J., Joanny, J.F., and Sykes, C., Reconstitution of an actin cortex inside a liposome. *Biophys J*, 2009. 96(1): p. 192-8.
69. Kojima, H., Ishijima, A., and Yanagida, T., Direct Measurement of Stiffness of Single Actin-Filaments with and without Tropomyosin by in-Vitro Nanomanipulation. *Proceedings of the National Academy of Sciences of the United States of America*, 1994. 91(26): p. 12962-12966.
70. Liu, X.M., and Pollack, G.H., Mechanics of F-actin characterized with microfabricated cantilevers. *Biophysical Journal*, 2002. 83(5): p. 2705-2715.
71. Zhang, X.Q., Hu, X., Lei, H., Hua, J., and Zhang, Y., Mechanical force-induced polymerization and depolymerization of F-actin at water/solid interfaces. *Nanoscale*, 2016. 8(11): p. 6008-6013.
72. Tsuda, Y., Yasutake, H., Ishijima, A., and Yanagida, T., Torsional rigidity of single actin filaments and actin-actin bond breaking force under torsion measured directly by *in vitro* micromanipulation. *Proceedings of the National Academy of Sciences*, 1996. 93(23):

p. 12937.

73. Riveline, D., Ott, A., Jülicher, F., Winkelmann, D.A., Cardoso, O., Lacapère, J.J., Magnúsdóttir, S., Viovy, J.L., Gorre-Talini, L., and Prost, J., Acting on actin: the electric motility assay. *European Biophysics Journal with Biophysics Letters*, 1998. 27(4): p. 403-408.

74. Hunt, A.J., Gittes, F., and Howard, J., The Force Exerted by a Single Kinesin Molecule against a Viscous Load. *Biophysical Journal*, 1994. 67(2): p. 766-781.



S 4 APPENDIX

S 4.1 Movie captions

Supplementary movie S4.1.1. The empty GUV of Figure 4.2B during a 500 μs pulse of 220 V/mm. The scale bar in the movie is 5 μm . The actual duration of the movie is 19.62 ms.

Supplementary movie S4.1.2. The actin-encapsulated GUV of Figure 4.2C during a 500 μs pulse of 130 V/mm. The scale bar in the movie is 5 μm . The actual duration of the movie is 5.45 ms.

Supplementary movie S4.1.3. The disruption of the actin network of the actin-encapsulated GUV shown in Figure 4.5B. The GUV membrane is shown in red, and the actin network in green. The scale bar in the movie is 5 μm . The movie is speed up 34 times, the actual duration of the movie is 378 s.

S 4.2 Visualization of the actin shell

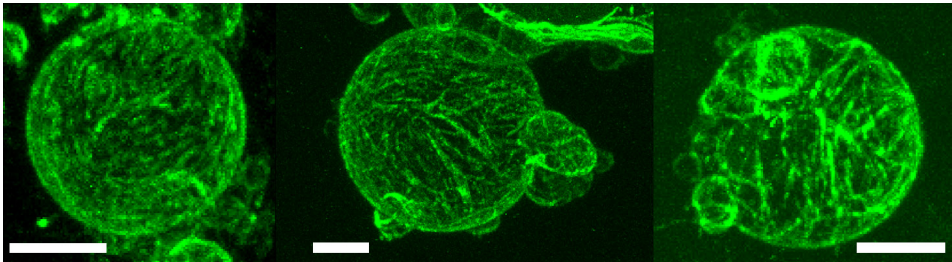


Figure S4.2.1. Three z-stacks of confocal images of the formed actin network. For these images, only the actin is fluorescently labelled. The scale bar in all images is 5 μm .

S 4.3 Polymerisation on the outside of the GUV

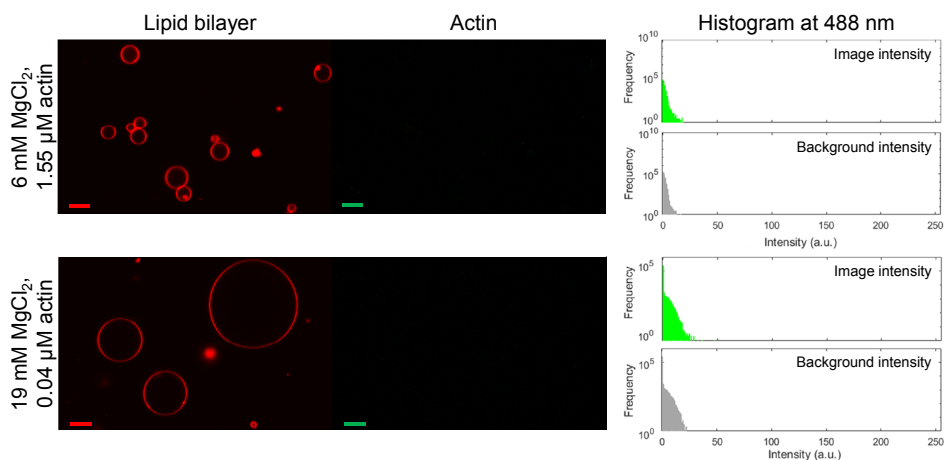


Figure S4.3.1. Polymerisation on the outside of empty GUVs. Top: Empty GUVs with an outside concentration of actin and MgCl_2 of the overnight-conditions (1.55 μM actin and 6 mM MgCl_2). Bottom: Empty GUVs with an outside concentration of actin and MgCl_2 during the electroporation experiments (0.04 μM actin and 19 mM MgCl_2). The red fluorescence signal shows the membrane, and the green fluorescence signal shows the actin. The histograms on the right gives the histogram of the intensity at 488 nm, the excitation wavelength for the actin network. The background intensity is obtained from empty GUVs in the absence of actin, imaged at the same conditions. In both cases, no polymerisation of the actin monomers on the outside of the GUVs and no significant increase in the intensity at 488 nm is observed. The scale bar in all images is 10 μm .

S 4.4 Photobleaching correction

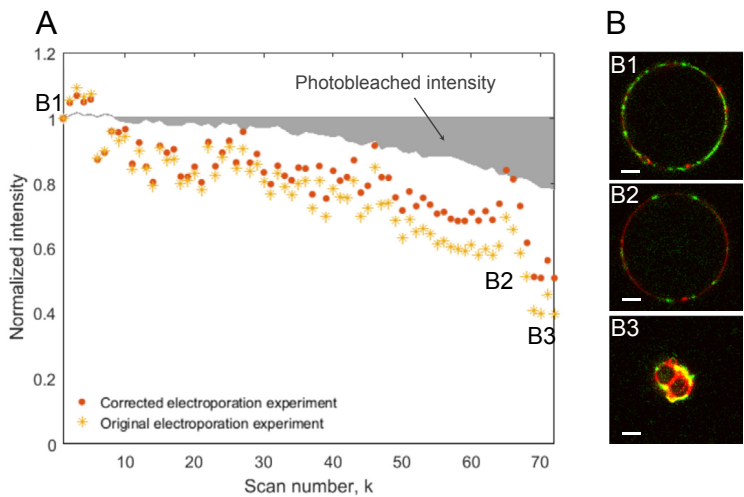


Figure S4.4.1. (A) The correction of the intensity loss of the actin, normalized over the initial intensity, during the electroporation experiments for photobleaching, as discussed in the main text. The time interval between the scans is 7.07 seconds. (B) Three images at different times during the experiment, indicated in the graph (B1, B2 and B3), where the signal of the membrane is depicted in red and the signal of the actin cortex in green. The scale bar in all images is 5 μm .

S 4.5 Background signal of confocal experiments

The fluorescent signal of the actin network is obtained by determining the gray value of a square surface that fits the maximum size of the GUV in the different imaging planes (indicated in red in Figure S4.5.1). Therefore, the intensity decrease that we observed upon the application of electric pulses includes both the actin network and actin in the bulk of the GUVs. Based on our estimates of the forces acting on the actin filaments during the pulse, electrophoretic forces can disrupt the actin network into single filaments. Consequently, one would expect that either the intensity in the bulk of the GUV increases (when the actin remains in the GUV), or intensity on the outside of the GUV increases if the membrane is permeabilized (i.e. the background). However, since the GUV concentration is dilute and the expelled actin can diffuse freely, we do not expect to be able to detect any increase in fluorescence of the background. The fluorescence intensity of the bulk actin inside the GUV can only be determined from the equatorial plane (indicated in blue in Figure S4.5.1), whereas the fluorescent intensity of the actin network can be obtained from the complete z-stack. Consequently, the mean intensity of the GUV is dominated by the fluorescent signal of the actin network, as can be seen in Figure S4.5.1B. As the electroporation experiments continue, photobleaching takes place, reducing the total actin signal, as can be seen in Figure S4.5.1C. Therefore, both the background fluorescent intensity and the inside fluorescent intensity approach the noise level of our camera. We are therefore unable to conclude whether the actin remains in the bulk of the GUV or is expelled. We did not observe any re-polymerization in any experiments at higher electric fields ($> 150 \text{ V/mm}$), suggesting that some actin may have been expelled, lowering the concentration on the inside of the GUV below the critical concentration for polymerization. However, it must be noted that as the GUVs are permeabilized by the electric pulse, other side effects may affect the re-polymerization of actin network (such as local pH fluctuations and local Mg^{2+} concentration changes).



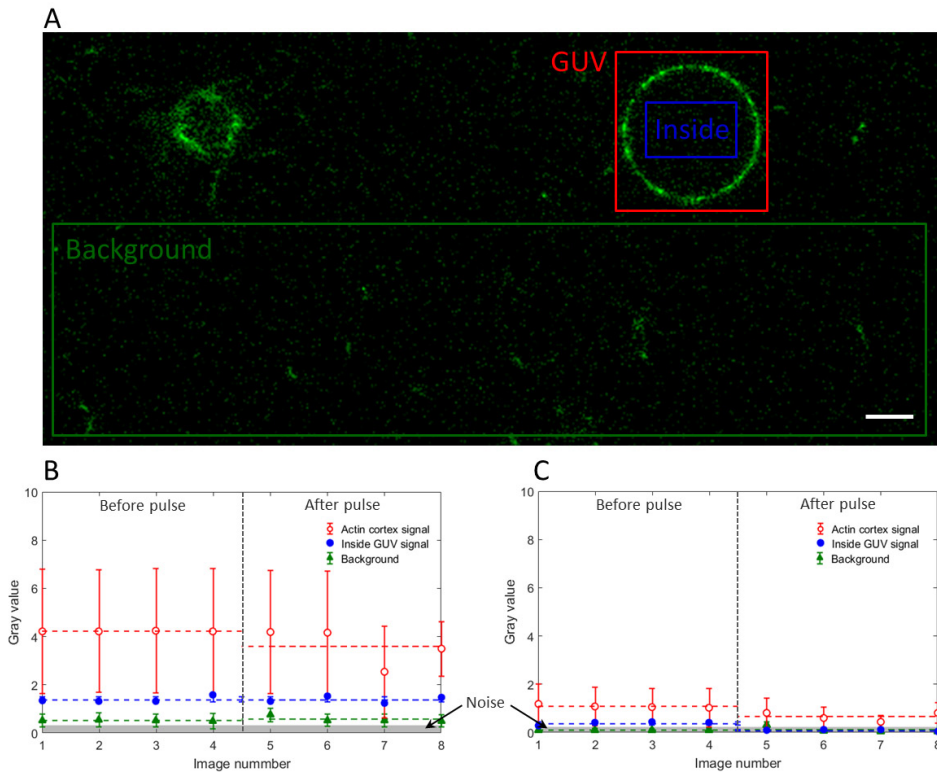


Figure S4.5.1. The gray levels of different regions of the confocal images. (A) A confocal image showing the areas of interest: background (red), inside of the GUV (blue) and the squared area around the GUV (red). (B) The gray values at the three regions of interest during the first pulse (~ 100 V/mm). (C) The gray values at the three regions of interest during the last pulse (~ 320 V/mm). The dotted lines indicate the mean values before and after the pulse. The error bar is $5\text{ }\mu\text{m}$.

S 4.6 Thickness of the actin network

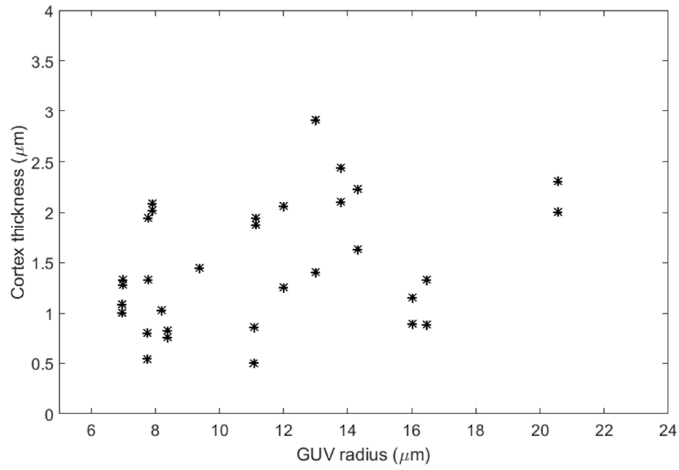


Figure S4.6.1. The relation between the thickness of the the actin cortexes and the radius of all reported GUVs. The thickness of the actin cortexes has been determined by use of the confocal images and are used as an estimate of the cortex thickness for the force calculations.

S 4.7 Electric field inside an electroporated GUV

We numerically calculated the electric field inside an electroporated GUV using Comsol Multiphysics software, similarly as in previous works [1, 2]. The model of a GUV exposed to an electric field E is built in a 2D axisymmetric coordinate system (Figure S4.7.1). A spherical GUV is positioned inside a cylindrical domain representing the external liquid. The exposure of the GUV to an electric pulse is modelled by assigning an electric potential to two opposite sides of the external domain (Figure S4.7.1). The electric potential distribution Ψ is calculated by

$$\nabla \left[\left(\lambda_{i,e} + \epsilon_{i,e} \frac{\partial}{\partial t} \right) \nabla \Psi \right] = 0 \quad (\text{S4.1})$$

where $\lambda_{i,e}$ and $\epsilon_{i,e}$ denote, respectively, the conductivity and the dielectric permittivity of the internal (subscript i) or external (subscript e) liquid. The GUV membrane is modelled via a boundary condition, which describes the continuity of the normal component of the electric current density \mathbf{J} across the membrane

$$\mathbf{n} \cdot \mathbf{J} = \left[G_m + C_m \frac{\partial}{\partial t} \right] \Psi_m \quad (\text{S4.2})$$

where \mathbf{n} denotes the unit vector normal to the membrane surface, and G_m and C_m denote the membrane conductance and capacitance, respectively. The transmembrane voltage Ψ_m corresponds to the difference between the electric potentials on the two sides of the membrane. Membrane electroporation is included into the model by solving the ordinary differential equation, which describes the density of electropores created in the membrane under the influence of the induced transmembrane voltage [3]

$$\frac{dN}{dt} = \alpha \exp \left(\frac{\Psi_m^2}{V_{ep}^2} \right) \left(1 - \frac{N}{N_0} \exp \left(-q \frac{\Psi_m^2}{V_{ep}^2} \right) \right) \quad (\text{S4.3})$$

Since electropores conduct ions, they increase the membrane conductance, which in turn affects the transmembrane voltage. The increase in membrane conductance due to

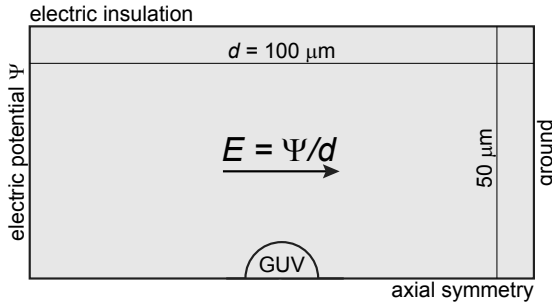


Figure S4.7.1. A 2-D schematic geometry of a spherical GUV exposed to an electrical field E inside a cylindrical domain representing the external liquid.

electropores is [2]

$$G_{ep} = N \frac{2\pi r_p^2 \lambda_p}{\pi r_p + 2d_m} \quad (\text{S4.4})$$

where r_p , λ_p , and d_m are the pore radius, conductivity of the solution inside the pore, and membrane thickness, respectively. The total membrane conductance G_m in equation (S4.2) is calculated at each time step as the sum of the passive membrane conductance G_{m0} and the conductance due to electropores G_{ep} . The values of the model parameters are given in Table S4.7.1.

Figure S4.7.2.A shows the magnitude of the electric field inside and around the GUV at the end of 150 V/mm pulse (500 μ s). Note that the electric field values are normalized with respect to the applied electric field, $E_{app} = 150$ V/mm. Figure S4.7.2.B depicts the electric field inside the GUV at two points beneath the membrane. The first point is located at the pole of the GUV (where the membrane normal is parallel to the applied electric field) and the second point is located at the equator of the GUV (where the membrane normal is perpendicular to the applied electric field). At both points the electric field is directed parallel to the applied electric field. As shown, the maximum electric field induced inside the GUV after the electroporation is about $0.2 E_{app}$ and $0.8 E_{app}$ for the vesicle size of $R = 10$ μ m.

Table S4.7.1. Model parameters

Parameter	Symbol	Value	Reference
GUV radius	R	10 μ m	Experiment
Electrical conductivity of internal and external fluid	$\lambda_i \lambda_e$	0.3 S/m	*
Dielectric permittivity of internal and external fluid	$\epsilon_i \epsilon_e$	80	[4]
Passive membrane conductance	$G_{m0} = \lambda_{m0}/d_m$	0.25 S/m ²	[4]
Membrane conductivity	λ_{m0}	10 ⁻⁹ S/m	[4]
Membrane capacitance	C_m	0.7 μ F/cm ²	[4]
Membrane thickness	d_m	4 nm	[4]
Conductivity of solution inside the pore	$\lambda_p = \lambda_i = \lambda_e$	0.3 S/m	[4]
Pore radius	r_p	1 nm	*
Electroporation parameter	α	10 ⁹ m ⁻² s ⁻¹	[3]
Characteristic voltage of electroporation	V_{ep}	0.258 V	[3]
Electroporation constant	q	2.46	[3]
Equilibrium pore density	N_0	15 \times 10 ⁹ m ⁻²	[3]
Applied electric field	E_{app}	150 V/mm	Experiment
Pulse duration	t_{pulse}	500 μ s	Experiment
Pulse rise time	t_{rise}	1 μ s	Arbitrary

* The conductivity was estimated as the conductivity of an aqueous solution of 19 mM, MgCl₂; we took tabulated values [5] for 53 mM (0.5 % mass) MgCl₂ and 106 mM (1.0 % mass) MgCl₂ and used linear extrapolation to obtain the conductivity of 19 mM MgCl₂.

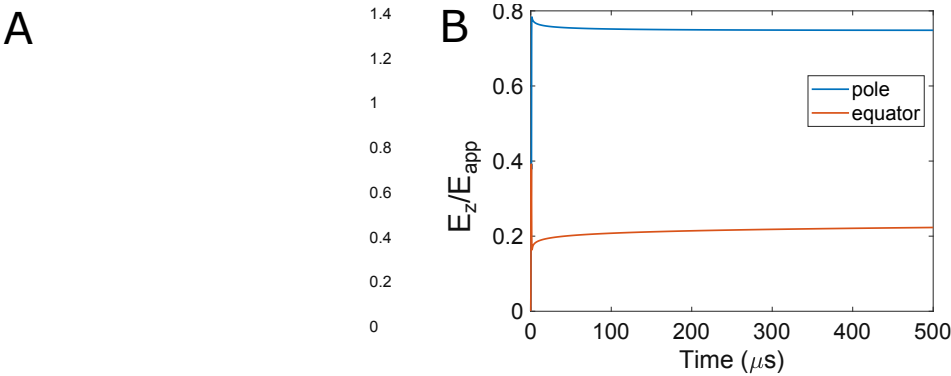


Figure S4.7.2. Magnitude of the electric field inside and around a GUV of size 10 μm exposed to an electric field of 150 V/mm. The electric field is directed from left to right. As shown, the maximum induced electric field inside occurs around the poles.

S 4.8 Actin intensity versus transmembrane voltage

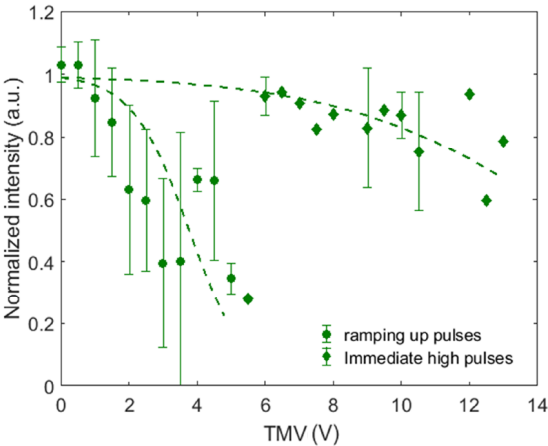


Figure S4.8.1. The averaged normalized intensity of the actin cortex of all GUVs plotted against the calculated transmembrane voltage (TMV). Since the transmembrane cannot increase as soon as the membrane is permeabilized, the estimated TMV is a theoretical value. The GUVs have been exposed to ramping up pulses (ranging from 10 – 300 V/mm with steps of approximately 10 V/mm) and immediate high pulses (ranging from 300 – 1000 V/mm with steps of approximately 200 V/mm), where only 2 to 4 pulses were applied of increasing field. It shows that the intensity decreases above the critical TMV of 1 V, which is in the electroporative regime.

S 4.9 References

1. Retelj, L., Pucihar, G., and Miklav, D., Electroporation of Intracellular Liposomes Using Nanosecond Electric Pulses - A Theoretical Study. *IEEE Transactions on Biomedical Engineering*, 2013. 60(9): p. 2624-2635.
2. Rems, L., Ušaj, M., Kandušer, M., Reberšek, M., Miklavčič, D., and Pucihar, G., Cell electrofusion using nanosecond electric pulses. *Scientific Reports*, 2013. 3: p. 3382.
3. DeBruin, K.A., and Krassowska, W., Modeling Electroporation in a Single Cell. I. Effects of Field Strength and Rest Potential. *Biophysical Journal*, 1999. 77(3): p. 1213-1224.
4. Chan, K.L., Gascoyne, P.R., Becker, F.F., and Pethig, R., Electrorotation of liposomes: verification of dielectric multi-shell model for cells. *Biochimica Et Biophysica Acta-Lipids and Lipid Metabolism*, 1997. 1349(2): p. 182-196.
5. Haynes, W.M., *CRC handbook of chemistry and physics*. 2014: CRC press.





5

Conclusions and outlook



5.1 CONCLUSIONS

The objective of this thesis is to unravel the mechanism of electroporation at the cellular level by modifying the simplified model of an empty GUV. GUVs provide the unique opportunity to decouple the electroporation mechanism of the membrane from the complex biological responses of a living cell triggered during electroporation. They are easy to prepare, tuneable in size and versatile in composition. Most studies have focused on GUVs composed of fluid-phase lipids, similar to the first study in this thesis. These fluid-phase GUVs exhibit the formation during the pulse of macro-pores, that reseal afterwards in hundreds of milliseconds. This phenomenon is often accompanied with shrinkage of the GUV, due to the electrical forces acting on the fluid-phase membrane. The three observations of macro-pore formation, fast resealing of the pore and shrinkage of the vesicle are universal for all fluid-phase GUVs, independent of the molecular architecture of the lipids. The majority of the cell membrane consists of fluid-phase lipids. However, these observations on pure fluid-phase GUVs are inconsistent with the observations of living cells. Therefore, fluid-phase GUVs cannot describe the pores of a living cell, showing that more cellular components are involved than solely a fluid-phase membrane.

By further developing the vesicle as a simplified model of the cell, we are bridging the gap between the electroporation of a single cell and of an empty GUV. The cellular membrane consists of a heterogeneous composition of lipids combined with rigid domains, and connected to the framework of the actin cortex. In this thesis, we have focused on these two aspects, the heterogeneity of the membrane and the actin-cortex adjacent to the membrane, of which the conclusions will be discussed below.

5.1.1 Empty vesicles in electric fields

Empty fluid-phase GUVs have been used to determine the response of the membrane to electric fields. Non-electroporative fields cause electrodeformations of the vesicles, due to the Maxwell stress. The degree of deformation is governed by the elastic stretching modulus of the membrane. In the presence of ions, based on the pulse duration, strength and conductivity ratio of the internal and external solutions ($\chi = \lambda_i / \lambda_e$, where λ_i and λ_e represent the conductivity of the internal and external solutions) the GUV can be deformed either along the electric field lines into a prolate shape ($\chi > 1$) or perpendicular to the field lines into an oblate shape ($\chi < 1$). The two deformations are caused by the different charging kinetics of the membrane on both sides. Similarly, GUVs in the presence of ions can deform along or perpendicular to the electric field lines, causing squared shapes: tube-like deformations ($\chi > 1$), square-like deformations ($\chi \approx 1$) and disk-like deformations ($\chi < 1$). During electroporative pulses the deformations are associated with macro-pores in the fluid-phase GUVs. The formation of the macro-pore is mainly related to the increase in the membrane tension caused by the electric field.

As the pore grows and the internal solvent leaks out, the induced tension is relaxed. The closure velocity of the pore is determined by the edge tension of the pore and the leak-out of the internal solvent. In addition to the macro-pores, a size reduction of the fluid-phase GUVs is observed after the pulse. The size reduction can occur through vesicle formation or tubulation or a combination of the two. However, the mechanism underlying these observations is unknown. In summary, electroporation of fluid-phase GUVs is associated with macro-pore formation together with a GUV size reduction on the form of small vesicle formation and tubulation.

To move towards understanding the response of the heterogeneous cell membrane to electric fields, GUVs with different membrane compositions have been studied. Firstly, the addition of cholesterol to the fluid-phase lipid bilayer induces a two-phase liquid system of liquid ordered and liquid-disordered domains. Based on the architecture of the lipids and the cholesterol percentage, the cholesterol can both strengthen and weaken the membrane, leading to either an increase or a decrease of the critical transmembrane voltage for electroporation. Secondly, mixing two different fluid-phase lipids with a different critical electroporation transmembrane voltage results in an intermediate critical value. Thirdly, the electroporation mechanism of gel-phase GUVs appears different, showing wrinkling and cracks in the membrane instead of the electrodeformations and macro-pores of the fluid-phase GUVs related to the Maxwell stresses. Additionally, the phase-state determines the critical transmembrane voltage for electroporation, which is significantly larger for gel-phase GUVs than for fluid-phase GUVs. In conclusion, a heterogeneous membrane results in an intermediate critical transmembrane voltage of the bilayer and gel-phase lipids alter the electroporation mechanism of the GUVs due to their high bending rigidity.

5.1.2 The response of a heterogeneous membrane to the electric pulse

We have observed that a different electroporation mechanism is operative in fluid-phase membranes than in gel-phase membranes. Electrical tension acting during the electric pulses applied in electroporation experiments can remove fluid-phase lipids from a GUV, due to the low surface viscosity of the lipids. On the contrary, pure gel-phase GUVs have a much higher surface viscosity, inhibiting area loss of the GUV during the pulse, resulting in buckling. Additionally, the gel-phase lipids prevent macro-pore formation. Consequently, fluid-phase GUVs exhibit macro-pore formation accompanied with lipid loss whereas gel-phase GUVs display buckling.

Additionally, we have found the electroporation mechanism of binary GUVs, depending on the gel-phase lipid percentage. Domains of rigid gel-phase patches in a fluid-phase membrane increase the electrical stability of the membrane. An increased buckling effect of these GUVs at higher electric fields shows that the electric field can again remove the fluid-phase lipids while the gel-phase lipids remain within the GUV. Based on the



estimates of the efflux of the GUVs, the pore-sizes appear to be in the same order as observed for the fluid-phase GUVs. Moreover, macro-pores have been observed for GUVs with a high percentage of gel-phase domains ($\sim 80\%$), indicating that the rigid gel-phase domains are not the limiting factor for the pore growth during the pulse. Therefore, the gel-phase domains in the fluid-phase membrane (1) increase the electrical stability of the membrane, (2) impose buckling at higher electric fields when most fluid-phase lipids have been removed by the electric field, and (3) do not affect the expansion of the pores to macro-pores. In conclusions, the findings in this chapter shed light on the role of gel-phase domains in the cell membrane, providing an increased electrical stability to the membrane while the pore size, and thus the transport across the membrane, is not affected.

5.1.3 Electroporation of an actin-supported membrane

One of the main findings of this thesis is that the presence of the cortex limits the expansion of the pore during the pulse, suppressing the formation of macro-pores. These resulting microscopically unobservable permeable structures (pore-like structures or not) in the membrane are more consistent with the structures reported for living cells. Possibly, the growth of the pores is limited to the mesh size of the actin network. Additionally, the presence of the actin cortex suppresses significant lipid loss. Similarly to the gel-phase membrane, the increased rigidity of the membrane due to the actin cortex does not allow lipid loss by the electrical stress. Only after disruption of the cortex, lipid loss can take place. Finally, the rigidity of the membrane due to the presence of the actin cortex reduces the deformation of the GUVs during pulsation with respect to empty fluid-phase GUVs. Increasing the electric fields beyond the electroporation threshold have shown to initiate disruption of the actin cortex, triggered by the electrophoretic forces acting on the filaments during the pulse. In summary, the actin cortex controls the electroporation mechanism as follows: (1) it suppresses the formation of macro-pores, most probably due to the mesh size of the actin-cortex, (2) the increased rigidity of the actin-supported GUV limits the deformation during the pulse, and (3) multiple electroporative pulses can disintegrate the actin-cortex. The findings of this chapter both reveal the role of the actin-cortex during electroporation, suppressing electrodeformation and macro-pore formation, and create new opportunities to reveal the contribution of the intracellular components in the electroporation of cells.

5.2 OUTLOOK

In this thesis, we have shown the electroporation mechanisms of GUV systems approaching towards a living cell. By preparing binary-phase GUVs and actin-supported lipid bilayers, we have systematically increased the knowledge on the electroporation of

a living cell. Developing these more complex vesicle systems to study in electric fields is the first step towards a fundamental understanding of the electroporation mechanism(s). Further exploiting the abilities in the synthetic biology to produce more complex vesicle systems is required to understand electroporation at the single cell level. Additionally, the physical structure of the electro-pore is still unknown. Moreover, dense vesicle systems can create a path towards the control of the electroporation of cell tissue and engineering cell tissue creates the opportunity to systematically study the very complex system of the human tissue. In conclusion, to fully control electroporation for the use of various applications, we must firstly expand the complexity of the vesicle system, secondly zoom in to the subcellular level, thirdly study dense vesicle systems as a step towards tissue electroporation and finally zoom out to the tissue level by studying engineered cellular systems, as will be discussed in the following sections.

5.2.1 Further increase complexity of the GUV

To increase our knowledge on the electroporation mechanism(s) step-by-step, the GUV as a model for the cell can be expanded [1, 2]. The vesicle systems used in this thesis have already shown how more complex GUVs can alter the response of GUVs in electric fields. The binary GUVs show that gel-phase lipids increase the electrical stability of the membrane, without affecting the possibility of macro-pore formation (Chapter 3). In addition, we have found that the actin-cortex does inhibit the formation of macro-pores in the GUV and also increases the life-time of the pores (Chapter 4). However, these vesicle systems are still far from modelling the living cell. Synthetic biology has developed even further, enabling us create more complex GUV systems [3, 4]. Adjacent to the membrane, incorporation of anchoring proteins, such as ezrin, radixin and moesin proteins [5, 6], provide a more realistic interaction between the cortex and membrane. Moreover, cross-linking proteins, like fimbrin, α -actinin and myosin II, determine the integrity of the cortex [7]. Furthermore, in addition to the actin filaments adjacent to the membrane, micro-tubules can be grown in GUVs, mimicking the crowded interior of the cell. The function of these tubules can be expanded even further by adding motor proteins, among which dynein and kinesin, that move across the tubules [8, 9]. Consequently, electroporation studies of these more complex systems can reveal two parts of the single cell electroporation mechanism: first of all these studies would reveal the role of the membrane properties, whether or not influenced by adjacent cellular components, and second of all they would create an insight on the contribution of the interior of the cell to membrane electroporation.

In addition to the fundamental mechanism of membrane electroporation governed by the cellular components, the more extended model of the cell can shed light on the electroporation mechanism of macromolecules, such as DNA plasmid. Experiments on gene delivery to living cells have shown a more complex delivery mechanism for these large molecules, of which the exact mechanism remains unknown. Different suggestions



are the transport of the genes through electrophoretic forces, vesicular uptake through pulse-mediated membrane-gene interaction and pulse-mediated ion-channel transport [10, 11]. Subsequently, after gene-delivery through the membrane, the DNA must reach the nucleus of the cell in order to induce gene expression [12, 13]. On the one hand, the crowded interior of the cell may inhibit free diffusion of the DNA. On the other hand, the molecular motors on the microtubules can provide active transport of the DNA towards the nucleus [1, 2]. The suggested modifications to the GUV model discussed above enable to study both the transport of the genes through the membrane and the transport of the genes inside the crowded cell.

5.2.2 Single pore imaging

Direct visualization of individual electropores in the membrane is challenging due to the small sizes of the electropores and the fast dynamics. Rapid freezing of cells after electroporation has been one of the first attempts to reveal pores [14]. However, this study has led to debate about the side effects of this rapid freezing technique [15]. Sengel and Wallace [16] have cleverly used fluorescent microscopy on planar droplet interface bilayers. By using this method, they have enabled the visualisation of single pores, their distribution of the pores in heterogeneous lipid bilayers and their diffusive behaviour. Additionally, Jeuken attempted to image individual pores with atomic force microscopy (AFM), providing a resolution in the nanometre scale [17]. No pores have been observed, possibly due to the relatively slow imaging technique in the order of minutes with respect to the fast dynamics of the pores.

Using high-speed AFM would combine both the nanometre resolution with the ability to do fast imaging with a temporal resolution of hundreds of milliseconds to seconds. Moreover, this imaging technique can be carried out under physiological conditions. Preliminary results of electroporation experiments using high-speed AFM on planar lipid bilayer supported by a gold support are promising. Applying second range pulses while scanning with similar temporal resolution has shown potential defects in the bilayer (Figure 5.1). Simultaneous conductivity measurements indicate the membrane is permeabilized during these observations. These are the first results of this high-speed AFM electroporation setup. Further exploring these samples can be used to study the pore size as a function of pulse strength and duration. Increasing the probability to find the pores would be to use a two-phase system, where it would be expected that the pores mainly form in the fluid-phase domains. Due to the difference in heights of the gel- and the fluid-phase domains, the two phases can be distinguished from each other. Consequently, these high speed AFM experiments on planar lipid bilayers can unravel the physical structure of the defects formed during electroporation.

Similarly to the actin-encapsulated GUVs, the lipid bilayer model can be expanded by the addition of the actin-cortex below the bilayer. Using this experimental setup of high-

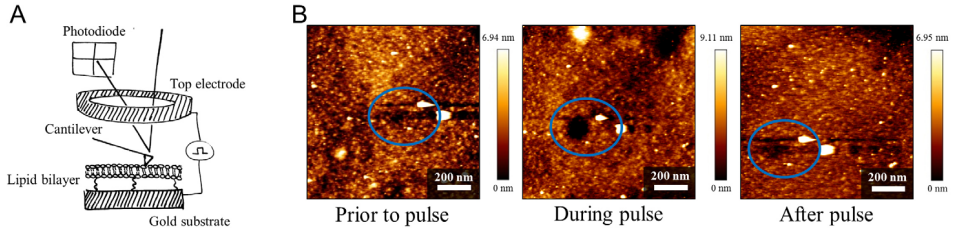


Figure 5.1. (A) A schematic of the high-speed AFM setup for electroporation, not to scale. (B) Three snapshots of a high-speed AFM experiment, prior to, during and after pulsing. Multiple pulses of 12.5 seconds at 600 mV have been applied on a POPC lipid bilayer, supported by a gold substrate. Highlighted in blue is the area where a defect is observed during the pulsing. Images are taken at 12.8 seconds per image.

speed AFM and supported bilayer on gold, the influence of the cortex on the pore size can be directly revealed. Therefore, this experimental setup combining high-speed AFM imaging with an actin-supported bilayer can provide a step towards finding the physical pore structure in cell membranes during electroporation

5.2.3 Reveal shielding effect of multiple GUVs

The work discussed in this thesis up is mainly focussed on the electroporation mechanism at the single cell level. These studies mainly focus on the fundamental mechanism(s) of electroporation. However, *in vitro* electroporation of cell suspensions is used for clinical and medical applications [18-20]. Low cell density suspension (< 1 vol% cells) can be approximated by the single cell electroporation. However, cell suspensions from 10 vol% cells and cell clusters exhibit an affected transmembrane voltage [19, 21, 22]. Additionally, dense cell suspensions, like cell pellets, can bridge the gap going from single cell insights to cell tissue systems [23]. The presence of multiple cells in the electric field leads to electric shielding effects [21, 22, 24] and requires higher electric pulses in order to electroporate the cells [25]. The larger the cell fraction, the lower the percentage of electroporated cells and the slower the resealing of the cells. In addition, the molecular transport is slowed down by the presence of multiple cells [23, 26, 27]. Systematic studies on cells in suspension can be done by using multiple GUV systems. Subsequently, by controlling the distribution of the GUVs on a substrate, dependence of the shielding effect on the distance between the GUVs can be determined. Due to the size-control of the GUVs, the relation between the size of the GUVs and the shielding effect can be obtained. Subsequently, using the vesicle models developed in this thesis can be used for more systematic studies. This insight can provide a better use of *in vitro* electroporation and simultaneously offer insights in *in vivo* electroporation of the tissue.

5.2.4 Systematic study on engineered cellular tissue

Electroporation of tissue is already used in several medical applications like electrochemotherapy, nonthermal tissue ablation and transdermal drug delivery [28]. Using electroporation for these medical applications, the main challenge is to control the electric field in the cell tissue, consisting of a heterogeneity of closely packed cells. *In vivo* experiments have shown great promise of the usage of electroporation on tissue for medical purposes [28]. By using predictive analytical methods to determine the number of electrodes, the geometry of the electrodes and the pulse properties (e.g. shape, strength, number), an effective treatment can be established in advance [29-32]. These studies are mainly focussed on the top down approach, studying the complex system itself.

Engineering tissue-like materials can be used as a bottom-up approach to unravel electroporation at the tissue level. From mid-1980, the field of tissue engineering has been introduced and has grown into a prospecting field enabling biomaterial engineering [33, 34]. The dermal and transdermal tissue have been successfully engineered [33] and microfluidic devices have been used to engineer cell tissue, tumour cells on a chip, and even the growth of organ tissue, the so-called “organ-on-a-chip” [35-38]. In these studies, both the artificial growth of actual tissue cells is used and the mimicking of certain human tissue by use of natural polymers. Both these approaches can enhance the progress in the development of electroporation applications as transdermal drug delivery and gene therapy. A recent example of the integration of tissue engineering with electroporation is the electrotransfer study of DNA into a three-dimensional reconstructed human dermal tissue [39, 40]. An extracellular matrix has been made from cell sheets of dermal fibroblasts, comparable to the dermis of the skin. The electric pulse experiments on this engineered skin tissue has shown that genes can successfully be electrotransferred into the tissue and also electrotransfection has been observed. Another example of using tissue engineering to study the electroporation of tissue is by mimicking the heterogeneous tissue with a potato slice immersed in two kinds of gel phantoms [41]. These potato samples are used to validate their numerical model to predict the current density distribution of the inhomogeneous tissue. These two examples illustrate how engineered cell tissue can expand our knowledge of tissue electroporation.

Exploiting these opportunities to engineer cell tissue would improve the use of tissue electroporation in medical applications. Microfluidic devices have shown great promise in culturing cells, providing the spatial control of cell growth [42, 43]. Using this approach, successful engineering of tumour models [36] and cell tissue have been achieved. Additionally, it enables easy visualisation and the integration of electrodes in the chips. Microfluidic concepts have already been used for single cell electroporation as single cell electroporation, cell screening and electrofusing [44-49]. Consequently, it would be a great system to systematically study the electroporation mechanism of cell tissue experimentally, enabling direct translation of the obtained results to medical applications.

5.3 REFERENCES

1. Lodish, H., Berk, A., Zipursky, S.L., Matsudaira, P., Baltimore, D., and Darnell, J., *Molecular cell biology*. 4th ed. Vol. 29. 2001, New York: W. H. Freeman and Company.
2. Vaughan, E.E., and Dean, D.A., Intracellular Trafficking of Plasmids during Transfection Is Mediated by Microtubules. *Molecular Therapy*, 2006. 13(2): p. 422-428.
3. Schwille, P., *Bottom-Up Synthetic Biology: Engineering in a Tinkerer's World*. Science, 2011. 333(6047): p. 1252-1254.
4. Schwille, P., and Diez, S., Synthetic biology of minimal systems. *Critical Reviews in Biochemistry and Molecular Biology*, 2009. 44(4): p. 223-242.
5. Gilden, J., and Krummel, M.F., Control of Cortical Rigidity by the Cytoskeleton: Emerging Roles for Septins. *Cytoskeleton (Hoboken, N.J.)*, 2010. 67(8): p. 477-486.
6. Fehon, R.G., McClatchey, A.I., and Bretscher, A., Organizing the cell cortex: the role of ERM proteins. *Nature Reviews Molecular Cell Biology*, 2010. 11: p. 276.
7. Chaffey, N., Alberts, B., Johnson, A., Lewis, J., Raff, M., Roberts, K. and Walter, P. *Molecular biology of the cell*. 4th edn. Annals of Botany, 2003. 91(3): p. 401-401.
8. Vale, R.D., Microtubule-based motor proteins. *Current Opinion in Cell Biology*, 1990. 2(1): p. 15-22.
9. Rosazza, C., Meglic, S.H., Zumbusch, A., Rols, M.P., Miklavčič, D., *Gene Electrotransfer: A Mechanistic Perspective*. *Current Gene Therapy*, 2016. 16(2): p. 98-129.
10. Portet, T., Favard, C., Teissié, J., Dean, D.S., and Rols, M.-P. , Insights into the mechanisms of electromediated gene delivery and application to the loading of giant vesicles with negatively charged macromolecules. *Soft Matter*, 2011. 7(8): p. 3872-3881.
11. Escoffre, J.-M., Portet, T., Wasungu, L., Teissié, J., Dean, D., and Rols, M.-P., What is (Still not) Known of the Mechanism by Which Electroporation Mediates Gene Transfer and Expression in Cells and Tissues. *Molecular Biotechnology*, 2009. 41(3): p. 286-295.
12. Rosazza, C., Escoffre, J.M., Zumbusch, A., and Rols, M.-P., The actin cytoskeleton has an active role in the electrotransfer of plasmid DNA in mammalian cells. *Molecular therapy : the journal of the American Society of Gene Therapy*, 2011. 19(5): p. 913-921.
13. Golzio, M., Teissié, J., and Rols, M.-P., Direct visualization at the single-cell level of electrically mediated gene delivery. *Proceedings of the National Academy of Sciences*, 2002. 99(3): p. 1292-1297.
14. Chang, D.C., and Reese, T.S., Changes in membrane structure induced by electroporation as revealed by rapid-freezing electron microscopy. *Biophysical Journal*,



1990. 58(1): p. 1-12.

15. Chernomordik, L.V., 5 - Electropores in Lipid Bilayers and Cell Membranes A2 - Chang, Donald C, in *Guide to Electroporation and Electrofusion*, B.M. Chassy, J.A. Saunders, and A.E. Sowers, Editors. 1992, Academic Press: San Diego. p. 63-76.

16. Sengel, J.T., and Wallace, M.I., Imaging the dynamics of individual electropores. *Proceedings of the National Academy of Sciences*, 2016. 113(19): p. 5281-5286.

17. Jeuken, L.J.C., AFM Study on the Electric-Field Effects on Supported Bilayer Lipid Membranes. *Biophysical journal*, 2008. 94(12): p. 4711-4717.

18. Pavlin, M., Kandušer, M., Reberšek, M., Pucihar, G., Hart, F.X., Magjarevic, R., and Miklavčič, D., Effect of Cell Electroporation on the Conductivity of a Cell Suspension. *Biophysical Journal*, 2005. 88(6): p. 4378-4390.

19. Pavlin, M., Leben, V. , and Miklavčič, D., Electroporation in dense cell suspension—Theoretical and experimental analysis of ion diffusion and cell permeabilization. *Biochimica et Biophysica Acta (BBA) - General Subjects*, 2007. 1770(1): p. 12-23.

20. Golzio, M., Rols, M.-P., and Teissié, J., In vitro and in vivo electric field-mediated permeabilization, gene transfer, and expression. *Methods*, 2004. 33(2): p. 126-135.

21. Susil, R., Šemrov, D., and Miklavčič, D., Electric Field-Induced Transmembrane Potential Depends on Cell Density and Organization. *Electro- and Magnetobiology*, 1998. 17(3): p. 391-399.

22. Pavlin, M., Pavselj, N., and Miklavčič, D., Dependence of induced transmembrane potential on cell density, arrangement, and cell position inside a cell system. *IEEE Transactions on Biomedical Engineering*, 2002. 49(6): p. 605-612.

23. Abidor, I.G., Li, L.H., and Hui, S.W., Studies of cell pellets: II. Osmotic properties, electroporation, and related phenomena: membrane interactions. *Biophysical Journal*, 1994. 67(1): p. 427-435.

24. Pucihar, G., Kotnik, T., Valič, B., and Miklavčič, D., Numerical Determination of Transmembrane Voltage Induced on Irregularly Shaped Cells. Vol. 34. 2006. 642-652.

25. Rems, L., and Miklavčič, D., Tutorial: Electroporation of cells in complex materials and tissue. *Journal of Applied Physics*, 2016. 119(20): p. 201101.

26. Pucihar, G., Kotnik, T., Teissié, J., and Miklavčič, D., Electropermeabilization of dense cell suspensions. *European Biophysics Journal*, 2007. 36(3): p. 173-185.

27. Canatella, P.J., Black, M.M., Bonnicksen, D.M., McKenna, C., and Prausnitz, M.R., Tissue Electroporation: Quantification and Analysis of Heterogeneous Transport in Multicellular Environments. *Biophysical Journal*, 2004. 86(5): p. 3260-3268.

28. Yarmush, M.L., Golberg, A., Serša, G., Kotnik, T., and Miklavčič, D., Electroporation-Based Technologies for Medicine: Principles, Applications, and Challenges. *Annual Review of Biomedical Engineering*, 2014. 16(1): p. 295-320.
29. Miklavčič, D., Šemrov, D., Mekid, H., and Mir, L.M., A validated model of in vivo electric field distribution in tissues for electrochemotherapy and for DNA electrotransfer for gene therapy. *Biochimica et Biophysica Acta (BBA) - General Subjects*, 2000. 1523(1): p. 73-83.
30. R. E. Neal, I., Garcia, P.A., Robertson, J.L., and Davalos, R.V., Experimental Characterization and Numerical Modeling of Tissue Electrical Conductivity during Pulsed Electric Fields for Irreversible Electroporation Treatment Planning. *IEEE Transactions on Biomedical Engineering*, 2012. 59(4): p. 1076-1085.
31. Langus, J., Kranjc, M., Kos, B., Šuštar, T., and Miklavčič, D., Dynamic finite-element model for efficient modelling of electric currents in electroporated tissue. *Scientific Reports*, 2016. 6: p. 26409.
32. Edhemovic, I., Gadzije, E.M., Breclj, E., Miklavčič, D., Kos, B., Zupanec, A., Mali, B., Jarm, T., Pavliha, D., Marcan, M., Gasljevic, G., Gorjup, V., Music, M., Vavpotic, T.P., Cemazar, M., Snoj, M., and Serša, G., Electrochemotherapy: A New Technological Approach in Treatment of Metastases in the Liver. *Technology in Cancer Research & Treatment*, 2011. 10(5): p. 475-485.
33. Vranckx Jan, J., and Hondt Margot, D., Tissue engineering and surgery: from translational studies to human trials, in *Innovative Surgical Sciences*. 2017. p. 189.
34. Howard, D., Buttery, L.D., Shakesheff, K.M., and Roberts, S.J., Tissue engineering: strategies, stem cells and scaffolds. *Journal of Anatomy*, 2008. 213(1): p. 66-72.
35. Huh, D., Hamilton, G.A., and Ingber, D.E., From 3D cell culture to organs-on-chips. *Trends in Cell Biology*, 2011. 21(12): p. 745-754.
36. Tsai, H.-F., Trubelja, A., Shen, A.Q., and Bao, G., Tumour-on-a-chip: microfluidic models of tumour morphology, growth and microenvironment. *Journal of The Royal Society Interface*, 2017. 14(131).
37. Velve-Casquillas, G., Le Berrea, M., Piel, M., and Tran, P.T., Microfluidic tools for cell biological research. *Nano today*, 2010. 5(1): p. 28-47.
38. Yi, L., and Lin, J.-M., Development and Applications of Microfluidic Devices for Cell Culture in Cell Biology. *Molecular Biology*, 2017. 6(1).
39. Madi, M., Rols, M.-P., and Gibot, L., Efficient In Vitro Electroporation of Reconstructed Human Dermal Tissue. *The Journal of Membrane Biology*, 2015. 248(5): p. 903-908.



40. Moinecha, M., Rols, M.-P., and Laure, G., Gene Electrotransfer in 3D Reconstructed Human Dermal Tissue. *Current Gene Therapy*, 2016. 16(2): p. 75-82.
41. Bernardis, A., Bullo, M., Campana, L.G., Di Barba, P., Dughiero, F., Forzan, M., Mognaschi, M.E., Sgarbossa, P., and Sieni, E., Electric field computation and measurements in the electroporation of inhomogeneous samples, in *Open Physics*. 2017. p. 790.
42. van Duinen, V., Trietsch, S.J., Joore, J., Vulto, P., and Hankemeier, T., Microfluidic 3D cell culture: from tools to tissue models. *Current Opinion in Biotechnology*, 2015. 35: p. 118-126.
43. Halldorsson, S., Lucumi, E., Gómez-Sjöberg, R., and Fleming, R.M.T., Advantages and challenges of microfluidic cell culture in polydimethylsiloxane devices. *Biosensors and Bioelectronics*, 2015. 63: p. 218-231.
44. Strömberg, A., Karlsson, A., Ryttsén, F., Davidson, M., Chiu, D.T., and Orwar, O., Microfluidic Device for Combinatorial Fusion of Liposomes and Cells. *Analytical Chemistry*, 2001. 73(1): p. 126-130.
45. Strömberg, A., Ryttsén, F., Chiu, D.T., Davidson, M., Eriksson, P.S., Wilson, C.F., Orwar, O., and Zare, R.N., Manipulating the genetic identity and biochemical surface properties of individual cells with electric-field-induced fusion. *Proceedings of the National Academy of Sciences*, 2000. 97(1): p. 7-11.
46. Dahl, J.B., Lin, J.M., Muller, S.J., and Kumar, S., Microfluidic strategies for understanding the mechanics of cells and cell-mimetic systems. *Annual review of chemical and biomolecular engineering*, 2015. 6: p. 293-317.
47. Hu, N., Yang, J., Joo, S.W., Banerjee, A.N., and Qian, S., Cell electrofusion in microfluidic devices: A review. *Sensors and Actuators B: Chemical*, 2013. 178: p. 63-85.
48. Saito, A.C., Ogura, T., Fujiwara, K., Murata, S., and Nomura, S.M., Introducing Micrometer-Sized Artificial Objects into Live Cells: A Method for Cell–Giant Unilamellar Vesicle Electrofusion. *PLoS ONE*, 2014. 9(9): p. e106853.
49. Santra, T.S., and Tseng, F.G., Recent Trends on Micro/Nanofluidic Single Cell Electroporation. *Micromachines*, 2013. 4(3): p. 333-356.



Acknowledgements

Yes, it is done! After years of living in the lab, cracking my brain over debugging matlab scripts, and writing writing writing, my scientific journey has come to an end. It has been a tough and amazing journey, and I never expected to get this far. The PhD has brought me high peaks and deep valleys, and I could not have gone through it without so many amazing people, which I would like to thank all. Words cannot describe how grateful I am for all help I have had during these years, that brought me to this milestone. Or, to say it more scientifically: it is challenging to find the words. And scientist as I've become, I am ready to accept the challenge.



First of all, **Pouyan**, this journey has been incredible and I owe it all to you. You offered me this position and with that you gave me the opportunity to take this step. Thank you so much for this opportunity. We have come such a long way together, as your first PhD, I have seen you grow in leading your own section, expanding the group with more PhDs and Post Docs and coaching all of us. Simultaneously, you have helped me to grow into a more mature scientist and to develop myself both professionally and personally. I appreciate your endless enthusiasm. In addition, you gave me so many opportunities to present my work to the public at conferences, where you always tried to get me more relaxed prior to the talk and always gave me some positive words afterwards. Even during our meetings we discussed our work critically and you made sure that I would walk out with a positive vibe. It is amazing how much you cared for us, making sure we were doing fine both professionally and personally. Hopefully you can carry on this fashion of leading your own group, giving attention to both the professional and personal life of your PhDs.

Michiel, it was great to work with you. You have made me into a critical researcher. You understand the art of raising simple questions that lead to great answers, and form your papers as such. During these years, I have seen you further developing your managing career. I think it is exceptional how you managed to combine both your manager career and still staying close to science. You introduced me into the wonderful world of Delft, consisting of equations, theory and error analysis. You have helped me to cultivate this knowledge of numbers, equations and derivatives, and I would like to thank you for all your help to get me this far.

Aside from my promotor and co-promotor. I've greatly enjoyed my time with all members in Pouyan's electroporation group, passing by over the years: **Piotr, Shaurya, Lea, Aswin** and **Afshin**. **Piotr**, as the first post doc joining Pouyan's group, we have worked very closely. I am happy and grateful how you got me through my first time at Delft, introducing me to all the important people and teaching me all the tricks. I still remember the day you told me that we were working together for too long, since you could pick up my mood already when I entered the office. Nevertheless, I think you handled all my 'moods' as a real gentle man, always opening all doors for me. **Shaurya**, after about two years, you entered the little group of Piotr and me. It was great to have someone else working on electroporation. In addition, you introduced me to many amazing meals you made us for lunch, and always took care that we had some fruits and nuts around the four 'o clock dip. **Lea**, as soon as Shaurya and I heard that you would join the group, we were super excited. Finally, an actual electroporation expert would join our group. You came around the time that I did my first publications, and I was very happy with all your help coaching me through the paper and the review. You have helped me through the ups and downs of the writing and publishing. I appreciated that you stayed late for every (re)submission we had to make, helping me through the pages and pages of uploading and formalities during submission. You even joined me on some of the additional experiments the reviewers requested, as a moral support and gave me soothing words when I was struggling. **Aswin**, as the fresh newly-PhD, you inherit all our electroporation experiments. It was great to have your

refreshing energy around and your enthusiasm to start with new experiments. **Afshin**, you joined latest during my time, and you immediately helped me with our last paper. It was great to work closely with you so soon after your start in the group. And I am very happy with all your contributions our last paper.

When I joined the group, **Barbara** and **Yogesh** welcomed me as my office colleagues. **Barbara**, you immediately introduced me into the group and brought me up to speed on the latest gossip and the do's and don'ts within the group in the first week. **Yogesh**, you have been so welcoming, helping me with all my math problems and making Barbara and me awesome food at your place. **Durgesh**, as soon as a desk was available, you joined our office. Thank you for the numerous lunches we had at your place, after which we had to work with an after dinner dip. Your lively and optimistic vibes helped me through the PhD and I enjoyed how we commented on each other R&O meetings and how we have spent our evenings in the lab to accompany and support each other. **Andrea**, **David**, **Aris**, **Wenjie**, **Floris**, **Jesus**, **Hao**, **Hrushikesh**, **Fabio** and **Samir**, the first batch of PPE. We have had such a great time together. Dinners, fries at the Bierfabriek, drinks on Friday, pizza-night at Fabio's and of course the kohl-tour in Bremen. It was amazing how you welcomed me in the group and introduced me into Delft, sharing the perks of being a researcher. **Andrea**, I was so happy to have another girl in the group, our girls nights with you and your housemate were lovely. **Samir**, your endless enthusiasm was amazing, it was great to have you around, making sure there was never a dull moment. **Fabio**, with your Fabio-licious food, you always surprised us with some amazing snacks (with our without chili). **David**, the fun-Friday lunches were amazing, and thank you for opening your house for all events we wanted to throw. The unforgettable Sinterklaas event mixed with the Spanish tapas with all of you was the best! **Floris**, the one who was always up for a drink, and knew the places to go to for free drinks and food. Thank you for taking all of us to those places, making sure we had some hilarious moments. **Aris**, apparently you loved us so much, you came back to join the group again. Thank you for all your little happy chats to enlighten my days at Delft. **Wenjie**, it was a great pleasure to have you around. I still remember you funny screensaver with the rabbit holding a carrot and you buying a towel with a huge cat during our trip to Bremen. **Hrushikesh**, it was a joy to have you in the group and it is a shame that you left our group early. I hope you are doing well at your new job. **Jesus**, the Macarena-movie we made for David was epic. **Hao**, thank you for all the tea and noodles you made me during may days of hard work. These are just a few examples to illustrate my great times in Delft thanks to all of you. Thank you all for this lovely time. **Dominik**, **Maulik**, **Kartik**, **Hamid**, **Damiano**, **Erik**, **Josette**, **Yuije**, **Serhii** and **Fatemeh**, to me you belong to the second batch of PPE. I admit I was a bit more focussed on my work, though all of you made life in the office so much fun with the newly introduced pizza-Tuesdays after the colloquium, the joined Friday drinks with TP and let's not forget the PPE days and activities. **Dominik**, you always managed to bring life into the office, the lunch, the group meetings, basically everywhere. It was great to have you around. Thank you **Maulik**, for always helping me with all my math problems at any time of the day, and **Serhii** for sympathizing for my last phase coping with finalizing my thesis while starting a post doc.



You were in the same position as me, and I appreciated our discussions how to streamline two jobs simultaneously. I hope you'll manage to finish up soon.

Of course I would also like to thank the permanent staff of PPE: **Volkert, Ruud, Henk, Peter, Gabriele, Wim, Mojgan, Caroline** and **Stefan**. Thank you for all your support during my stay in Delft. **Ruud**, during our small encounters in the hallway, you always asked me fatherly how I was doing, thank you for caring. **Volkert**, for three years we worked together during the yearly MTP course. Thank you for all your endless patience, bringing me up-to-speed on my first engineering course and giving my private lectures so I could TA the students. **Henk** and **Peter**, thank you for all the enjoyable chats at the coffee machine. **Gabriele**, we have never worked together, though still you were open to meet with me and discuss my future career. Thank you for all the advice, and the genuine follow-up conversations. **Wim**, it was so much fun to work in the lab together, we both shared the interest for microscopy and it was great to exchange awesome microscopy images to show how pretty science can be. **Mojgan**, it was a joy to be around your lively and cheerful personality, always having great stories to tell. **Elly** and **Astrid**, I owe you so many thank you's! Without you, it would have been impossible to finish. You have both helped me numerous times to get my work high on the priority list of Michiel. **Astrid**, especially during the last months you have been of great help. Thank you for always helping me to get the thesis finished. **Evert**, your knowledge of cameras is amazing, thank you for your help improving my imaging techniques. **Marcel**, it was so much fun to work with you. You introduced me into the world of atomic force microscopy, and the JPK crash-course with Jörg was great! In addition, we shared the interest to communicate science beyond the scientific world, hopefully we will still work together in the future in the environment of the NTR. **Alex**, the electronics expert, you were involved to build all the electrical setups together with **Youp**, making the most fancy designs for 3D printed electrodes. Thank you both for all your help, building a complete new setup from scratch. **Bart**, thank you for all your help with LabView and **Duco** thank you for letting me use all your lab facilities. Finally, **Peter Verheijen**, the friendly and familiar face when I just entered Delft. Whenever you were in Delft, you came for a cup of coffee, showing me around and giving me advice. Thank you for being a listening ear and your advice throughout the years.

Over the years of research, so many students have helped me with the work in the lab. **Jord, Nienke, Sharon, Alexander, Max & Riemer, Loes & Max, Quinten, Vaishnavi, Lotte** en **Zoë**, thank you for all your contributions to the work. **Jord**, you were my first student during my first year. I have learned so much from our working together, thank you for giving me this experience. **Vaishnavi** and **Lotte**, your work has led directly to a publication, which is awesome. **Vaishnavi**, your first steps in the lab were the most crucial steps for me, finding out how to make GUVs with an encapsulated actin network. You have grown incredibly during your project, being the expert in the preparation of actin-encapsulated GUVs in the end and being an excellent trainer for Lotte. **Lotte**, you picked up on Vaishnavi's research quickly, and I am very happy with your results, which went directly into the paper. **Zoë**, it was a great pleasure to work with you. You joined our group

as a bachelor student and you enjoyed it so much that came you came back as a master student and even after your internship you came back just for fun! (and some work). You have worked on the most challenging project we had and your work was of great quality and I think you would make an excellent scientist.

No actin paper without the actin experts **Yuval** and **Gijsje**. Thanks for sharing all your knowledge on actin with me and for your super super fast response on every version of the manuscript.

Already during my first year I got introduced into the community of electroporation, during the EBT course, and every world congress or conference we would meet again. **Lea, Maurina, Amar, Elisa, Shirley, Damian, Mounir, Peter, Luis** and **Justin**, it was great to be in this community and you taught me so much about the theory behind electroporation and making vesicles, sharing experimental tricks and frustration.

Traveling to Delft, day by day, week after week, month after month, I was lucky to have the support via the whatsapp group: Forenzen app, the place to dump all complaints about commuting, without bothering our friends. **Lisa, Zsa zsa** and **Romy**, thank you for all the support during the crowded trains, smelly and loud people on the train, endless delays and many many more train sorrow during the two years of commuting. The pied-a-terre at the Vlamingstraat after the first year of travelling every day was a blast. **Caroline, Jaqueline, Defne, Amber, Josephine, Nikki, Merel** and **Liselotte**, it was amazing to live with all of you and I enjoyed you showing me the student life in Delft, including all do's and don'ts, and go's and do not go's. Your stories about life in Delft were amazing. **Defne** and **Amber**, we have spent so many home-made dinners, Harry Potter marathons and crazy nights. I am so glad I have met the both of you, you have made Delft so much fun and I still love seeing you two.

However, after one year of full-time commuting, and one year of part-time commuting and part-time living in Delft, the moment came to move closer to work full-time. **Anna, Guido, Esther, Arthur, Nataša** and **Robbert**, you have made Den Haag feel like a new home. **Nataša**, no matter the work load, every Sunday was our stress-free-zen-day, yoga followed by coffee at Pims where **Robbert** joined for his weekly portion of vlammetjes. This made every Sunday feel like a little holiday. Thank you for all the help with the cover and the lay-out of the booklet. Your endless creativity was of great help. **Esther, Arthur, Anna, Guido** and of course the little **Mies**, it is so great to live in Den Haag with all of you. Always ready to check out the latest events in the city and sharing the same love for design and furniture. Organizing game-nights and beach picnics together with **Linda, Vincent** and **Niels**, and even moving the Christmas dinner to Den Haag together. These evenings of "a journey around the world" and "Yvette van Boven versus Ottolenghi the cook-off" with the home brewed wine of Niels were unforgettable. **Ruben** and **Rebecca**, you two went even further than Den Haag and moved from Amsterdam to South Africa and from South Africa to Switzerland. You always choose great locations for a relaxing holiday and it was great to visit you at every new place. I cannot wait to find out you next



exotic location.

Luckily, I could always fall back on my loyal friends of way before this delft-era. **Dide** and **Jaco**, we met during the master in Utrecht and we have been friends ever since. **Dide**, even though our roads separated after the master, you starting a PhD at Utrecht and me starting in Delft, we kept meeting up to enjoy a glass of wine, sharing ours visions of women in science. I hope you are doing well in Bern together with **Manuel**. **Jaco**, I am glad we chose a similar research field and we would see each other every once in a while at a conference. Your endless enthusiasm for science is amazing, and as soon as you moved to Delft you could not wait to give me a tour through your lab. No matter where you will end up, I am sure that this science-love of yours will definitely be fully appreciated. **Romy**, **Sieske**, **Jorien** and **Barbara**, our friendship already started during the bachelors (and bar we actually go even more back). It all started when we were exploring our first steps of independency as fresh students in Amsterdam. Now, more than ten years later, we have spread over different parts of The Netherlands entering the working life, though seeing you girls is still as much fun and crazy as when we met. A weekend with you girls is both re-energising and exhausting. Hopefully, we can continue this till the end of days. **Dennis** and **Arno**, thank you for coping with our weird little traditions and sorry in advance for all the lunacy. Last and certainly not least, **Rebec**, **Esmée** and **Saar**, my friends that go all the way back to Hilversum. I am so happy that we are still in touch after so long. I love how we are so different and still support each other through thick and thin. **Ben**, you often surprised me with an awesome home-cooked meal, amazing! And thank you for all your genuine interest in my work.

Romy and **Sieske**, you two are not only my friends, you are also my paranymphs for the defence. Therefore, I wanted to give you some extra words. All three of us pursued the ambition to do a PhD and I have always felt as if we did it together. All in the far corners of the Netherlands, though connected via the gmail chat. Our daily chats discussing the perks of being a PhD and exchanging survival guides for women in science, complaining about the muscular environment. Without our daily chats I could not have made it through this time. Our conversations were complaining though witty and always encouraging to get me through the days. **Rom**, your defence was amazing and I was glad to be part of it. **Sies**, I cannot wait for yours.

To all the **Oelen**, you have welcomed me into the family as if I am a part of it. **Bregje** and **Alain**, together with the boys **Tristan**, **Sacha** and **Bodi** you always bring colour to all our gatherings, whether it is chaotic pancake events at Hans en Grietje or a birthday at home. **Carline**, **Daniel**, **Liv** and **Levi**, despite the great distance, you are very close to me. It is great to see you grow into a family. **Wim** and **Ineke**, thank you for all your support, your loving messages and caring words.

Dear **Karindra**, my amazing sister and roll model. I admire all talents you have, being a scientist by day and a musician by night, and your perseverance do to both full power. You are a great sister to look up to and our caring relation is dear to me. Us crossing our

scientific roads now, brings us even closer. **Erik**, the beacon of calm in this chaotic life of music and science. Your refreshing view brings a nice twist to our conversation and despite your profession in music it is relieving to see how you are one of the few that does not shy away from science.

Yanti and **Cor**, I feel privileged to come from a progressive family as ours. Coming from a family with a full-time working mother and a father with a home-office, you have always encouraged us to follow our hearts and taught us that the sky is the limit. In doing so, you have raised two ambitious daughters that do not shy away from this muscular world. It is great to see how you two complement each other and to receive your infinite love and support during all my calls during the bike-ride home. Your always wise advice was amazing.

Rutger, my little ray of sunshine every day, last and far but not least. So many years together and you still make me happy every day. What would I have done without you. No manuscript, email or figure has left our house before you had gone through it. I think it is exceptional how engaged you have been to my work. Your loving support whenever I was insecure about my work, during my sleepless nights and moody days has been endless and amazing. I am so happy you were with me in this turbulent journey and *“er zijn nog honderdduizend dingen om in de toekomst te gaan doen”* (Lucky Fons III).



Curriculum Vitae

Dayinta was born on the 24th of January 1989 in Amsterdam, The Netherlands. In 2010 she obtained her Bachelor degree in Bèta-Gamma, majoring in Chemistry at the University of Amsterdam, The Netherlands. After graduating, she spend one year teaching Chemistry as an extracurricular course for kids between the age of eight and twelve and traveling through South-East Asia. From 2011 till 2013 she pursued the Masters Nanomaterials: Chemistry and Physics at the Utrecht University, The Netherlands. During her last year, from March 2013 till August 2013, she conducted a research project at the University of Oxford, United Kingdom. In November 2013 she started her PhD in the Department of Chemical Engineering at the Delft University of Technology under the supervision of Prof. dr. ir. Michiel T. Kreutzer and Dr. Pouyan E. Boukany. Since November 2017 she started as a Postdoctoral Researcher in the same university, collaborating between the departments Civil Engineering and and Chemical Engineering.



List of publications

Dayinta L. Perrier, Afshin Vahid, Vaishnavi Kathavi, Lotte Stam, Yuval Mulla, Gijssje H. Koenderink, Michiel T. Kreutzer and Pouyan E. Boukany, *Unraveling the response of a biomimetic actin cortex to electric pulses in vesicles*, under submission.

Dayinta L. Perrier, Lea Rems, Michiel T. Kreutzer, and Pouyan E. Boukany, *The role of gel-phase domains in electroporation of vesicles*, Scientific Reports, 8, 4758 (2018).

Dayinta L. Perrier, Lea Rems, and Pouyan E. Boukany, *Lipid vesicles in pulsed electric fields: Fundamental principles of the membrane response and its biomedical applications*, Advances in Colloid and Interface Science, 24 (2017) 248-271.

Frank Versluis, Daphne M. van Esland, Serhii Mytnyk, Dayinta L. Perrier, Fanny Trausel, Jos M. Poolman, Chandan Maity, Vincent A. A. le Sage, Sander I. van Kasteren, Jan H. van Esch, and Rienk Eelkema, *Negatively charged lipid membranes catalyse supramolecular hydrogel formation*, Journal of the American Society, 28, 138 (2016).



